PULSE TRAIN ANALYSIS APPLIED TO THE RE-EVALUATION OF DEADTIME CORRECTION FACTORS FOR CORRELATED NEUTRON COUNTING

by

Louise Gail Evans

A thesis submitted to
The University of Birmingham
for the degree of
DOCTOR OF PHILOSOPHY

School of Physics and Astronomy
The University of Birmingham

2009

Abstract

Temporally-correlated neutron counting, including the passive neutron coincidence counting (PNCC) and passive neutron multiplicity counting (PNMC) techniques, is widely used at nuclear fuel cycle facilities for the non-destructive assay (NDA) of plutonium (Pu). Correlated event rates are used to quantify mass values of spontaneously fissile nuclides and derive total Pu mass. These methods are limited in accuracy by uncertainty in the deadtime correction. A pulse train analysis method has been developed and applied to the re-evaluation of deadtime correction factors for correlated neutron counting.

The Monte-Carlo transport code MCNPX^{TM} was used to generate a time-stamped list of neutron captures in ^{3}He. Event times were processed in software to create neutron pulse trains akin to list mode data. The action of multiplicity shift register (MSR) electronics was modelled in software to analyse these pulse trains. Prior to MSR analysis, stored pulse trains could be perturbed in software to apply the effects of deadtime. In this work, an updating (paralyzable) deadtime model was chosen to replicate existing theoretical approaches to deadtime correction.

Traditional deadtime correction methods for temporally-correlated neutron counting have been found to be accuracy limiting in cases where highly correlated rates occur over a short coincidence gate width i.e. high instantaneous rates associated with high multiplicity bursts. Here, empirical results are presented which support the development of an alternative formalism for both the traditional Singles and Doubles deadtime correction factors for PNCC. Deadtime effects are found to be dependent on the level of correlation in the pulse train yet independent of gate fraction, which is set by the shift register gate structure, for Singles deadtime correction factors. Doubles deadtime correction factors were found to have a slight dependence on gate fraction.

Research work was conducted at the University of Birmingham, UK in close collaboration with Canberra Industries, Inc., USA.

to Mum, Dad & Lucy

Nothing in life is to be feared. It is only to be understood.
- **Marie Curie** 1867 - 1934

In Loving Memory of Grandad Drury.
I'm still expecting the wheel barrow...

Acknowledgements

Over the course of my research and writing this thesis, there have been many people who have made an important contribution or helped me along the way. I therefore wish to express my deepest thanks to those people here.

Firstly, I would like to thank my industry supervisor and mentor, Stephen Croft; for his continuing advice, endless patience, numerous comments and above all, inspiration. I also thank Stephen for co-authoring my papers and proof-reading this thesis (notably, even on a weekend). I can only aspire to one day be as knowledgable.

Thanks are also due to my University supervisor, Paul Norman; for accepting my application to study on the PTNR MSc course in the beginning and for the opportunity to conduct my research at Birmingham. Paul is a truly excellent teacher and has been a source of great support and encouragement over the past four years. Thank you to Paul for proof-reading this thesis.

Many, many thanks to the rest of the research collaboration, who have been instrumental to this thesis work: the team of scientists at Canberra Industries; with special mention to Nabil Menaa, Sasha Philips, Bob McElroy and Pauline Blanc. Thanks are also due to Ram Venkataraman; for arranging for me to gain valuable practical experience at Meriden. The laboratory supervision from Nabil during time spent at Canberra Industries and his continuing support have also proved invaluable to composing this thesis. Kate Leduc should not go unmentioned for making other necessary arrangements for this trip and conferences.

A special mention to Jacqueline Croft; for looking after me during my stay in the US, the 'to do' list and being the best 'boot buddy' one could hope for.

Thank you to colleagues at Canberra UK, for their support in the final stages of writing this thesis: Colin Wilkins, Malcolm Wormald, Kenneth Lambert, Mike Henry, Eloisa Alvarez and Mercedes Lis. Thanks also to Patrick Chard for help with MCNPX.

Thank you to the other people that have made my research possible. Thank you to Martyn Swinhoe, Los Alamos National Laboratory; for advice and comments in the early stages of developing the pulse train analysis method. Thank you to David Weaver, University of Birmingham and Cristina Lebunetelle, OECD NEA Data Bank; for the MCNPX^{TM} code distribution. Thank you to Tom Turner, UKAEA; for help during the first year.

A huge thank you to EPSRC; for the provision of funding; Norma Simpson; for always knowing the answer and Anna Jenkin; for fielding a constant stream of questions on travel expenses.

Thank you to Andrew Worrall, National Nuclear Laboratory; for time and advice. In particular, for valuable input into the fuel cycle section of this thesis, the provision of presentation materials and pointing me in the direction of useful reading material.

I am also grateful to colleagues in the Nuclear Physics Group: Garry Tungate; for his encouragement from my first day in the Physics department. Martin Freer; for reviewing my CV and therefore enabling me to continue my research career and begin to answer some of the questions that remain from this thesis. Paul Jagpal and Victor Ziman; for helping me with my computing needs. Thanks to the current and former 'inhabitants' of E320 and E320a for sharing the journey: Thomas ('Ramone') Burton, Kasia Baczynska, Peter Haigh, Monjur Ahasan, Leon Gaillard, Anthony Timmins, Dave Price, Paul McEwan, Thomas Bloxham, Mark Bissell, Matt Gardner, Nick Ashwood, Neil Curtis, Carl Wheldon, Lee Barnby, Dave Forest, Mareike Ruffer, Essam Elhalhuli, Thomas Munoz and Simeon Spencer. Thanks also to current and former members of the PTNR research group; Debbie Curtis, Andrew Davis, Mike O'Brien, Tim Ware and Andrew Hetherington.

A special mention to my dearest friends: Anna Hitti, Emma Catton, Sarah Price, Kate Limb, Anna Jackson, Margaret O'Hara, Kasia Baczynska, Geraldine Huet, Tanya Reardon and Anna Price; for your friendship and continuing support. Anna H; University life would not have been the same without you. Margaret and Sarah; for getting me away from my desk and out to lunch at least once a week. Kate and Anna J; for helping me survive the 'politics' of Langley's Road and for continuing to make Birmingham a great city to live in. Emma and Tanya; for a memorable first year with the highest number of cups of tea consumed and Tanya's wonderful cooking (truly the dinner party 'hostess with the mostest'). Thanks to Vlad Penev; for helping me stay calm through running (even if I can't walk for a day or so afterwards). Thanks also to Peter Brookes for proof-reading this thesis.

Thank you to my Parents; for their support (both emotional and financial) from literally day one. Thank you to my ('big little') sister, Lucy; for being a great friend and supporter. Thank you to my Grandparents; for being their wonderful selves and for always listening. Grandad Drury; you are dearly loved and very much missed.

Finally, a special thank you to my partner and best friend, Tom; for his love, patience and support. This continued even when Tom had his own thesis to write.

Figure 1: Research Collaboration. From left: Nabil Menaa, Bob McElroy, Stephen Croft, Louise Evans (author), Ram Venkataraman, and Sasha Philips.

Contents

List of Figures

List of Tables

List of Abbreviations

AMSR	Advanced Multiplicity Shift Register
AWCC	Active Well Coincidence Counter
CF	Correction Factor
DA	Destructive Assay
DDA	Differential Die-Away
DTCF	Deadtime Correction Factor
ESARDA	European Safeguards Research and Development Association
GUF	Gate Utilization Factor
HEU	Highly Enriched Uranium
HLW	High Level Waste
HPGe	Hyper Pure Germanium
IAEA	International Atomic Energy Agency
IEA	International Energy Agency
ILW	Intermediate Level Waste
INMM	Institute of Nuclear Materials Management
LANL	Los Alamos National Laboratory
LEMC	Large Epi-Thermal Multiplicity Counter
LEU	Low Enriched Uranium
LLW	Low Level Waste
LLWR	Low-Level Waste Repository
LMDA	List Mode Data Acquisition
LWR	Light Water Reactor
MSR	Multiplicity Shift Register
NDA	Non-Destructive Assay
NPT	Non-Proliferation Treaty
MCNP™	Monte Carlo N-Particle code
MCNPX™	Monte Carlo N-Particle eXtended
MOX	Mixed (Plutonium and Uranium) Oxide
MSR	Multiplicity Shift Register
ORNL	Oak Ridge National Laboratory
PNCC	Passive Neutron Coincidence Counting
PNMC	Passive Neutron Multiplicity Counting
PSMC	Plutonium Scrap Multiplicity Counter

QA	Quality Assurance
QC	Quality Control
Shake	10 ns
SNM	Special Nuclear Material
STI	Signal Triggered Inspection
te	Metric Tonne
	= 1000 kg
TMU	Total Measurement Uncertainty
TNC	Total Neutron Counting
TRU	Transuranic
	TRU waste Z > 92, Half-life > 20 years
VLLW	Very Low Level Waste
WG	Weapons Grade
WM	Waste Management

Notation

α	Alpha Ratio *Ratio of random (α,n) neutrons to spontaneous fission neutron production rates*
δ	System Deadtime Parameter
D	Doubles Rate
D_c	Measured Doubles Rate
D_m	Deadtime Corrected Doubles Rate
ϵ	Detection Efficiency *Counts per particle emitted*
F	Fission Rate
g	Specific Fission Rate
K_S	Vanishing Singles Rate Deadtime Correction Factor Multiplier
K_D	Vanishing Doubles Rate Deadtime Correction Factor Multiplier
m	Mass of Fissile Material
$m(^{240}\mathbf{Pu_{eff}})$	^{240}Pu Effective Mass
$\overline{\nu}_{i1}$	First Moment of Induced Fission
$\overline{\nu}_{s1}$	First Moment of Spontaneous Fission
$\overline{\nu}_{i2}$	Second Moment of Induced Fission
$\overline{\nu}_{s2}$	Second Moment of Spontaneous Fission
$\overline{\nu}_{i3}$	Third Moment of Induced Fission
$\overline{\nu}_{s3}$	Third Moment of Spontaneous Fission
R	Reals Rate
S	Singles Rate
S_c	Deadtime Corrected Singles Rate
S_m	Measured Singles Rate
τ	Die-away Time
T	Totals Rate
T_r	Triples Rate
T_{r_c}	Deadtime Corrected Triples Rate
T_{r_m}	Measured Triples Rate

Chapter 1

INTRODUCTION

This chapter explains the motivations for conducting research into the physics of Non-Destructive Assay (NDA) techniques. The discussion is set in the broader context of the nuclear fuel cycle. Challenges facing nuclear materials management are discussed, identifying some of the ways in which nuclear measurements need to evolve to meet these challenges. The importance of simulation as a research tool is highlighted. First, several research questions are posed. These are addressed in later sections of this work.

1.1 Scope

Temporally-correlated neutron counting techniques are potentially limited in accuracy by traditional deadtime correction methods. Measured correlated count rates are reduced due to deadtime thus, if not performed accurately, deadtime correction itself may lead to uncertainties in derived total plutonium (Pu) mass values. For safeguards measurements, target accuracies of less than 0.25% may be needed in demanding cases to maintain material balance areas and, even with careful item specific calibration, variations between items mean that dead time corrections are significant. This is discussed in a recent paper by Croft, *et al* [1]. It is costly to retrofit new hardware to existing assay systems to reduce the effects of deadtime, therefore it is advantageous to develop and implement new deadtime correction algorithms as an alternative approach to ameliorate this problem. There has been a general trend to field neutron instruments with higher efficiencies and shorter die-away times and hence these designs present the need for improved deadtime treatments. For these reasons, deadtime correction methods for temporally-correlated neutron counting are currently being re-visited by both the waste characterisation and safeguards communities in the nuclear industry.

Developments in list mode data acquisition (LMDA) have also stimulated growing interest in direct analysis of neutron pulse trains. In principle LMDA provides a complete record of the experiment and can be analysed in such a way as to simulate multiplicity shift register (MSR) action and investigate the MSR algorithms used for conducting neutron assay online. Examples of recent studies include those conducted by Bondar [2], Swinhoe, *et al* [3] and Peerani, *et al* [4]. This study thus began with the following research question in mind:

- *Can existing neutron pulse train analysis methods be extended to include a full systematic study of deadtime behaviour and effects in passive neutron counting systems?*

The first objective was therefore to research existing pulse train analysis techniques and extend their application to a systematic investigation of deadtime behaviour in correlated neutron counting, over a range of operational conditions of a multiplicity counter. A study of this nature has not been conducted by the community until now [1] [5], but provides a convenient means to study the validity of both the theoretical models of deadtime and empirical approximations. List mode data is now available for comparison and multiplicity data has been added to the Monte-Carlo transport code MCNPX^{TM} [6], which make this an opportune time to conduct an investigation of this nature. Following on from this work, further research questions developed:

- *Are there differences between the deadtime correction factors for uncorrelated (e.g. AmLi) and correlated neutron sources (e.g. Cf)?*
- *To what extent does multiplication (e.g. Pu items) impact the deadtime correction factors (impact the existing theoretical approaches to deadtime correction)?*

These research questions are part of a larger study to re-evaluate deadtime correction factors for correlated neutron counting in commercial applications and to develop a unified approach to deadtime correction for different multiplicity distributions. Broader questions are being addressed by other researchers in this field:

- *How does the multiplicity distribution impact deadtime correction factors?* [7] [8]
- *Are existing algorithms for the shift register the most efficient? i.e. is there merit to an improved sampling regime for the MSR?* [9]

1.2 Non-Destructive Assay

The term Non-Destructive Assay (NDA) covers a range of techniques for the measurement of both radioactive waste and special nuclear material (SNM); for example, fissile plutonium (^{239}Pu), uranium (^{233,235}U) and enriched uranium, held at nuclear fuel cycle facilities. NDA techniques are used for the characterisation (e.g. elemental or isotopic composition) and quantification (e.g. mass, activity) of these materials when contained or stored within sealed packages and waste drums. These containers are collectively known as "assay items". It is an essential feature of NDA that items are not opened or changed when conducting NDA measurements, hence preserving the physical and chemical state of the nuclear material under assay [10]. This type of nuclear measurement is therefore non-destructive in nature, involves the assay of the bulk item *in situ* and generally *in toto*, and relies on the detection of emitted penetrating radiation. The detected radiation can be correlated to specific radionuclides present and used to determine their characteristics and quantity [11].

NDA techniques for SNM were originally developed for nuclear materials safeguards measurements, requiring a rapid assay without interfering with the item [12]. NDA techniques therefore present certain advantages over Destructive Assay or Destructive Analysis (DA) which involves the collection of *samples* from the bulk material for radiochemical analysis [10]: NDA requires no preparation or transportation of radioactive samples and therefore no residual waste forms are created, operator radiation exposure is greatly reduced for NDA compared to DA, NDA measurements are faster than destructive techniques leading to higher assay throughput in fuel cycle facilities and a corresponding reduction in cost [12].

Moreover NDA of the bulk item is potentially more accurate than a physical sampling (often accompanied by radiochemical analysis) because the finite number of samples may not be representative of the bulk nuclear material, depending on the homogeneity of the item. For example, the distribution of radioisotopes and therefore radioactivity may not be uniform across the item. DA methods therefore require a strategy to homogenise and sample the item, ensuring a representative sampling scheme is obtained [11]. Typically, samples need to be sent to a laboratory for preparation, prior to analysis. This imposes further time and cost restraints on this choice of assay method. Sample preparation and transportation of radioactive materials to a laboratory may also result in the generation of unwanted secondary wastes. NDA does not require a sampling scheme and is thus free from the classical sampling error otherwise associated with DA. Bulk assay also obviates the need for repeated measurements to improve precision [11].

Advantages of NDA techniques have meant that their application has extended beyond nuclear safeguards measurements to other aspects of nuclear materials management for both safety and security. At present, NDA techniques are employed for a wide variety of applications at nuclear fuel cycle facilities, including: radioactive waste characterisation, process flow monitoring, enrichment monitoring, and spent fuel verification [12], among other examples given in section 1.4.

There are, however, disadvantages of NDA in comparison to DA. Unlike DA, NDA relies on the detection of emitted radiation outside a container, which may be a large waste drum or shipping container. Emitted radiation may therefore be subject to unwanted "matrix effects" such as attenuation or absorption as it traverses the surrounding matrix material, leading to uncertainty in the assay result. This means that NDA is usually less accurate than DA [12], provided the DA sampling protocol is representative. Typically DA samples are small compared to the overall volume of the item and so the dilemma is whether the samples collected, together and after homogenisation, are truly representative of the whole. This is a statistical problem. Depending on the nature of the material and practically acceptable sampling strategy the sampling errors can be large. Very often however sampling is not an option since the item can not be readily opened.

In many cases NDA measurements must be used in conjunction with DA, or results interpreted using process knowledge relating to the isotopes present in the waste form. Furthermore, NDA simply cannot be applied to the assay of some radionuclides. For example, pure β emitters are measured using DA, due to the short range of β particles in matter. Very long lived radionuclides are a further example.

Radioactive waste and nuclear material arise in a variety of physical and chemical forms which also have to be taken into account during the selection of an appropriate assay technique. For example, the assay of Pu metal generally requires neutron measurements for accurate absolute mass determination due to gamma ray self-absorption and the large attenuation of the gamma ray signal in dense waste drum matrices [12]. Calorimetry may also be applied to the assay of Pu; for example, PuO_2 and Pu metal product [13].

Table 1.1 provides a summary of the relative advantages and disadvantages of NDA and DA methods.

NDA	DA
Non-Destructive	Destructive
In-situ	Transportation of Radioactive Samples
Measurement of bulk item, generally *in-toto*	Physical sampling
Radiometric measurements	Radiochemistry
Radioactively "clean"	Residual waste forms, secondary wastes
Matrix Effects: attenuation, self-absorption, short range of α and β particles	Sampling error, non-homogeneity of matrix
Rapid measurement	Time consuming, expensive

Table 1.1: NDA vs DA

Reducing total measurement uncertainty (TMU) values in NDA measurements is the goal of current research, which would in turn lead to a reduced reliance on DA. Typically, DA techniques may be up to 10 times more accurate than an NDA result, however this does not merit the use of these techniques if the sampling errors are large i.e. imperfect sampling performed with exact analysis, as opposed to an NDA assay on the whole item performed imperfectly; as considered by Bronson [14]. Trade-offs between cost, time, simplicity and secondary waste generation come in to play during the selection of an appropriate assay technique, and it depends crucially on what is known about the assay items beforehand. NDA is generally the preferred approach when prior knowledge about an item is not available. Limitations in accuracy must therefore be investigated to enable the application of NDA techniques to continue to broaden to a greater range of measurement scenarios and more demanding items. Research can also lead to improvements in the way measurements are both conducted and interpreted.

1.3 NDA Techniques

This section provides an outline of the main NDA techniques currently applied in the nuclear fuel cycle. It is not intended to be extensive since several texts exist; these include the Los Alamos National Laboratory (LANL) *Passive Non-Destructive Assay of Nuclear Materials* [12] and the US Nuclear Regulatory Commission (NRC) manual *Active Non-Destructive Assay of Nuclear Materials* [15].

Three main classifications of NDA techniques are currently available: gamma-ray spectroscopy, neutron counting and calorimetry. Detecting emitted gamma radiation, neutrons and heat output, respectively. These techniques can be thought of as forming the "NDA triangle" shown in figure 1.1, with an assay radionuclide e.g. Pu at the centre. High Resolution Gamma Ray-Spectroscopy (HRGS) measurements are used to identify specific radionuclides present in assay items from their gamma-ray energy spectra. Neutron measurements are used to detect the presence of and determine the mass of U and transuranic (TRU) isotopes such as plutonium (^{238,239,240,241,242}Pu), americium (^{241}Am) and curium (^{242,244,246,248}Cm), as these isotopes emit neutrons during both spontaneous and induced fission. Calorimetry is useful for determining total Pu mass under certain conditions where neutron measurements are limited in accuracy. It is especially useful for determining Pu content in mixed oxide fuel (MOX) where a high background from (α, n) reactions would otherwise mask a useful neutron assay signal.

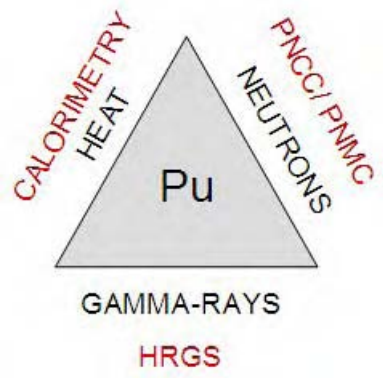

Figure 1.1: NDA Triangle

NDA measurements may be either passive or active, depending upon the radiation emission process. Passive measurements rely on counting the natural radiation emissions from an item following a spontaneous decay; these can be gamma rays from nuclear transitions following α or β decay, gamma rays following nuclear reactions or neutrons born in spontaneous fission. Heat generation from radioactive decay, due to the interaction of decay products in the surrounding material, is also classed as a passive process. Hence, all three groups of NDA techniques can be used in the passive mode.

Passive gamma measurements alone are used for assay. However, the interpretation of results from passive neutron measurements and calorimetry requires known isotopics from relative HRGS measurements or declared isotopic composition. Passive gamma measurements therefore accompany both passive neutron measurements and calorimetry where limited process knowledge is available. For this reason, HRGS can be thought of as forming the base of the NDA triangle in figure 1.1.

Items containing Pu lend themselves well to passive assay due to the relatively high spontaneous fission rates of the even-even isotopes: ^{238,240,242}Pu; ^{240}Pu being the dominant nuclide and the effective mass of ^{240}Pu the main assay parameter.

Active measurements, alternatively, are required where spontaneous fission neutron emission rates (or spontaneous fission yields) are not high enough to provide a detectable signal for assay. Measurement of the fissile isotope ^{235}U is conducted actively due to the low spontaneous fission rates of odd-even nuclei and corresponding low neutron yields. An active measurement uses an external interrogation source to stimulate emissions from the assay item, which may be a gamma ray, x-ray or neutron source. Gamma ray sources are more commonly used for transmission correction methods to account for spatial inhomogeneities in the waste matrix [11]. Neutron sources utilise the following reactions to induce fission within the assay item and therefore stimulate neutron emission [12]: (α,n) reactions (e.g. AmLi); spontaneous fission (e.g. ^{252}Cf) in the case of the Cf Shuffler assay system; and T(d,n) 14 MeV pulsed neutron generators for Differential Die-Away (DDA).

This thesis is concerned with passive neutron NDA measurements. The main area of research is the study of deadtime correction factors for correlated neutron counting, specifically the techniques of Passive Neutron Coincidence Counting (PNCC) and Passive Neutron Multiplicity Counting (PNMC).

1.4 Nuclear Fuel Cycle

Nuclear measurements, including NDA techniques, are widely used at nuclear fuel cycle facilities. The term nuclear fuel cycle is defined by the International Atomic Energy Agency (IAEA) [10] as: "A system of nuclear installations and activities connected by streams of nuclear material." Broadly, this refers to all facilities and processing stages required to fabricate nuclear fuel and generate power in a nuclear reactor, followed by the direct storage or reprocessing of the spent nuclear fuel at the end of its useful lifetime in the reactor core and subsequent waste management. However, the nuclear fuel cycle can greatly vary between countries; from a single reactor supplied with fuel from abroad, to a fully developed cycle which includes all the aforementioned processes [10].

The main stages of the UK nuclear fuel cycle are illustrated in figure 1.2 with arrows indicating the flow of nuclear material [16]. Not all stages of the UK fuel cycle take place in the UK itself, thus material is transported between countries. For example, U mining and milling are carried out overseas; mainly in Canada, Australia and Kazakhstan [17]. Stages are described here to highlight where radioactive waste and SNM arise within the cycle and thus where material monitoring is required. The different stages mean U and Pu may arise in many forms. LLW, ILW and HLW in the figure refer to Low-Level Waste, Intermediate-Level Waste and High-Level Waste, respectively; which are defined in section 1.5.1:

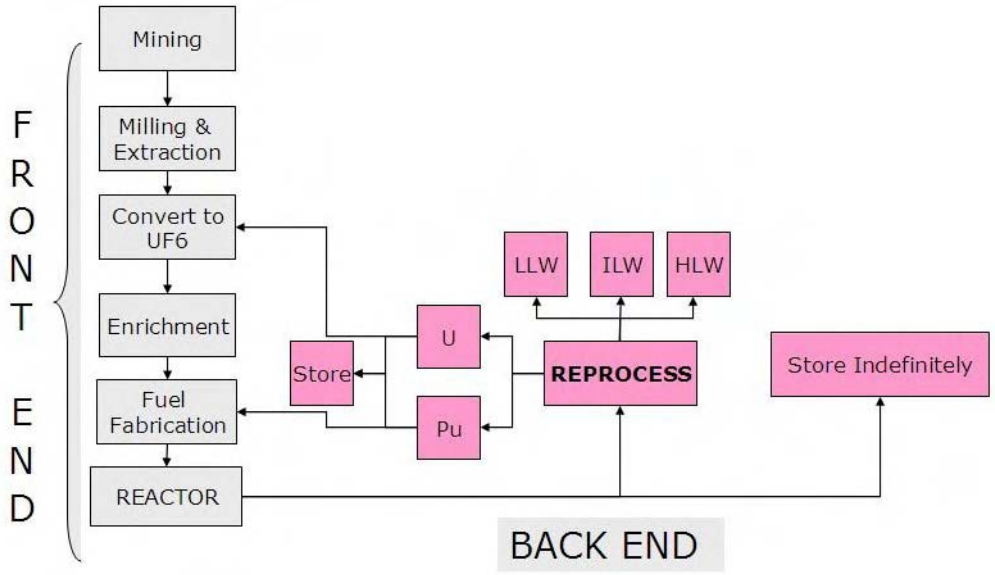

Figure 1.2: Overview of the UK Nuclear Fuel Cycle - Courtesy of A. Worrall, NNL

1.4.1 Front End Nuclear Fuel Cycle

Worrall, Barré and Wilson provide detailed descriptions of the nuclear fuel cycle in references [16], [17] and [18]. The "front end" of the fuel cycle refers to all activities prior to power generation in a nuclear reactor. Each activity takes place in a designated facility or plant. Front end activities include: mining of the raw U ore, milling of the ore and extraction of U concentrate (U_3O_8), conversion of U to UF_6, enrichment (increasing the concentration of the fissile isotope ^{235}U within the U), fabrication of the fuel and its arrangement into assemblies, and loading of the fuel in the reactor core. The composition of reactor fuel varies with reactor type, therefore enrichment of the fuel is not always a requirement; for example, Candu reactors operate using Natural U metal fuel (∼99.3% ^{238}U, 0.7% ^{235}U).

1.4.2 Pu Production in Nuclear Fuel

Nuclear fuel is exposed to a high neutron flux during irradiation in a reactor core e.g. $\sim 10^{14}$ n.cm^{-2}s^{-1} thermal flux in a Light Water Reactor (LWR). Fissile[1] ^{235}U has a high capture cross-section for thermal neutrons, resulting in the fission of ^{236}U* (thermal fission). Fertile[2] ^{238}U may also lead to fission following capture of neutrons at higher energies (fast fission). Nuclear fission results in fuel burn-up (i.e. a reduction in the proportion of fissionable isotopes in the fuel) and the production of highly radioactive (and in some cases, long-lived) fission products. The quantity of these fission products in spent fuel is therefore related to fuel burn-up, allowing for radioactive decay.

Neutron capture reactions occuring within the fuel that do not lead to fission can lead to the production of other isotopes - the actinides, including transuranic (TRU) isotopes - via a series of neutron capture reactions and β decays. Examples of minor actinides in spent fuel include: neptunium (^{237}Np), americium (^{241}Am) and curium (^{242}Cm). Fissile ^{239}Pu is produced following neutron capture on ^{238}U. Further neutron captures lead to the production of the transuranic (TRU) isotopes ^{240}Pu, ^{241}Pu and ^{242}Pu. However the production of ^{244}Pu is inhibited by the β decay of ^{243}Pu. The final composition of spent fuel at the time of removal from the reactor includes a high proportion of U (∼95%), some Pu (∼1%), and smaller amounts of fission products and minor actinides [16] [17].

[1] *Fissile* = Isotopes that can undergo fission following neutron capture at all neutron energies.

[2] *Fertile* = Isotopes that can capture neutrons leading to the direct production of fissile isotopes or production via daughter products.

The *isotopic composition of Pu* in a given spent fuel assembly is dependent upon the reactor type, the initial U enrichment, the irradiation period of the fuel in the reactor and the reactor operating conditions [19].

Figure 1.3 illustrates the series of neutron capture reactions and decay mechanisms that lead to the production of actinides in nuclear fuel, when exposed to a high neutron flux in a nuclear reactor core. For passive neutron NDA measurements, the region of interest of the chart of the nuclides is shown, indicating the proton (Z) and neutron (N) numbers (i.e. isotopes) of U and TRU nuclides. The red arrows in the figure indicate neutron capture reactions that lead to the production of higher N isotopes. This occurs when the neutron is captured, but the isotope does not undergo immediate fission or decay. Neutron rich isotopes are β-unstable and therefore decay via β particle emission, resulting in the conversion of a neutron to a proton. Thus the proton number of the nuclide increases by one, but its mass number is unchanged. This decay mode is indicated by black arrows on the diagram.

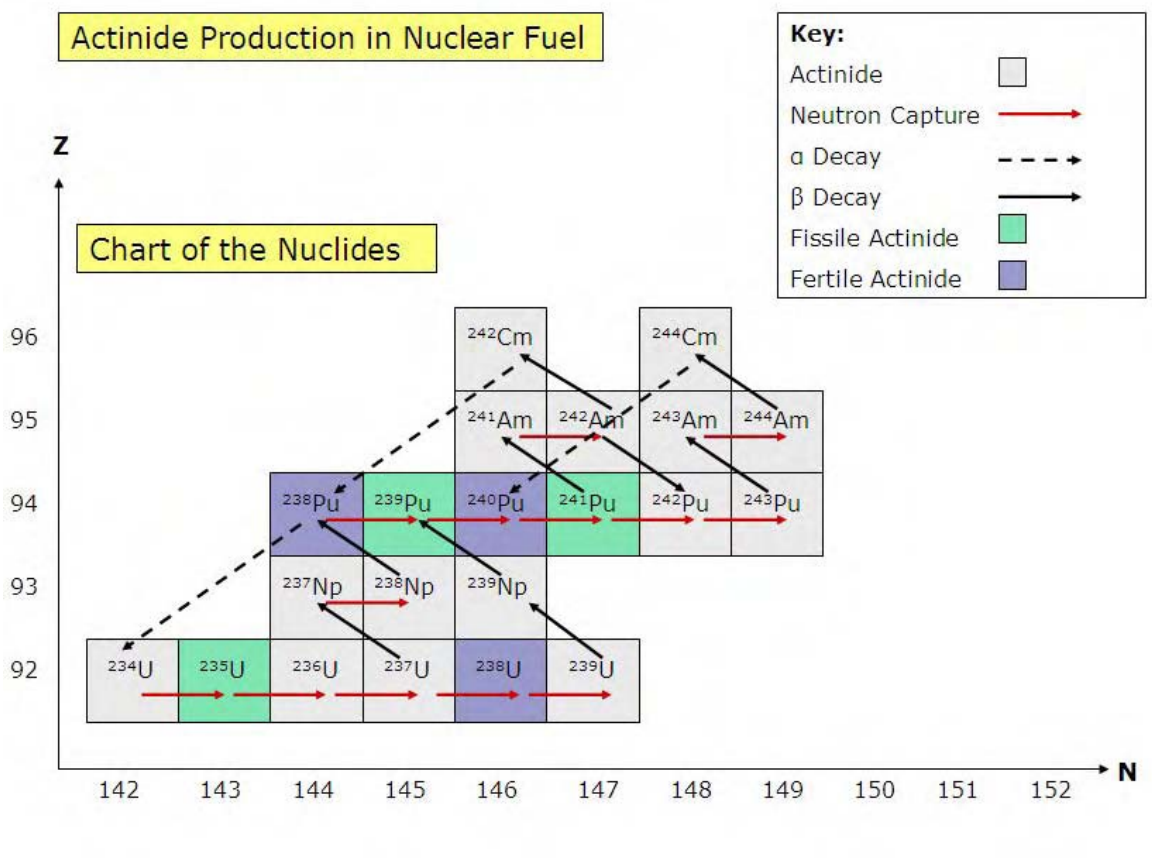

Figure 1.3: Actinide Production in Nuclear Fuel: When exposed to a neutron flux in a nuclear reactor

1.4.3 Back End Nuclear Fuel Cycle

The "back end" of the nuclear cycle refers to all activities following power generation. After de-fuelling of the reactor core, spent fuel has to be managed safely. The nuclear fuel cycle may operate as an open ("once-through") or closed cycle, based on different approaches to spent fuel management in a given country. In both cycles, spent fuel assemblies are usually stored in a water pond at the reactor site for $\sim$ 5-6 years for cooling. There are cases where an air-cooled store is used; for example, storage of Candu reactor spent fuel [16]. In an open fuel cycle, spent fuel is considered waste and continues to be stored, pending final disposal. In the closed fuel cycle approach, spent fuel is treated and reprocessed to recover U and Pu. The resulting separated Pu can be mixed with tails U as mixed oxide (MOX) fuel for recycling in a reactor [17]. Recycling has the advantage of minimising the total volume of waste going to a repository, as well as extracting the fissile material for potential subsequent re-use in reactors (Pu and reprocessed U) [16]. Since U and Pu are considered to be useful in this approach and therefore recyclable, it is only the fission products and actinides which are treated as waste and are ultimately disposed [17]. An alternative management option is spent fuel storage with provision for eventual retrieval of the fuel [16].

Although the UK manufactures MOX fuel, to date this fuel is exported as UK reactor designs do not currently utilise this fuel type. This is due to the higher cost of MOX fuel compared to UO_2 fuel, the technical modifications required to the reactors and the associated safety cases [20]. The use of MOX fuel may be a potential option for a programme of new reactor build in the UK [19]. Future fuel cycle options will be addressed in section 1.6.1 on challenges facing nuclear materials management which have a potential impact on nuclear measurement technologies.

1.5 Applications of Nuclear Measurements in the Nuclear Cycle

Nuclear fuel cycle activities lead to the production of nuclear materials and radioactive waste. The safe storage and transportation of nuclear materials is therefore a requirement throughout the fuel cycle. Nuclear measurements are an integral part of the safe management of nuclear materials at all stages of the cycle for tracking and accounting for nuclear material, thus ensuring its safe handling and storage, and avoiding clandestine use.

1.5. APPLICATIONS OF NUCLEAR MEASUREMENTS IN THE NUCLEAR CYCLE

Non-Destructive Assay provides the physical measurements which underpin safety, security and safeguards [12]:

Safety

- Criticality safety,
- Waste characterisation,
- Plant process control,
- Verification of process quality assurance (QA),
- Regulatory compliance, and
- Environmental monitoring.

Security

- Access control, and
- Homeland security (e.g. portal monitoring at borders and points of entry).

Safeguards

- IAEA safeguards inspection,
- Inventory management (e.g. verification of radioactive inventory and inventory changes),
- Nuclear materials accountancy and control,
- Surveillance and plant monitoring,
- Undeclared activities,
- Site perimeter radiation monitoring,
- Enrichment monitoring,
- Spent fuel verification, and
- Shipper-receiver differences.

1.5. APPLICATIONS OF NUCLEAR MEASUREMENTS IN THE NUCLEAR CYCLE

Figure 1.4 is an illustration of applications of nuclear measurements in the nuclear fuel cycle. The techniques of PNCC and PNMC are commonly applied to both waste characterisation and nuclear safeguards. These applications will now be described.

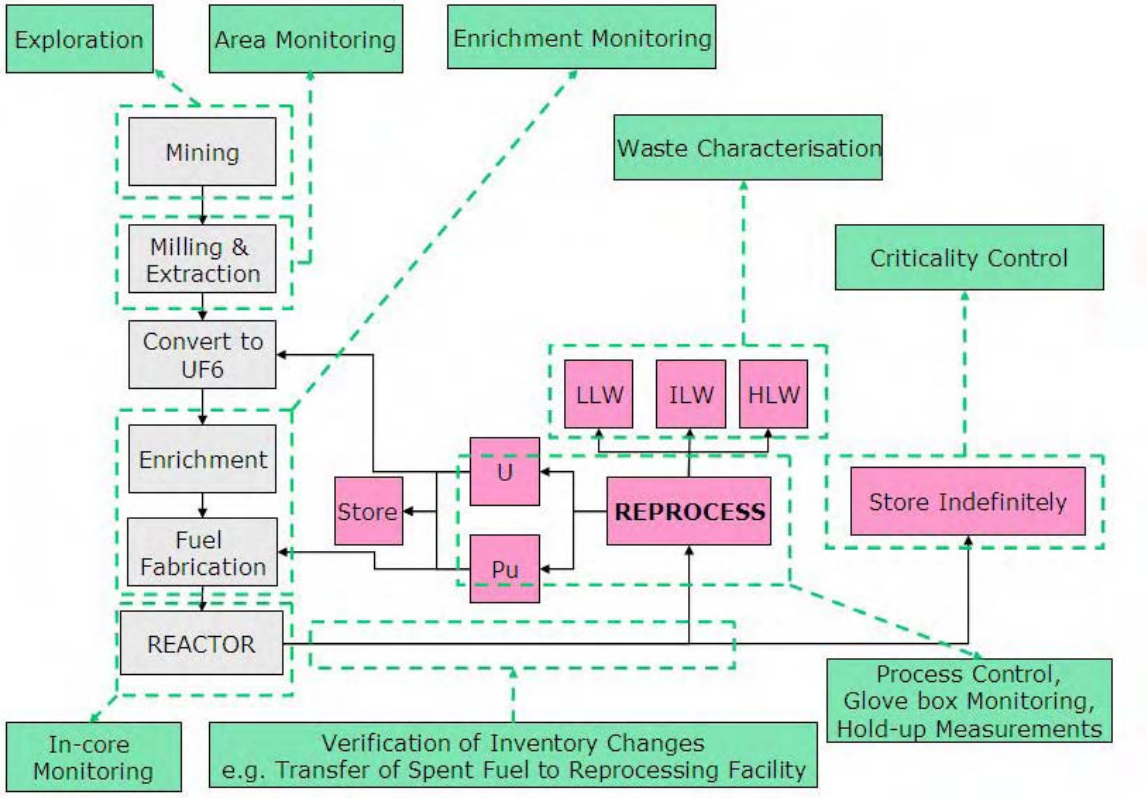

Figure 1.4: Examples of NDA Applications in the UK Nuclear Fuel Cycle

1.5.1 Radioactive Waste Characterisation

Radioactive waste is defined by the IAEA [10] as: "nuclear material in concentrations or chemical forms which do not permit economic recovery and which is designated for disposal." The main contribution to the UK's radioactive waste inventory is from the nuclear power industry. Radioactive waste arises as a result of nuclear fuel cycle activities, as previously described. Radioactive waste may also arise from the decommissioning of reactor sites and from military nuclear programmes - both weapons and propulsion. Other minor contributions to UK radioactive waste volumes arise from the use of nuclear materials in industry, medicine and research laboratories [21].

The radioactive waste classification system in the UK is based on the type and quantity of radioactivity contained within the waste form and its heat generating capacity. There are three main classifications of radioactive waste in the UK, as defined in [21]:

- High-Level Waste (HLW)
- Intermediate-Level Waste (ILW)
- Low-Level Waste (LLW)

Table 1.5.1 provides a summary of this classification system, based on information presented in the 2007 UK Radioactive Waste Inventory [21]. The table includes a description of each classification and gives examples of waste forms, together with their designated disposal route.

According to the 2007 inventory [21], Very-Low Level Waste (VLLW) is a sub-category of LLW. This includes waste containing levels of radioactivity low enough for disposal alongside non-radioactive waste in landfill sites - less than 400 kBq per m^3 of beta/gamma activity or less than 40 kBq of β/γ activity for single items.

Radioactivity limits are given in table 1.5.1 to distinguish between LLW and ILW. These limits are defined in legislation to ensure that background levels of radioactivity are not exceeded in storage or disposal sites for the purpose of environmental protection. Measurement of the total radioactivity (using NDA, DA or a combination) contained within a waste drum is used to determine whether it can be disposed of as LLW or has to be consigned to an ILW store. ILW storage is more expensive than LLW disposal due to the additional shielding requirements.

UK Radioactive Waste Classification			
Classification	Description	Examples	Disposal Route
HLW	Significant heat generation due to the high concentration of radioactivity. Heat generation has to be taken into account in the design of storage or long-term repository facilities with additional cooling and shielding.	The highly active nitric acid solution or liquor containing the waste products from spent fuel re-processing, including fission products and actinides.	No long-term disposal route currently available. Liquid HLW is conditioned (i.e. immobilised into a stable vitrified borosilicate glass) and packaged for storage at the Sellafield site, Cumbria.
ILW	No significant heat generation. Containing levels of radioactivity greater than the upper limits defined for LLW.	Metal items (mainly steel) including fuel rod cladding, reactor components and plant equipment. Graphite from moderator blocks in dismantled reactor cores (Magnox, AGR stations). Pu Contaminated Materials (PCM). Scrap metal. Sludges from the treatment of liquid waste effluents.	No disposal route currently available. ILW is packaged and stored on the site where it was produced pending final disposal in the proposed national waste repository. ILW holdings include a ILW store at Harwell and storage facilities at Sellafield.
LLW	Containing levels of radioactivity not exceeding 4 GBq/te of α or 12 GBq/te of β/γ activity.	Operational wastes including protective clothing, gloves, laboratory and site equipment used on a nuclear plant. Waste forms are mainly paper, plastics and scrap metal items. Decommissioning wastes such as contaminated soil and building rubble.	Most solid LLW is currently disposed of at the national Low Level Waste Repository (LLWR) near the village of Drigg in Cumbria.

Table 1.2: UK System of Radioactive Waste Classification

Figure 1.5: Low-Level Waste: (a) UK LLW Repository near Drigg (b) 208ℓ Drum of LLW Items (c) LLW Drum following Supercompaction into a 'Puck' for Volume Reduction

The safe and cost effective storage and ultimate disposal of radioactive waste relies on knowing the type of radionuclides present in a waste form and their quantity. Waste characterisation is therefore an essential part of effective waste management. Another part of waste management is minimising secondary waste arisings or secondary waste forms where possible [16]. As previously mentioned, NDA techniques obviate the need for physical sampling of the item therefore no residual waste forms are created. NDA therefore meets this requirement, whereas DA does not. Waste volumes should also be minimised where practicable. Figure 1.5 provides a good example: (a) shows an aerial photograph of the UK national LLW repository near Drigg [22]. Drums of LLW shown in photograph (b) [16] are supercompacted to reduce their volume before final disposal in the repository. A 208ℓ LLW drum following supercompaction is shown in photograph (c) [22].

1.5.2 Nuclear Safeguards Measurements

Nuclear materials and nuclear technology have beneficial and peaceful applications in energy (i.e. nuclear power) and medicine (i.e. nuclear imaging, nuclear medicine). However, the civilian use of nuclear technology grew rapidly from military use, but not exclusively (e.g. Radium). In 1953, Eisenhower addressed the members of the United Nations General Assembly during his *Atoms for Peace speech* [23]. Eisenhower publicly acknowledged this "dual nature" of nuclear fission and agreed to transfer nuclear reactor technology from military to civilian use. This speech paved the way for the development of an independent international body to safeguard fissile materials and therefore prevent nuclear proliferation[3]. The IAEA was thus established in 1957 [17] and still exists in this founding role today and promotes peaceful uses of nuclear technology.

The fundamental objectives of the IAEA (under the IAEA statute) are to encourage member states to be "open and transparent" regarding the use of nuclear materials in all their nuclear facilities and to declare all peaceful activities. Activities are monitored to ensure no illicit diversion of nuclear material and that any undeclared nuclear materials or clandestine activities can be detected. Nuclear measurements play a central role in this monitoring process. Results from inventory verification measurements and facility surveillance allow the IAEA to draw independent conclusions regarding nuclear fuel cycle activities in a country. This ensures that a country is compliant with peaceful use commitments via non-proliferation[4] agreements, such as the 1968 Treaty on the Non-Proliferation of Nuclear Weapons (NPT) [17].

Correlated neutron counting techniques such as PNMC are used to non-destructively determine mass values of spontaneously fissile materials for nuclear materials accountability and control. PNMC is an NDA technique employed by IAEA inspectors for materials accountability measurements, verification measurements and excess weapons materials inspections [24].

[3] *Nuclear Proliferation* = Where a greater number of countries acquire nuclear weapons. This is sometimes referred to as "Horizontal Proliferation" [17].

[4] *Non-proliferation* = Political or technical measures implemented to reduce the spread of nuclear weapons.

1.6 Technology Trends and Research Needs for Neutron NDA Systems

1.6.1 Challenges Facing Nuclear Materials Management

Several pressing challenges currently face the field of nuclear materials management. These challenges represent key drivers for further research into nuclear measurements and NDA techniques, for both waste management and safeguards, in ways which will now be described.

Global Expansion of Nuclear Power

An increase in world energy demand and growing concerns over climate change, coupled with an increasing dependence on diminishing supplies of fossil fuels, have led to the planned global expansion of nuclear power, or "nuclear renaissance". In many countries (e.g. China, Japan, France, Finland), new civilian nuclear build is underway and is being planned in others (e.g. UK). Even countries such as Sweden, that have previously had a 'phasing out' of nuclear power, are showing a renewed interest in new nuclear build.

Expansion of Nuclear Fuel Cycle Facilities and Activities

A global expansion of nuclear power leads to the growth of activities across the nuclear fuel cycle and a corresponding expansion of nuclear power plants and fuel cycle facilities. New technologies are being considered and evaluated; under many multi-national partnerships, for example, the Generation IV programme. As a result, the need for both nuclear materials safeguards and facility surveillance is increased. Safeguards measurements are also evolving: there is a greater requirement for remote monitoring, remote review and a reduction in operator intervention. Sprinkle [25] stated that safeguards measurements should incorporate advances in detection, automation and information technology. It was also noted that a new generation of safeguards technologies is needed, to adapt to new waste processes and reactor technology.

The concept of "safeguards by design" is also being considered i.e. the opportunity for new build facilities to plan and include safeguards measurements during the design phase.

Increased Security Climate

Increasing security concerns are also placing greater emphasis on nuclear safeguards. These include concerns over general acts of terrorism on nuclear plants, and theft of radioactive materials leading to the production of improvised, explosive radiation dispersal devices ("dirty bombs").

New Fuel Cycles

Potential new fuel cycles present the challenge of new materials and measurement scenarios i.e. potentially harder to assay items. Current measurement solutions need to be adapted to meet the needs of new fuel cycles (e.g. thorium cycle) and new materials. New reprocessing techniques (e.g. pyroprocessing) change the nature of the material being measured.

Resources

Resources commonly used for neutron detection in both waste and safeguards applications are becoming limited. There is currently a shortage of supply of ^{3}He and demand is increasing sharply. Other options of detector materials are being considered.

1.6.2 Technology Trends

Technology trends in NDA systems can be used to predict trends in future counter designs and thus highlight where research into NDA physics is required. Here, the need for research into deadtime correction algorithms will be discussed in the context of future counter designs, since this is the main subject of this thesis.

There are several practical motivations driving an investigation into deadtime correction factors for PNMC. Evolution of counter design features, together with an extension of the technique to a greater range of applications and the assay of more demanding items, are likely to result in the need for improved deadtime treatments.

Evolution of Neutron Counter Designs

There has been a general trend to field neutron instruments with higher efficiencies and shorter die-away times (see section 2.3.2). Figure 1.6 shows two recent neutron multiplicity counter designs: the Canberra PSMC-01 Pu Scrap Multiplicity Counter [26] and the Canberra LEMC Large Epithermal Multiplicity Counter [27].

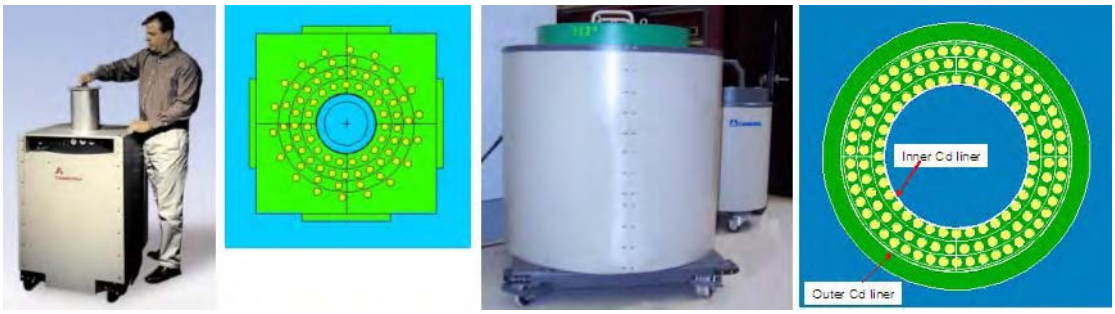

Figure 1.6: Evolution of neutron counter designs. From left: Canberra PSMC-01 Pu Scrap Multiplicity Counter; MCNP^{TM} model of the PSMC-01; Canberra LEMC Large Epithermal Multiplicity Counter; MCNP^{TM} model of the LEMC.

Table 1.3 illustrates the difference in design features between the LEMC and the PSMC-01. The LEMC has an increased number of ^{3}He gas proportional tubes and higher fill pressure than the PSMC-01, and thus higher efficiency for neutron capture. The LEMC also has a smaller die-away time than the PSMC-01.

Design Feature	PSMC-01	LEMC
Number of ^{3}He Tubes	80	126
^{3}He Partial Pressure	4 atm	10 atm
Rings	4	3
Counter Efficiency, ϵ	$> 50\%$	51%
Die-away Time, τ (μs)	50	24
Cavity Dimensions:		
Inner Diameter	200 mm	400 mm
Cavity Height	400 mm	500 mm
Outer Dimensions:		
Footprint	661 mm $\times$ 661 mm	889 mm $\times$ 889 mm
Height	992 mm	1156 mm

Table 1.3: Evolution of neutron counter design features: comparison of design features between the Canberra PSMC-01 Pu Scrap Multiplicity Counter and the Canberra LEMC Large Epithermal Multiplicity Counter.

Future generations of neutron counters and their applications will trend towards the following [1]:

- Increased neutron detection efficiencies (currently $\epsilon \sim 50\%$),
- Shorter capture time distributions and hence reduced die-away times (currently $\tau \sim 30$ - 40 μs),
- Higher sustained count rates as a result of increasing the range of masses of assay items e.g. ILW, high rate safeguards applications,
- Assay of impure items with high (α, n) rates i.e. an increased ratio, α, of (α, n) neutrons to neutrons born in spontaneous fission,
- Increased induced fission as a result of self-interrogation, and
- High self-leakage multiplication, M_L, resulting in long fission chains.

1.6.3 Research Needs

A reduced counter die-away time means that neutrons are detected over shorter timescales, requiring counter operation at shorter coincidence gate widths. For a given detection efficiency, ϵ, higher instantaneous count rates will be imposed by this reduction in gate width, potentially with a corresponding increased item count rate (high sustained rate). High instantaneous count rates mean there is an increased likelihood of detecting a large number of events in a single coincidence gate width, hence detecting higher multiplicities of events resulting in the multiplicity histogram extending to high order. Consequently, there is an increased likelihood of overlapping events or pulse pile-up and thus deadtime losses. When the instantaneous counting rate is high, the uncertainties in the applied deadtime corrections can be the accuracy limiting factor in the derived count rates. This subject will be discussed in greater detail in chapter 6.

Since the underlying physical behaviour of deadtime to date has not yet been thoroughly investigated in PNMC, there is a corresponding physics motivation to investigate the analytical forms of the deadtime correction factors themselves to improve general understanding.

1.6. TECHNOLOGY TRENDS AND RESEARCH NEEDS FOR NEUTRON NDA SYSTEMS

Koskelo [28] addressed technology trends in NDA systems and future research needs during the 2008 meeting of the Institute of Nuclear Materials Management (INMM) NDA Users Group. The following research topics were highlighted as being important for neutron NDA systems:

- Deadtime correction algorithms.
- Faster, more capable electronics e.g. Canberra JSR-14, JSR-15, list mode data acquisition (LMDA).
- ^{3}He has been the staple detector material for neutron systems, but is in short supply and hence is expensive i.e. new detector materials need to be investigated. Need for high efficiency, shorter die-away time and low deadtime.
- The cost of High Density Polyethylene (HDPE) has increased (tracks oil prices). This presents a need to develop new moderator and shield materials.
- New and improved mathematics e.g. add-a-source method, cosmic ray interference, and coincidence vetoes.
- Sourceless calibration i.e. computation.
- Combination of NDA systems and surveillance - integrated, remote, unattended.
- Networked systems for unattended and fully automated systems. This is a capability that will be required for IAEA inspections and will also reduce operator costs.
- Reporting back remotely e.g. results of IAEA safeguards inspections, or systems requiring maintenance, via the introduction of flags in software etc.
- Encryption and identification.
- Remote data analysis.
- Expert systems with automated local review, remote expert review. Reduce the need to send experts to site.

1.7 Simulation Applied to NDA Physics Research

This section discusses one aspect of meeting the NDA challenge in more detail. Simulation can be applied to a wide range of research problems in NDA physics. The principal advantage of simulation is the ability to extend the range of research problems that can be addressed which cannot be solved by empirical work alone, or have proven to be challenging practically. Simulation has several advantages (over calculational methods and, in some cases, over experimental work):

- Forward calculations - complete control over input parameters and problem definition,
- Convenient means to validate empirical correlations,
- Simulation allows full systematic study of dead-time behaviour (MSR parameters, input channels, detection geometry),
- Support developments in detector design and the design of future counters,
- Reduces the need for physical calibration standards,
- Variety of post-processing algorithms,
- List mode data available for comparison, making benchmarking practically viable,
- Newer versions of transport codes now available, not previously available, and
- Allows full range of detection geometries to be modelled and investigated. In turn this can support developments in detector design by simulating design features envisaged for the next generation of multiplicity counters. Facilitating the modelling of high efficiency systems, allowing a larger range of materials to be assayed.

Simulation is also a useful tool for detector design studies. Figure 1.7 shows an example of an MCNP^{TM} Model for a neutron counter: a Canberra PSMC-01 Pu Scrap Multiplicity Counter. This type of MCNP^{TM} model is created for each counter to optimise counter design features e.g. number of ^{3}He gas-filled proportional tubes, thickness of HDPE moderator etc. Simulation can therefore aid the development of future NDA systems.

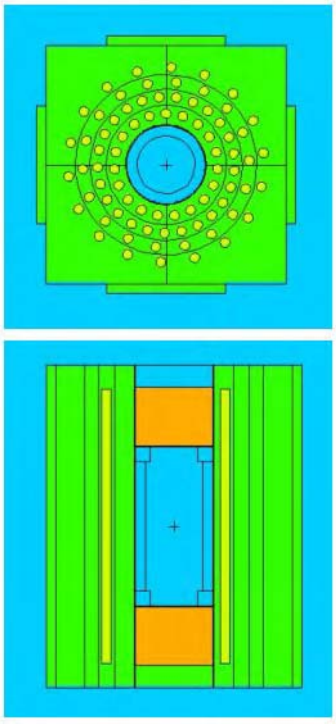

Figure 1.7: MCNP^{TM} Model of a Canberra PSMC-01 Pu Scrap Multiplicity Counter - courtesy of R.D. McElroy, Canberra Industries, Inc.

Simulation provides a convenient means to examine the range of applicability of current analytical models. The deadtime algorithms researched in this work provide a good example. Studies of this nature are made possible by the availability of nuclear data, for example, the inclusion of multiplicity distributions in MCNPX. Advances in computation and the availability of list mode data for comparison, such as the data used for the inter-comparison exercise reviewed in chapter 5, also support work in this area.

Chapter 2

THEORETICAL ASPECTS OF CORRELATED NEUTRON COUNTING

A review of theoretical aspects of temporally-correlated neutron counting is presented in this chapter, prior to an account of practical aspects in Chapter 3. Concepts of temporal correlations, neutron multiplicity, time correlation analysis, neutron pulse train analysis, multiplicity shift register (MSR) action, the analytical point model, and deadtime (both updating and non-updating) are introduced to aid understanding of later discussion.

2.1 Temporal Correlations

The detection of temporally-correlated neutrons from spontaneous fission provides a unique time signature for the non-destructive assay of spontaneously fissile nuclides. Passive neutron counting methods for waste assay and nuclear safeguards utilise ^{3}He for neutron detection. Detected neutrons are indistinguishable in energy, therefore counting methods rely on this time signature to distinguish between temporally-correlated neutrons (from both spontaneous and induced fission) emitted from assay items and single, random-in-time neutrons arising from background events (e.g. from (α, n) reactions).

Temporal correlations arise from the fact that prompt neutrons are emitted from spontaneous fission events in groups or time-correlated 'bursts'. Each 'burst' of prompt neutrons is emitted within $\sim 10^{-14}$ seconds [29] of the initial fission event. These neutrons are therefore closely correlated in time. Correlated event rates are used to quantify mass values of special nuclear materials, such as Pu. Items containing Pu lend themselves well to passive assay due to the relatively high spontaneous fission rates of the even-even isotopes: ^{238,240,242}Pu; ^{240}Pu being the dominant nuclide and the effective mass of ^{240}Pu, $m(^{240}\mathrm{Pu}_{\mathrm{eff}})$ the main assay parameter. For the NDA of spent nuclear fuel, the spontaneous fission of ^{244}Cm is the major contributor to the neutron emission.

Pu isotopes also decay via α-particle emission, therefore (α, n) reactions may occur if light elements are present in fuel cycle materials and in contact with the Pu; for example, Pu oxide (PuO_2) or fluoride (PuF_3). Other light elements such as Al, Mg and Be present as impurities also lead to high (α, n) yields [12]. These reactions provide an additional background source of single, random-in-time neutrons. Temporal correlations therefore allow neutron measurements to be conducted in the presence of high background. The contribution of background (α, n) neutrons to the detected signal can be quantified using the ratio α of (α, n)-to-(spontaneous fission, n) production rates. Typical α values range from 0 for metallic Pu up to ~ 35 for weapons grade (WG) Pu fluoride [30].

2.1.1 Item Characteristics

In most circumstances, a variety of materials are present within the assay item. The following parameters therefore need to be determined in order to fully interpret the response of neutron counters; as explained in references [30] [31]:

1. Effective mass of ^{240}Pu, $m(^{240}\mathrm{Pu}_{\mathrm{eff}})$, derived from the specific fission rates, g, of isotopes present in the assay item.

2. Multiplication, M, which includes the contribution to neutron numbers from induced fissions within the item.

3. Ratio, α, of the neutrons produced by (α,n) reactions to those produced by spontaneous fission.

4. Efficiency of counting system, ϵ, which includes the spatial variation of efficiency across the assay system and the effect of the energy of the detected neutrons. Matrix Effects (e.g. moderating, reflecting and absorbing properties) can also have an effect on the detection efficiency.

2.2 Correlated Neutron Counting

2.2.1 Techniques

Temporally-correlated neutron counting techniques include:

- Passive Neutron Coincidence Counting (PNCC), and
- Passive Neutron Multiplicity Counting (PNMC).

2.2.2 Passive Neutron Coincidence Counting (PNCC)

Standard PNCC is used to obtain two measured count rates: Totals and Reals. Total neutron events (Totals) or pairs of neutron events (Reals) are detected within a defined coincidence gate width. The Reals response is a function of all the spontaneously fissile isotopes, including the even isotopes of plutonium: ^{238}Pu, ^{240}Pu, ^{242}Pu; as well as other isotopes such as: ^{242}Cm, ^{244}Cm, ^{252}Cf, and a small contribution from ^{238}U.

Four unknown parameters need to be determined in order to fully interpret the neutron counter response (as described in section 2.1.1): $m(^{240}\mathrm{Pu}_{\mathrm{eff}})$, M, α and ϵ. It is assumed that α is known when applying PNCC to waste assay. Efficiency, ϵ can be obtained from the calibration of the assay system with known sources. By equating the two measured Totals and Reals count rates to the first two point model equations (see section 2.2.4), 2.6 and 2.7 respectively, assay results can be used to solve for two unknown parameters: M and $m(^{240}\mathrm{Pu}_{\mathrm{eff}})$ [30].

The measured response is expressed as an effective mass of ^{240}Pu, $m(^{240}\mathrm{Pu}_{\mathrm{eff}})$. This represents the mass of ^{240}Pu that would give the same coincidence response as that obtained from all the even isotopes in the assay item [12]. The effective mass of ^{240}Pu is thus given by the following [32]:

$$m(^{240}\mathrm{Pu}_{\mathrm{eff}}) = 2.52\ m(^{238}\mathrm{Pu}) + m(^{240}\mathrm{Pu}) + 1.70\ m(^{242}\mathrm{Pu}) \tag{2.1}$$

The co-efficients will vary slightly based on the energy dependence of the detectors used in the counting system [12]. A coupled measurement of the isotopic composition of the Pu is used to relate the measured $m(^{240}\mathrm{Pu}_{\mathrm{eff}})$ to the total Pu mass [33].

2.2.3 Passive Neutron Multiplicity Counting (PNMC)

Passive neutron multiplicity counting (PNMC), based on Multiplicity Shift Register (MSR) electronics (a form of time correlation analysis) is used to differentiate between coincidence events involving different numbers of neutrons [31]. Three measured count rates are obtained: Singles, Doubles, and Triples. To date the technique of PNMC has been routinely applied to the assay of Pu metal, oxide, scrap, residues, waste and Pu oxide in excess weapons materials [24].

Neutron Multiplicity Distribution

The number of prompt neutrons emitted from individual spontaneous fission events is known as the neutron multiplicity, ν [24]. This quantity may vary between zero to six or more, with the shape of the multiplicity distribution governed by the mass of the fissile nuclide and the kinematics of the fission process [29]. The average neutron multiplicity increases with the mass of the spontaneously fissile nuclide. The neutron multiplicity distribution is therefore characteristic of the nuclide. Table 2.1 provides a comparison of neutron multiplicity data for two different spontaneously fissile nuclides: ^{252}Cf and ^{240}Pu; where $P(\nu)$ is the probability of a spontaneous fission event occurring with multiplicity ν. Values in the table were taken from Ensslin, *et al* [24], based on the evaluation by Zucker and Holden [34]. The quantities $\overline{\nu_1}$, $\overline{\nu_2}$ and $\overline{\nu_3}$ are the first, second and third moments of spontaneous fission, respectively; which will be explained in the next section.

ν	P(ν) ^{252}Cf s.f.	P(ν) ^{240}Pu s.f.
0	0.002	0.066
1	0.026	0.232
2	0.127	0.329
3	0.273	0.251
4	0.304	0.102
5	0.185	0.018
6	0.066	0.002
7	0.015	
8	0.002	
$\overline{\nu_1}$	3.757	2.156
$\overline{\nu_2}$	11.962	3.825
$\overline{\nu_3}$	31.812	5.336

Table 2.1: Spontaneous Fission Multiplicity Distribution for ^{252}Cf and ^{240}Pu.

These neutron multiplicity distributions are normalised to one [24]:

$$\sum_{\nu=0}^{\nu_{max}} P(\nu) = 1 \tag{2.2}$$

Figure 2.1 provides an illustration of the neutron multiplicity distributions for AmLi (α, n) reactions, alongside both ^{240}Pu and ^{252}Cf spontaneous fission. A common neutron source used for assay system calibration is AmLi. AmLi emits single neutrons via (α, n) reactions and can therefore be regarded as having a multiplicity distribution $\nu = 1$, with 100% emission probability.

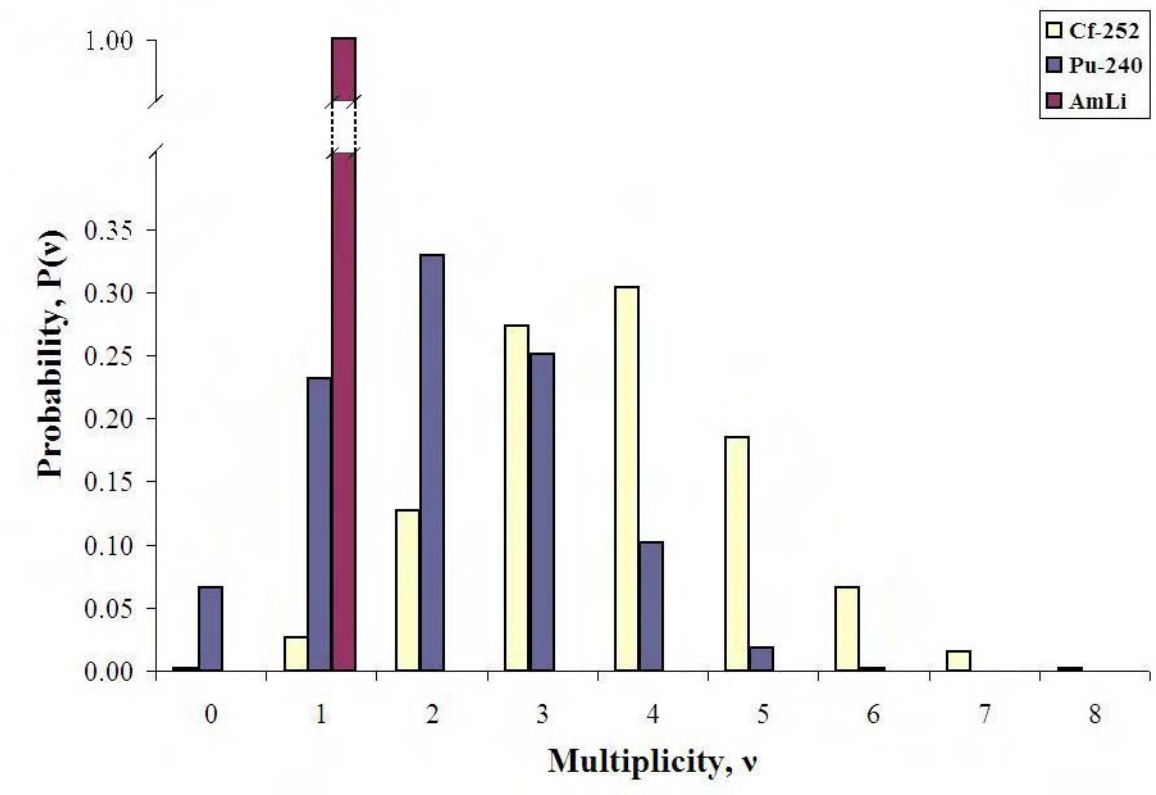

Figure 2.1: Neutron Multiplicity Distributions for AmLi, ^{240}Pu and ^{252}Cf neutron sources.

Moments of the Multiplicity Distribution

The first moment of the multiplicity distribution, $\overline{\nu_1}$, describes the average number of prompt neutrons emitted per spontaneous fission event, or mean multiplicity. The first moment is therefore given by the following expression [24]:

$$\overline{\nu_1} = \sum_{\nu=1}^{\nu_{max}} \nu \cdot P(\nu) \tag{2.3}$$

The second moment of the neutron multiplicity distribution is then given by the following expression [24]:

$$\overline{\nu_2} = \sum_{\nu=2}^{\nu_{max}} \nu \cdot (\nu - 1) \cdot P(\nu) \tag{2.4}$$

By extension, the third moment of the neutron multiplicity distribution can be calculated from the following [24]:

$$\overline{\nu_3} = \sum_{\nu=3}^{\nu_{max}} \nu \cdot (\nu - 1) \cdot (\nu - 2) \cdot P(\nu) \tag{2.5}$$

Correlated Count Rates

PNMC is used to differentiate between coincidence events involving different neutron multiplicities [31]. A multiplicity shift register (MSR), which is described in section 2.3.6, is used to count the number of times events are observed at each multiplicity to build up a multiplicity histogram. Multiplicity analysis is based on the use of factorial moments [30]: the first moment of the detected multiplicity distribution gives the total number of single neutron events recorded. The response of a PNMC counter allows both the Singles and Doubles rates to be calculated as in PNCC, and extends this analysis to Triples counting.

By equating the Singles, Doubles and Triples rates to the three point model equations, 2.6, 2.7 and 2.8 respectively, assay results can be used to solve for three unknown parameters. PNMC can be used to solve for M, α and ϵ in the case where a neutron counter is calibrated with known masses. For safeguards measurements, it is generally assumed that ϵ is known and assay results are used to solve for m($^{240}\mathrm{Pu}_{\mathrm{eff}}$), M and α [30].

In principle, the extension of PNMC to higher orders, for example; Quads (four neutron coincidence events) yields four measured count rates allowing for the solution of four unknown parameters. Temporally correlated counting techniques can then be applied to the assay of more complex items, such as the case where the α ratio is unknown [30] which may be of benefit to future fuel cycles.

Multiplicity counting also provides useful features such as the filtering out of spallation neutrons from the interaction of background cosmic ray events in counter shielding, occurring in coincident bursts greater than the number of neutrons emitted from fission.

Singles and Doubles vs. Totals and Reals

Note that PNMC Singles and Doubles rates are numerically equivalent to Totals and Reals rates obtained from PNCC. However, during an assay, Singles and Doubles rates are derived from the measured multiplicity histograms (see section 2.2.4) while the Totals and Reals rates are obtained directly from the the shift register hardware (see section 2.3.6).

2.2.4 Analytical Point Model

The results obtained from PNCC and PNMC are commonly interpreted using a model representing characteristics of the neutron source and detector, known as the Point Model by Böhnel [35]. Böhnel's Point Model equations define the Singles (equation 2.6), Doubles (equation 2.7) and Triples (equation 2.8) rates in terms of the item characteristics described in section 2.1.1. Equations 2.6, 2.7 and 2.8 are the first three factorial moments of the detected combined multiplicity distribution of both spontaneous fission and (α, n) neutrons; as discussed in detail by Ensslin, *et al.* [24].

The Singles rate, S (or Totals) is given by the following expression [35]:

$$S = m\ g\ M\ \epsilon\ \overline{\nu_{s1}}\ (1+\alpha) \tag{2.6}$$

where m is the mass of fissile material, g is the specific fission rate, M is the multiplication, ϵ is the detection efficiency, $\overline{\nu_{s1}}$ is the first moment of spontaneous fission (average number of prompt neutrons per spontaneous fission) and α is the alpha ratio. The Singles rate is the first factorial moment of the detected combined multiplicity distribution and is the sum of all the single neutrons detected; including neutrons from spontaneous fission, induced fission, and (α, n) reactions [24]. The terms in equation 2.6 therefore describe the following contributions to the Singles rate [30]:

- Single neutron events from spontaneous fission,
- Single neutron events from (α, n) reactions, and
- Single neutron events from induced fission - where the fission is induced by a neutron from a spontaneous fission or an (α, n) reaction.

The Doubles rate, D (or Reals) is given by [35]:

$$D = \frac{m\ g\ M^2\ \epsilon^2\ f_d}{2}\left\{\overline{\nu_{s2}}\ +\ \left(\frac{M-1}{\overline{\nu_{i1}}-1}\right)\ \overline{\nu_{s1}}\ \overline{\nu_{i2}}\ (1+\alpha)\right\} \tag{2.7}$$

where f_d is the Doubles gate fraction (see section 3.5.12), $\overline{\nu_{s2}}$ is the second moment of spontaneous fission, $\overline{\nu_{i1}}$ is the first moment of induced fission and $\overline{\nu_{i2}}$ is the second moment of induced fission.

The terms in equation 2.7 describe the following contributions to the Doubles coincident rate [30]:

- Spontaneous fission Doubles,
- Induced fission Doubles - induced by a spontaneous fission neutron where no other spontaneous fission neutron is detected (if it were one of two spontaneous fission neutrons emitted it would be a triple), and
- Induced fission Doubles - induced by an (α, n) neutron.

The Triples rate, T_r is given by [35]:

$$T_r = \frac{m\ g\ M^3\ \epsilon^3\ f_t}{6} \cdot \left\{ \overline{\nu_{s3}} \ + \ \left(\frac{M-1}{\overline{\nu_{i1}}-1} \right) [3\ \overline{\nu_{s2}}\ \overline{\nu_{i2}} \ + \ \overline{\nu_{s1}}\ \overline{\nu_{i3}}\ (1+\alpha)] + \ 3 \left(\frac{M-1}{\overline{\nu_{i1}}-1} \right)^2 \ \overline{\nu_{s1}}\ (1+\alpha)\ \overline{\nu_{i2}}^2 \right\} \tag{2.8}$$

where f_t is the Triples gate fraction, $\overline{\nu_{s3}}$ is the third moment of spontaneous fission and $\overline{\nu_{i3}}$ is the third moment of induced fission. The terms in equation 2.8 describe the following contributions to the Triples coincident rate [30]:

- Spontaneous fission Triples,
- Induced fission Triples - induced by a spontaneous fission neutron where no other spontaneous fission neutron is detected,
- Induced fission Double plus spontaneous fission Single,
- Induced fission Single plus spontaneous fission Double, and
- Induced fission Triples - induced by an (α, n) neutron.

Expressions 2.6, 2.7 and 2.8 for the Singles, Doubles and Triples rates can be used to solve for the mass of spontaneously fissile material, expressed as an effective mass of ^{240}Pu, $m(^{240}\mathrm{Pu}_{\mathrm{eff}})$.

2.3 Time Correlation Analysis

2.3.1 Temporally-Correlated Detection

Standard multiplicity counter designs use ^{3}He gas-filled proportional counters embedded in High Density Polyethylene (HDPE) for the detection of neutrons. Nuclear safeguards measurements are commonly conducted using cylindrical well counters with several rings of ^{3}He detectors surrounding a central cavity in which the assay item is placed (see section 3.2.1 for further detail on counter design features). Neutrons from fission are emitted essentially isotropically and are slowed in the HDPE so that the likelihood of absorption in the ^{3}He active volume is increased. The cluster of neutrons following a spontaneous fission event is slowed and migrates in the moderator. The detection is therefore spread out in time and amongst the array of ^{3}He tubes. The use of multiple rows of counters facilitates high efficiency measurements at high speed via the detection of neutrons from individual fission events. The pattern is usually chosen to minimise the spatial and energy dependence of detection and to control the timing characteristics of the counter; for example, with the use of liners such as Cd.

2.3.2 Die-Away Time

The characteristic time for a neutron, once thermalised, to undergo capture or leak from the system is known as the die-away time, τ and is characteristic of the specific detector. Note typically the die-away time is measured relative to a neutron trigger and the trigger is likely a thermal neutron. If the trigger is a fast neutron, then a thermalisation time comes into play.

2.3.3 Neutron Pulse Trains

Neutron pulse trains are the stream of digital electronic pulses representing the time-stamp of neutron captures in the detector; produced following amplification and discrimination of the analogue signal from the detector output. Neutron pulse trains are stored in the Multiplicity Shift Register (MSR) to carry out time correlation analysis by overlaying coincidence gating. The neutron pulse train from a counter contains the time-stamp of neutron captures originating from all source events: both spontaneous fission and background (α, n) reactions. Pulse trains therefore provide a complete record of an assay. Correlated event data must be extracted and accurately corrected for the effects of deadtime.

2.3.4 Rossi-Alpha Distribution

Coincidence gating is based on the detection of temporally correlated events occuring during a gate width T_g following an initial trigger from a fission event occuring at $t = 0$. The probability of detecting a neutron from the same fission event falls exponentially with time; as shown in figure 2.2. This is known as the Rossi-Alpha distribution [36]. Neutrons from the same fission event as the initial trigger event are detected in the $R+A$ (reals + accidentals) gate. The contribution from random background events is measured in a delayed gate known as the A (accidentals) gate, set far apart enough in time so as not to be related to the initial fission event.

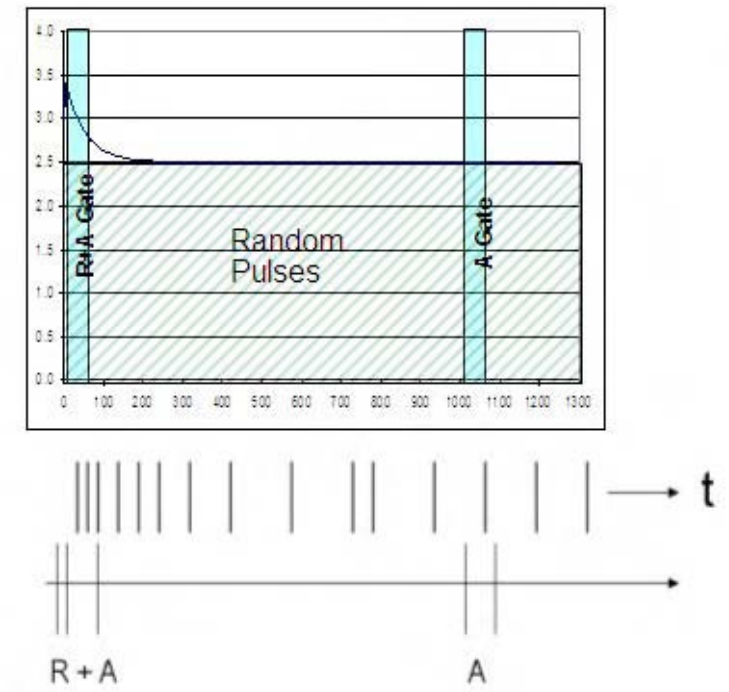

Figure 2.2: Above: Rossi-Alpha Distribution. Below: Schematic of neutron pulse train containing correlated and random-in-time events.

2.3.5 Pulse Train Analysis

A neutron pulse train contains a complete record of an assay. It is now practically viable to store this pulse train using List Mode Data Acquisition (LMDA). Neutron pulse trains provide the input to correlation analysers, such as the MSR.

2.3.6 Multiplicity Shift Register (MSR)

The Multiplicity Shift Register (MSR) provides a method of time correlation analysis. Each event in the stored pulse train acts as a trigger event and can therefore be compared to every other event in the pulse train, using forward-in-time sampling. The trigger extends a pre-delay, T_p (see section 3.5.8) followed by a $R + A$ gate, then a delayed A gate after a time interval, T_L has elapsed. For PNCC measurements, the total number of events occuring within the $R + A$ gate and A gate are calculated and are used to calculate the Reals via the difference between the counts in these two gates: $R = (R + A) - A$. For PNMC measurements, the number of events occuring within the $R + A$ gate and A gate are recorded in an accumulator and are then transferred to individual scaler totals at the time of the next trigger event. This generates a histogram of event data over the time period of the assay. Singles, Doubles and Triples are calculated by factorial moments analysis of the resulting MSR histograms; which is discussed in section 3.5.6. The action of the MSR is shown schematically in figure 2.3.

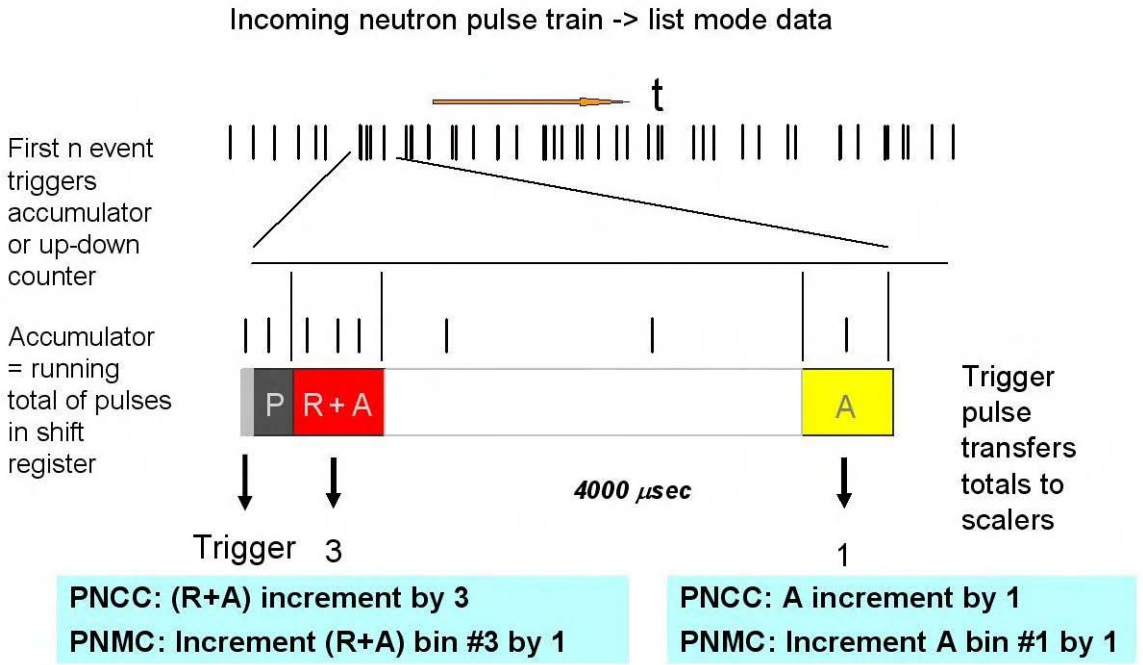

Figure 2.3: Multiplicity Shift Register Action.

2.4 Deadtime

This section provides a discussion of theoretical aspects of deadtime behaviour in PNMC systems and the basis of two familiar theoretical models of deadtime - both non-paralyzable (see section 2.4.3) and paralyzable (see section 2.4.4). Practical challenges associated with deadtime behaviour and correction for these effects are discussed in chapter 3. Deadtime is the time by which two events must be separated in order to be processed independently. Deadtime can be due to charge collection in a detector or arise as a result of pulse-processing in electronics. Events must be registered as two separate or distinguishable pulses in acquisition electronics.

2.4.1 System Deadtime Parameter, δ

Deadtime can be reasonably well characterised by an overall system parameter, δ. This includes contributions to the deadtime from the detector, amplifier, signal pile-up at the discriminator and synchronisation losses at the MSR input. Deadtime losses will be described in a practical context in section 3.4.

2.4.2 Theoretical Models of Deadtime

There are two dominant single-parameter theoretical models of deadtime, representing the two limiting cases: type I (non-paralyzable or non-updating) deadtime and type II (paralyzable, updating, extendable or cumulative) deadtime. These models were first proposed by Vincent [37].

2.4.3 Type I: Non-Paralyzable Deadtime

Type I deadtime takes the system deadtime parameter to be of fixed value, δ following every pulse that is counted. Vincent's equations describing deadtime can be found in Knoll's text [38]. Non-paralyzable deadtime can be modelled by the following equation:

$$n = \frac{m}{1 - m \cdot \delta} \tag{2.9}$$

where m is the recorded or measured count rate, n is the true interaction rate and δ is the system deadtime parameter.

2.4.4 Type II: Paralyzable Deadtime

Type II deadtime takes δ to extend from every pulse, whether counted or suppressed due to the arrival during the deadtime of the preceding pulse. For well defined passive neutron counters operated with fast electronics the major contributor to the deadtime is the action of the pulse discriminator (time above threshold) and the closest model is traditionally considered to be the paralyzable model. Paralyzable deadtime can be modelled by the following equation [38]:

$$m = n \cdot \exp(-n \cdot \delta) \tag{2.10}$$

where m is the recorded or measured count rate, n is the true interaction rate and δ is the system deadtime parameter, as before.

2.4.5 Deadtime Effects

The effect of deadtime is to perturb the neutron pulse trains and thus affect the measured count rates, thereby introducing a bias in the final assay result. Singles, Doubles and Triples count rates are increasingly affected by deadtime. The effect is complicated because the input pulse train is not random in time by definition of the assay problem. The higher orders are expected to be effected more since they correspond to the registration of a higher number of events in a time scale commensurate with the die-away time (a higher instantaneous rate).

Chapter 3

PRACTICAL ASPECTS OF CORRELATED NEUTRON COUNTING

This chapter provides an account of the characterisation of a neutron counter operated in passive multiplicity mode. It sets a practical context to the simulated parameters described in chapter 4. A neutron counter performance may be characterised by the following: high voltage (HV) plateau, (R + A)/A bias, die-away time, deadtime and efficiency at a given HV. Several operating parameters may be chosen by the user, based on these characteristics: operating voltage, pre-delay time, coincidence gate width, long-delay time, and both coincidence mode and multiplicity deadtime parameters. Careful selection of these operating parameters is needed if the 'best' neutron time correlation measurements are to be made using the counter. Operating parameters are therefore chosen based on these characterisation measurements and the physics behind this selection process is explained. Furthermore, the theoretical basis of neutron detection and origin of deadtime effects in the counter are also discussed as a precursor to a discussion of the simulation of neutron capture and deadtime behaviour in chapter 4.

3.1 Neutron Counter Characterisation

Characterisation measurements were performed by the author at the Meriden facility of Canberra Industries using an Active Well Coincidence Counter (AWCC): a Canberra JCC-51 [39]. The JCC-51 counter is a standard counter for neutron measurements with many units operating in the field, thus plenty of data exists for comparative studies and peer review. The ESARDA multiplicity benchmark exercise [4] is an example of an intercomparison study that uses list mode data taken using a JCC-51 counter as the reference case. This was used to benchmark the MSR software algorithms developed for this thesis work and is reviewed in chapter 5.

3.2 JCC-51 Counter

The Canberra JCC-51 counter [39] is based on the Los Alamos National Laboratory Active Well Coincidence Counter (AWCC) design. This instrument was first developed by Menlove in 1979 [40] for the active assay of ^{233}U and ^{235}U present in U fuel materials in field inspection applications. The current counter design is applied to the assay of bulk UO_2 samples, high-enrichment U (HEU) metals, UAl alloy scraps, light water reactor (LWR) fuel pellets and fuel materials containing ^{238}U, as detailed in the counter technical specification [39]. With the AmLi sources removed from the end plugs the AWCC also serves as a mid performance PNMC.

3.2.1 AWCC Design Features

Figure 3.1 shows a drawing of the JCC-51 counter geometry [39]. The counter uses forty-two ^{3}He proportional tubes for neutron detection. These ^{3}He tubes are arranged in two concentric rings surrounding a central assay cavity and embedded in high-density polyethylene (HDPE) to maximise detection efficiency.

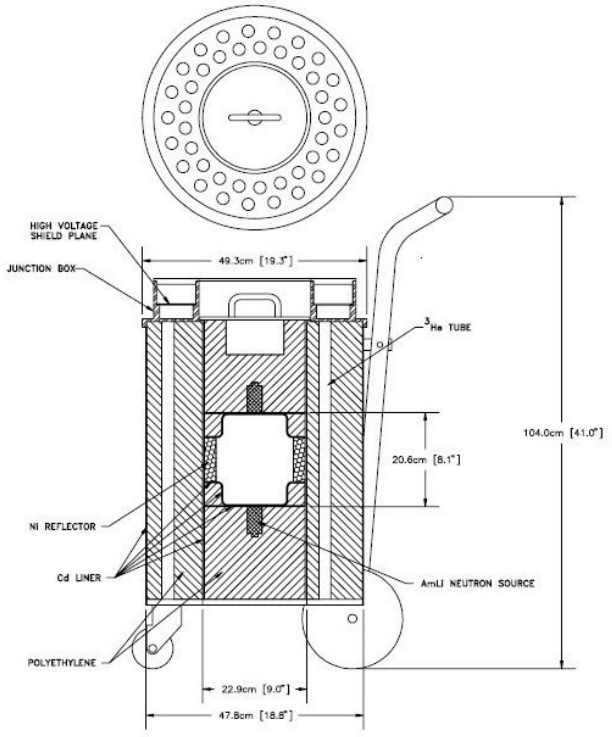

Figure 3.1: Canberra JCC 51 Active Well Coincidence Counter (Note the measurement cavity is reconfigurable; one arrangement is shown).

Neutron coincidence counters can be used in the passive mode for the assay of Pu. However, the assay of U generally requires active neutron interrogation, due to the low spontaneous fission neutron yields of the U isotopes ^{233}U and ^{235}U; as explained in chapter 1. ^{234}U and ^{238}U are always present with ^{235}U in practice and in special cases, especially for enrichments $\lesssim 18\%$ (Low Enriched Uranium or LEU), PNCC can be used. For UF_6, total neutron counting dominated by ^{234}U (α, n) induced reactions is commonplace. AmLi neutron sources are therefore present in the end plugs (both top and bottom) for conducting U assay by active neutron interrogation. Removal of these sources facilitates passive neutron counting for Pu assay [39]. The counter is designed to optimise performance; one aspect is the positioning of the AmLi sources within the polythene end plugs. This tailors the interrogation spectrum which improves the signal-to-interrogation neutron background ratio, as described by Menlove [40] in the report on the original counter design.

Figure 3.2 shows photographs of the JCC-51 counter on the test laboratory floor in the Meriden facility of Canberra Industries, taken whilst preparing for performing characterisation measurements using the counter. These measurements were performed in the passive mode without the use of an AmLi interrogation source.

Figure 3.2: Left: JCC-51 AWCC on the test laboratory floor in the Meriden facility of Canberra Industries. Right: The author is shown removing the end plug with Dr Nabil Menaa in attendance.

3.3 Neutron Detection

Calibration sources or assay items (in this case ^{252}Cf used as a surrogate for Pu, and AmLi chosen as a random source) are placed inside the central assay cavity. Neutrons from the source are emitted essentially isotropically and migrate in to the high-density polyethylene (HDPE) moderator surrounding the central cavity wall. ^{3}He gas proportional counters are embedded in the HDPE for neutron detection via the detection of charged reaction products of the ^{3}He(n, p)^{3}H reaction:

$$^{3}\mathrm{He} + \mathrm{n} \rightarrow \ ^{3}\mathrm{H} + ^{1}\mathrm{H} \tag{3.1}$$

with a reaction Q-value of 0.764 MeV. The thermal neutron (2200 ms^{-1}) cross-section for this reaction is 5330 barns. These values are quoted from the standard text by Knoll [38]. Neutrons from a given fission remain correlated in time during their lifetime in the system so that statistically a correlated signal can be extracted.

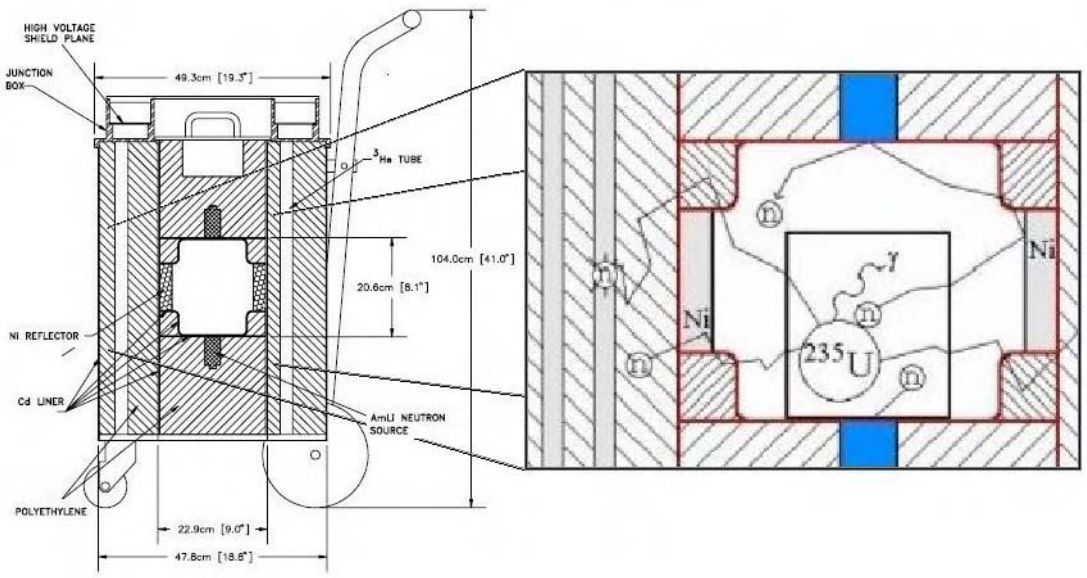

Figure 3.3: Neutron detection in the Canberra JCC-51 AWCC. Left: Drawing of the JCC-51 AWCC. Right: Schematic diagram of neutron emission from ^{235}U induced fission, migration of neutrons from the central cavity to the HDPE, neutron moderation in the HDPE, and detection in ^{3}He gas-filled proportional tubes.

Table 3.1 summarises the main parameters for the ^{3}He gas-filled proportional tubes used in the JCC-51, taken from the counter technical specification in [41].

Active length	50.8 cm
Diameter	2.54 cm
Fill Pressure	4 atm ^{3}He
Quench Gases (P-10)	Argon (Ar), Methane (CH_4)
Cladding	Aluminium (Al)
Operating High Voltage	1680 V

Table 3.1: ^{3}He Tube Parameters

The forty-two ^{3}He tubes are divided into six groups of seven, and each group is connected to one JAB-01 Amplifier/ Discriminator circuit board, to form a single detection channel, as described in the counter technical specification [39]. Three boards service each of the inner and outer rings of ^{3}He tubes. The six JAB-01 boards are mounted inside a sealed high voltage (HV) junction box at the top of the JCC-51 counter. The photograph on the left in figure 3.4 shows the HV junction box with the lid removed. The six JAB-01 boards can be observed in the photograph. The photograph on the right shows a single JAB-01 amplifier/ discriminator circuit board.

The main output signal is a TTL pulse train from all detector outputs. This pulse train provides the input to the MSR (i.e. JSR-12, JSR-14 or JSR-15 neutron multiplicity coincidence analyser). The JAB-01 is built around an Amptek-A111 integrated circuit. The logic pulse is formed when the shaped pulse crosses a fixed threshold. The gain is trimmed according to a factory calibration procedure and this results in a 1680 V operating point for these tubes.

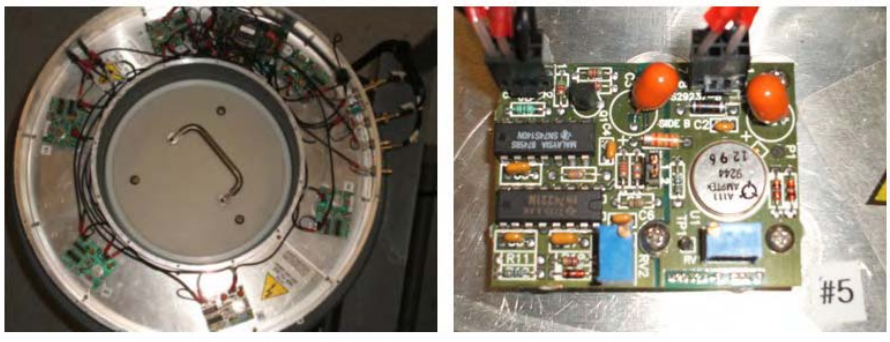

Figure 3.4: Signal Processing Electronics. Left: JCC-51 counter HV junction box with the lid removed. Right: JAB-01 amplifier/ discriminator circuit board.

3.4 Deadtime

3.4.1 Analogue signal from charge collection in the ^{3}He tubes

It is possible to observe deadtime effects from the detected analogue pulse alone. Figure 3.5 shows a range of analogue pulses from the collection of charge in the ^{3}He tubes of the JCC-51 counter. These shaped analogue pulses are the summed detector output from a single Canberra JAB-01 board, taken from test point TP1 before the discriminator.

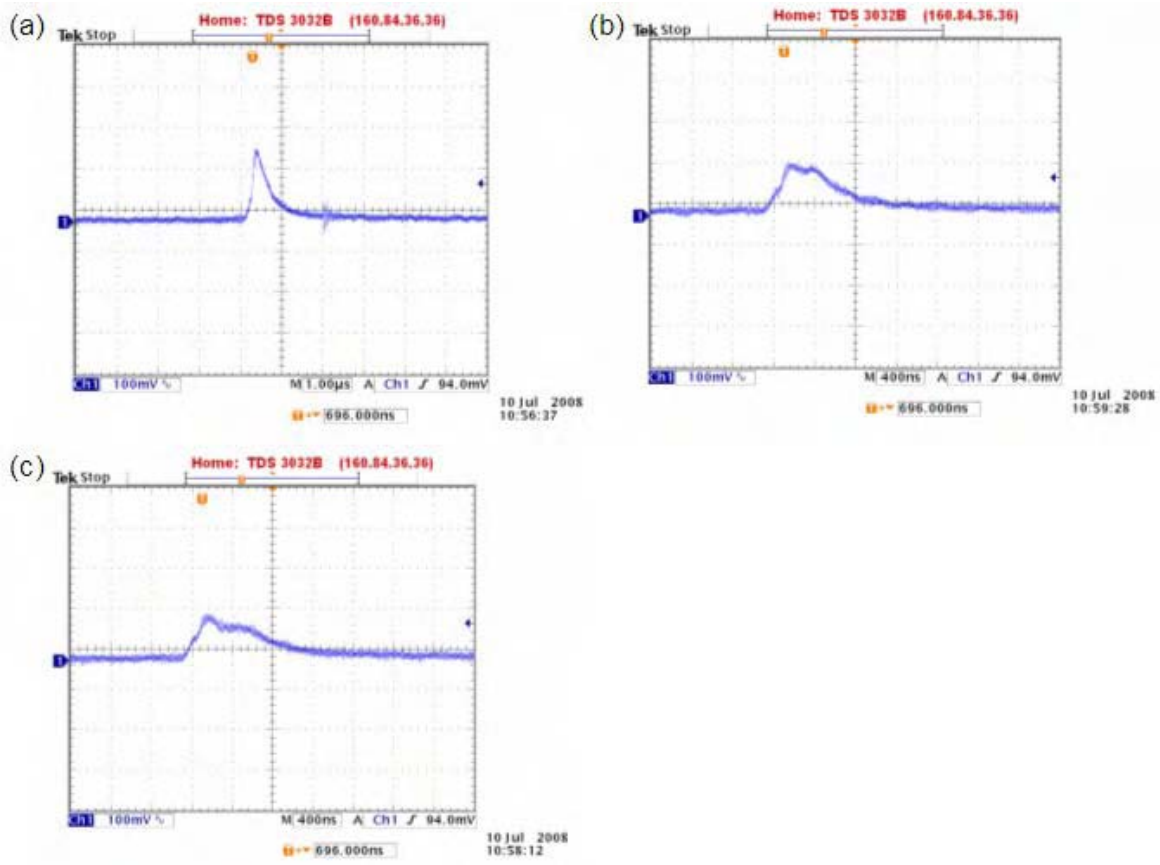

Figure 3.5: Analogue pulses from the collection of charge in the ^{3}He tubes of the JCC-51 counter; (a) single pulse; (b) suspected double pulse; (c) collection of pulses. These images were taken from the display of a digital storage oscilloscope with time base 400 ns/ division and amplitude 100 mV/ division.

Figure 3.5(a) shows a single pulse from a single charged particle event in a single detector. Figure 3.5(b) shows a suspected double pulse, possibly created from the interaction of two charged particles in the neutron counter.

Figure 3.5(c) shows a collection of pulses, created from multiple charged particle events. For pulse mode operation of the neutron counter, all pulses above a lower level threshold are registered from the detector [38]. When multiple particle events lead to a 'double pulsing' or pulse pile-up, the action of the pulse discriminator remains above threshold for longer than processing a single pulse, thus other pulses detected during this time period cannot be registered. This is the basis of the paralyzable model of deadtime. The action of the pulse discriminator is the dominant source of deadtime in a neutron counting system. Thus, the paralyzable model of deadtime is thought to be the most accurate representation of deadtime effects in the counter. In reality, deadtime is thought to be a combination of both paralyzable and non-paralyzable models as these represent the two extreme cases. The discriminator cannot re-trigger until the pulse falls below the threshold, but pulses show a large variation in shape hence their die-away time is not constant.

Since more than one detector is connected to a single JAB-01 board i.e. a single channel, a reduction in the deadtime effect could be achieved by a reduction in the detector-to-board ratio (increasing the number of detection channels).

3.4.2 Sources of Deadtime

The following list summarises the main sources of deadtime in a neutron counting system [12]:

- Detector charge collection time,
- Amplifier pulse shaping time,
- Amplifier baseline restoration time,
- Losses in the discriminator OR gate, and
- Synchronisation losses at the shift register input.

3.5 Characterisation Measurements

The following measurements were used to determine the performance characteristics of the JCC-51: HV plateau, die-away time, τ and effective deadtime parameter.

Characterisation measurements can be used to determine the basic neutron multiplicity counter operating or calibration parameters listed in table 3.2. A brief definition is given for each parameter [42]:

Basic Operating Parameters[5]	
Operating Parameter	**Description**
Operating HV	Optimal setting of the bias supply HV
Pre-delay time, T_p	Short coincidence time cut-off after each trigger event for recovery
Die-away time, τ	Time constant representing the characteristic time required to detect coincident neutrons over a given interval of the capture distribution measured by the shift register; an effective value over the fitted range
Coincidence gate width, T_g	Coincidence time window width
Coincidence mode deadtime parameters, a and b	Deadtime correction parameters for standard neutron coincidence counting
Multiplicity deadtime parameter, δ	Primary deadtime correction parameter for neutron multiplicity counting
Multiplicity deadtime parameter, c	Deadtime correction parameter for neutron multiplicity counting, applied only to Doubles rates
Multiplicity deadtime parameter, d	Deadtime correction parameter for neutron multiplicity counting, applied only to Triples rates
Efficiency, ϵ	Neutron detection efficiency for neutrons emitted in the centre of the empty assay cavity
Doubles gate fraction, f_d	Fraction of Doubles or Reals coincidence events which occur within the coincidence gate
Triples gate fraction, f_t	Fraction of Triples events which occur within the coincidence gate
Rho zero, ρ_0	Reference ratio of Reals-to-Totals neutron events for a non-multiplying metallic ^{240}Pu sample for use with the multiplication correction for neutron coincidence counting

Table 3.2: Basic operating parameters (to be determined from measurements of the JCC-51 performance characteristics) and corresponding definitions.

[5]The following operating parameters were determined based on measurements performed by the author: operating HV (see section 3.5.4), die-away time (see section 3.5.7), pre-delay (see section 3.5.8 and 3.5.9), coincidence gate width (see section 3.5.11), Doubles gate fraction (see section 3.5.12) and Triples gate fraction (see section 3.5.13).

3.5.1 Software

Data was taken using a JCC-51 AWCC and JSR-14 coincidence analyser (MSR). Analysis software included NDA2K, Assay Supervisor and Genie 2K (products of Canberra Industries).

3.5.2 ^{252}Cf Calibration Source

^{252}Cf is an important spontaneous fission source for both counter characterisation and determination of counter operational parameters, such as coincidence and multiplicity deadtime parameters. ^{252}Cf has a multiplication close to one ($M = 1$) i.e. no induced fission. ^{252}Cf can also be taken to have an alpha ratio of zero ($\alpha = 0$) because the (α, n) neutron yield is small for commercial Cf-oxides (present in calibration sources) compared to the spontaneous fission neutron yield. From work conducted by Croft [43], it is known that ^{252}Cf dilutely distributed in a pure heavy metal dioxide (UO_2) matrix generates (α, n) neutrons with a specific rate of 6.4×10^5 $ns^{-1}g^{-1}$ or equivalently 3.2×10^{-8} nBq^{-1}. The thick target yield may be scaled to other materials using the rules described by Croft and Yates [44] to show that for $^{252}Cf_2O_3$ an (α, n) neutron production of $\sim 2.6 \times 10^{-8}$ nBq^{-1} is expected. This is small compared with a spontaneous fission neutron production of ~ 0.12 nBq^{-1} in the case of ^{252}Cf.

A ^{252}Cf source was used for the JCC-51 characterisation measurements (source I.D. Cf-01-1). The calculated source activity on 1 July 2008 was 31026 ns^{-1} ($\pm$1.8%), where the uncertainty represents the $\pm 1\sigma$ value based on the certificate value and includes allowances for half-life, $T_{\frac{1}{2}}$, measurement time, and a minor correction for the presence of ^{250}Cf (13y).

3.5.3 HV Plateau

The HV plateau is characteristic of the ^{3}He proportional counters used in the JCC-51 and is the region of greatest stability for detection operation i.e. the least variation in detection efficiency for small changes in HV setting. The HV plateau region could be determined from a plot of count rate against HV. A ^{252}Cf neutron source was placed in the assay cavity and the Singles, Doubles and Triples count rates were recorded as a function of HV setting. The voltage was incremented by 20 V between 1200 V and 2200 V. Count rate data was acquired over a 30 s count time at each HV setting, using a coincidence gate width of 64 μs and a pre-delay setting of 4.5 μs, which are standard for this type of counter [39] [42]. Figure 3.6 shows the recorded data: Singles (S), Doubles (D) and Triples (T_r) count rates as a function of HV.

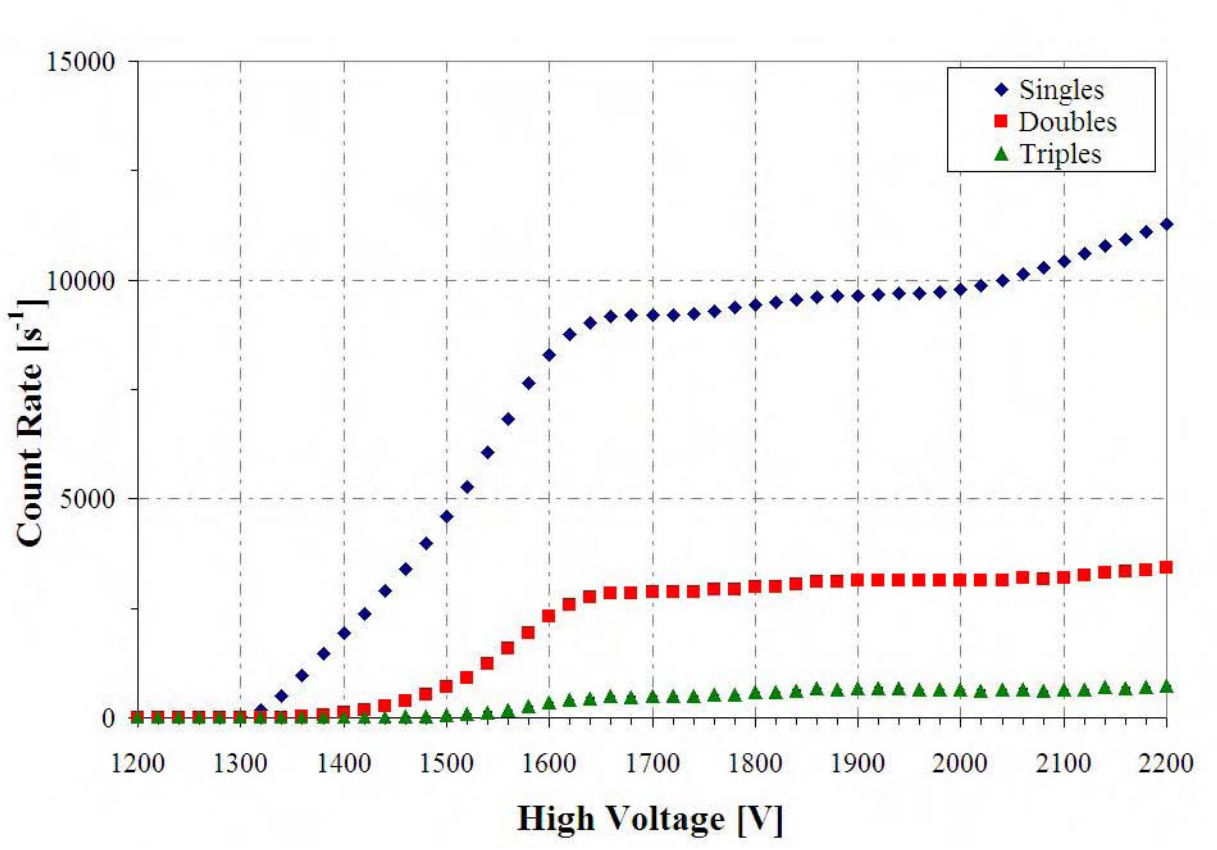

Figure 3.6: Measured HV Plateau for the JCC-51 AWCC: Measured Singles, Doubles and Triples count rates (from multiplicity analysis) vs. HV.

3.5.4 Operating HV

The optimal HV setting is determined from the measurement of this plateau region. The traditional method of determining the operating HV is to select a value ∼40V above the knee on the plot in figure 3.6. This is usually achieved visually by a technician. This places the operating voltage on the plateau and therefore in the region of greatest stability, yet also far below the γ-breakthrough. This reduces detector sensitivity to gamma radiation and also the sensitivity of efficiency to variations in HV setting [30]. The knee was measured and occurred at 1640 V. The JCC-51 operating voltage was therefore shown to be 1680 V.

Note the high voltage setting does not have direct relevance to the simulated neutron counter in chapter 4, but is included for completeness.

3.5.5 MSR Histogram Output

The MSR R + A and A histograms are output to the assay report. Figure 3.7 shows an example of this section of an assay report file.

Reals+Accidentals Histogram Total: 3.3232E+007
Accidentals Histogram Total: 3.3232E+007

Histogram Data

Bin Number	Real+Accid Counts	Real+Accid Probabilities	Accidental Counts	Accidental Probabilities
0	15089551	0.454068273306	20426598	0.614666819572
1	10436517	0.314051181078	8087685	0.243370518088
2	4919614	0.148038908839	3204293	0.096421957016
3	1888542	0.056829191744	1074081	0.032320700586
4	634142	0.019082328305	321153	0.009663973004
5	191356	0.005758202169	88329	0.002657951554
6	53558	0.001611644286	22618	0.000680609373
7	14087	0.000423899939	5596	0.000168391998
8	3491	0.000105049665	1242	0.000037373633
9	818	0.000024614903	317	0.000009539003
10	181	0.000005446574	64	0.000001925855
11	36	0.000001083297	12	0.000000361098
12	4	0.000000120366	0	0.000000361098
13	1	0.000000030092	0	0.000000361098

Figure 3.7: R + A and A Histograms from the Assay Report.

3.5.6 Calculation of Count Rates from the Multiplicity Histograms

The measured Singles, Doubles and Triples count rates, uncorrected for the effects of deadtime, can be calculated directly from the multiplicity histograms in the assay report. The measured Singles rate, S_m is the sum of all trigger events, equivalent to summation over the elements of the raw Accidentals histogram data, divided by the assay time, t given by the following equation:

$$S_m = \frac{1}{t}\sum_{i=0}^{255} A_i \tag{3.2}$$

The measured Doubles rate, D_m is given by the first factorial moment of the difference between the $R + A$ and A histograms:

$$D_m = \frac{1}{t}\sum_{i=1}^{255} i \cdot [(R+A)_i - A_i] \tag{3.3}$$

The measured Triples rate, T_{r_m} is given by the second factorial moment:

$$T_{r_m} = \frac{1}{t}\sum_{i=2}^{255} \frac{i \cdot (i-1)}{2} \cdot [(R+A)_i - A_i] - S_m \cdot D_m \cdot T_g \tag{3.4}$$

where T_g is the coincidence gate width. The assay time or experimental count time, t in each case represents the time between the first and final trigger events in the MSR.

Expressions 3.2, 3.3 and 3.4 are taken from the software algorithms detailed in the Canberra NDA2K User's Manual [45].

3.5.7 Die-Away Time

The die-away time, τ is used to characterise the temporal behaviour of the neutron counter i.e. the characteristic time required for fast neutrons to slow down in the HDPE moderator and be detected in ^{3}He for a given neutron counting system [30]. The die-away time was determined from measurements of the Reals coincidence rate as a function of coincidence gate width for a ^{252}Cf source. These measurements were performed for a fixed pre-delay setting of 4.5 μs over the following gate settings: 8, 16, 24, 32, 64 and 128 μs. Figure 3.8 shows the recorded Reals rate as a function of gate width.

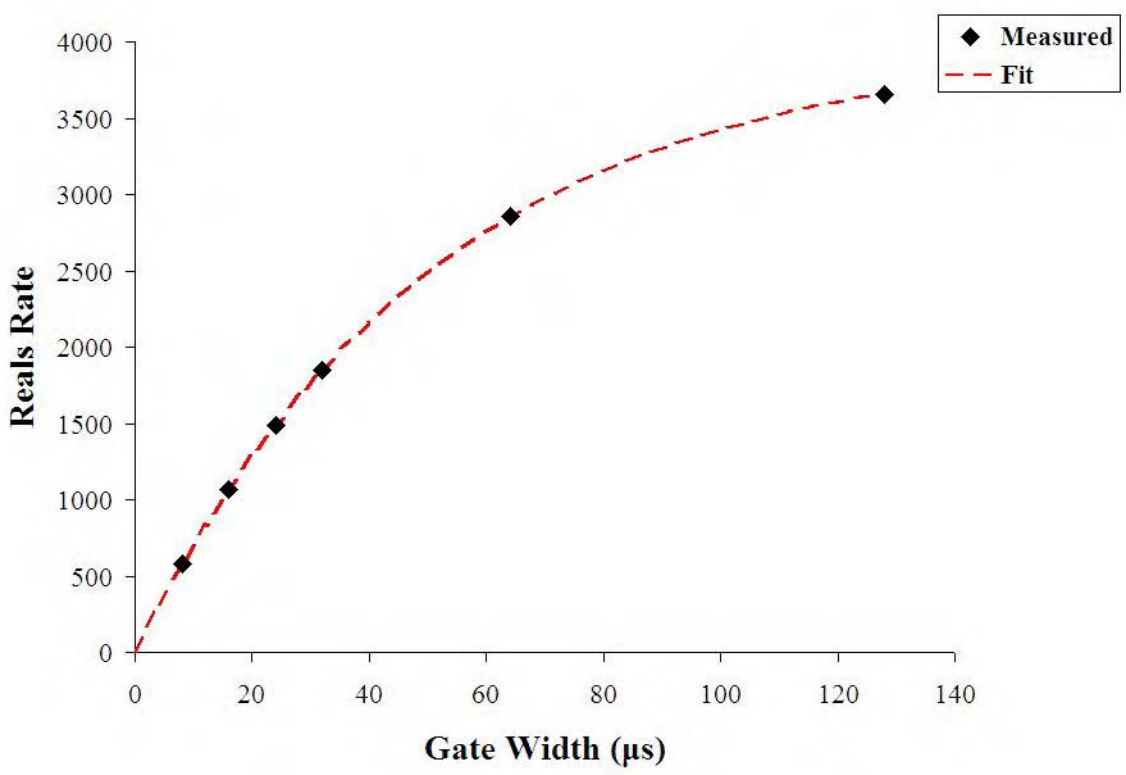

Figure 3.8: Die-away time determination for the JCC-51 AWCC using ^{252}Cf: measured Reals coincidence count rate vs. gate width.

For a given ^{252}Cf source, the Reals rate can be expressed by the following:

$$R = const \times f_d \tag{3.5}$$

where f_d is the Doubles gate fraction.

The Reals rate can be approximated by the following expression, for a near exponential chamber [30]:

$$R \approx R_0 \cdot \exp(\frac{-T_p}{\tau}) \cdot (1 - \exp(\frac{-T_g}{\tau})) \tag{3.6}$$

where R_0 is a constant. By fixing the pre-delay, the first two terms in the above expression remain constant, hence the measured Reals rate follows a saturating exponential form with increasing gate width. The measured Reals rate data as a function of gate width could therefore be fit to the following expression to determine the die-away time:

$$R(T_g) \approx const \cdot (1 - \exp(\frac{-T_g}{\tau})) \tag{3.7}$$

The die-away time for the JCC-51 was calculated by the author to be 51.31 μs $\pm$ 0.27 μs from a chi-squared, χ^2 minimisation fit of the measured data to the expected form of equation 3.7.

3.5.8 Pre-delay Setting using ^{252}Cf

During MSR pulse train analysis the coincidence gate width is not opened immediately following a start trigger pulse. Instead it is opened after a short period of time known as the pre-delay time, T_p has elapsed. The pre-delay setting can therefore be defined as the short coincidence time cut-off [42]. The function of the MSR pre-delay setting is to remove any bias in the $R + A$ and A histograms due to transient effects in the amplifier. The optimum pre-delay setting is therefore determined when the bias in the ratio of the mean Reals rate ($(R + A)$ - A) and the mean Accidentals rate (A) is a minimum. In other words, set the pre-delay to the lowest value where the bias is essentially zero:

$$(\frac{R + A}{A} - 1) \approx 0 \tag{3.8}$$

If the pre-delay setting is too small, then a bias may be introduced due to transients in the electronics following a detected event not clearing (e.g. baseline shift in the channel that fired). If the pre-delay is set too high, then real coincidences may be missed.

By analogy to equation 3.7, the Reals rate for a ^{252}Cf source as a function of pre-delay, for a fixed gate width, is given by the following expression:

$$R(T_p) \approx const \cdot \exp(\frac{-T_p}{\tau}) \tag{3.9}$$

The optimal pre-delay setting, T_p for the JCC-51 can be determined by adjusting the value of T_p until the Reals rate curve follows the form of equation 3.9. Historically at Canberra, a pre-delay setting of 4.5 μs is chosen for the JCC-51. $\tau \gg T_p$ therefore a linear behaviour is expected:

$$\exp(\frac{-T_p}{\tau}) \sim 1 - \frac{-T_p}{\tau} \tag{3.10}$$

Conventionally, T_p is not calculated but is chosen to be a small value (so Real coincidence events are not lost) but high enough for the transient to pass and the linear behaviour to be established.

3.5.9 Pre-Delay Setting using AmLi

AmLi calibration sources can be used to obtain the counter pre-delay setting, as an alternative to using ^{252}Cf. For a random neutron source, there should be no difference within sampling limits in the $R + A$ and A histograms.

3.5.10 Effect of Deadtime on Pre-delay Setting

It has been found by the author, through the simulation work detailed in chapter 4, that setting a pre-delay less than the overall system dead-time parameter also introduces an unwanted bias in the MSR histogram data. Therefore the following condition should be met when approximating the system deadtime to a single parameter, δ:

$$\mathrm{T_p} \gg \delta \tag{3.11}$$

This is not discussed in literature as the above condition is true for real experimental PNMC systems in use today, in the context of safeguards measurements. For example, high performance PNMC systems such as the Canberra PSMC-01 Pu Scrap Multiplicity Counter [26]; introduced in chapter 1 (see section 1.6.2). The PSMC-01 Counter has a deadtime parameter, δ of 46.22 ns $\pm$ 0.45 ns [42] and is operated with a pre-delay setting, T_p of 4.5 μs [42].

Ensslin, *et al.* [24] provide a survey of existing multiplicity counters in use at United States Department of Energy (DOE) facilities, which includes a list of counter deadtime parameters.

3.5.11 Gate Width Optimisation

The coincidence gate width setting, T_g determines the time window over which real coincidence events are detected. The optimal coincidence gate width setting can be determined from the same data used to calculate the die-away time, recorded over a range of gate settings using a fixed pre-delay of 4.5 μs. The gate width is chosen to minimise the uncertainty in the Reals rate i.e. to maximise the number of true coincidences measured. Figure 3.9 shows the measured relative Reals rate uncertainty as a function of coincidence gate width. From this plot, the minimum relative Reals rate uncertainty occurs at a coincidence gate width ≈ 35 μs. However, it is conventional to use a gate width setting of 64 μs for the JCC-51 counter to follow type tests on previous units.

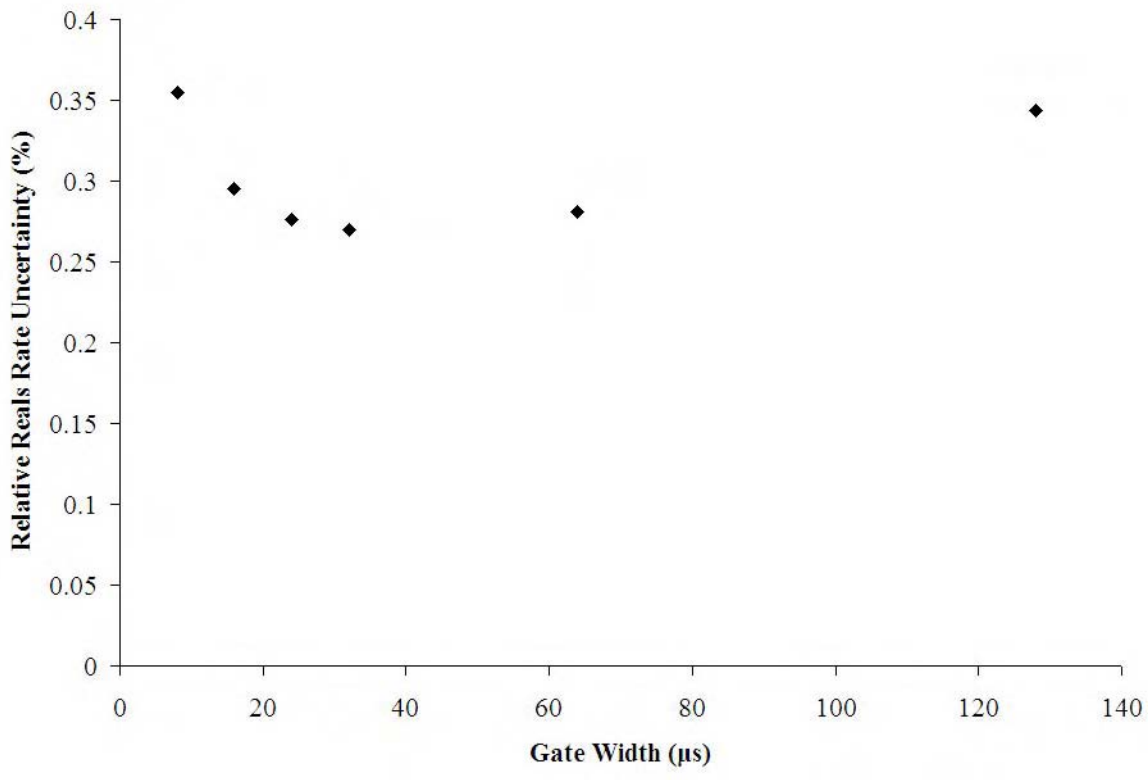

Figure 3.9: Gate width optimisation for the JCC-51 ACC: Measured relative Reals rate uncertainty (%) vs. gate width.

3.5.12 Doubles Gate Fraction

The Doubles gate fraction, f_d is defined as the fraction of Doubles or Reals coincidence events which occur within the coincidence gate [42], given by the following calculation using the counter die-away time [30]:

$$f_d = \exp\left(\frac{-T_p}{\tau}\right) \cdot \left(1 - \exp\left(\frac{-T_g}{\tau}\right)\right) \tag{3.12}$$

The Doubles gate fraction for the JCC-51 was calculated to be 0.6521 ± 0.0014 from the die-away time and MSR settings determined in sections 3.5.7, 3.5.8 and 3.5.11. In reality, the gate fraction is determined from the ^{252}Cf rates (deadtime and background corrected).

3.5.13 Triples Gate Fraction

The Triples gate fraction, f_t is defined as the fraction of Triples events which occur within the coincidence gate [42], given by the following relation [30]:

$$f_t = {f_d}^2 \tag{3.13}$$

The Triples gate fraction for the JCC-51 was calculated to be 0.425 ± 0.053 from a calculated Doubles gate fraction of 0.6521 ± 0.0014.

3.6 Deadtime Correction

The JCC-51 can be operated in both conventional coincidence counting mode and multiplicity mode. The measured count rates in each case need to be corrected for the effects of deadtime (rate-related) losses. The deadtime parameters are determined in separate ways for each mode. The method of deadtime correction for the rates obtained from conventional neutron coincidence counting (NCC) is empirical [46]. The method of deadtime correction for the rates obtained from multiplicity analysis is more complex and follows the method of Dytlewski [7], with two additional correction factors for the Doubles and Triples rates based on the method of Krick and Harker [47].

3.6.1 Conventional NCC Deadtime Correction

Traditionally, the count rates obtained from PNCC are corrected for deadtime using coincidence deadtime parameters, a and b extracted based on the expectation that the Reals-to-Totals ratio, $\frac{R}{T}$ for ^{252}Cf will be constant once corrected for deadtime. The measured Totals count rate, T_m is corrected for deadtime to obtain the true Totals rate, T_c by applying the following expression:

$$T_c = T_m \cdot \exp(\frac{a + b.T_m}{4}.T_m) \tag{3.14}$$

where a and b are empirical parameters to be determined for the system. This is the most commonly adopted approach and is referred to in a discussion by Swansen [46]: the factor 4 in the exponential is empirical. By analogy to equation 3.14, the measured Reals coincidence rate, R_m is corrected for deadtime to obtain the true Reals rate, R_c by applying the following expression:

$$R_c = R_m \cdot \exp((a + b.R_m).T_m) \tag{3.15}$$

Here, the traditional deadtime correction factors for PNCC are stated without discussion, but refer to section 6.2.

NCC Deadtime Parameters

Reals and Totals count rates were recorded from measurements of ^{252}Cf sources spanning a range of source intensities between 10^3 to 10^6 ns^{-1}. Coincidence deadtime parameter b was set equal to zero. Historically, setting $b = 0$ has been found to yield a lower χ^2 value. Coincidence deadtime parameter a was determined by performing a chi-squared, χ^2 minimisation on the Reals-to-Totals, $\frac{R}{T}$ ratios obtained from these measurements. Here, χ^2 is defined as the difference between the deadtime corrected ratios for each of the individual sources and the average value of these ratios, weighted by the uncertainty in the ratio [48].

Deadtime corrected Reals and Totals rates, R_c and T_c were calculated from measured count rates, R_m and T_m using expressions 3.15 and 3.14 while parameter a is varied.

3.6.2 Multiplicity Deadtime Correction

The count rates obtained from neutron multiplicity counting are corrected for deadtime using multiplicity deadtime parameters, δ, c and d (see table 3.2). System deadtime parameter δ is a measured parameter. Parameters c and d are treated as empirical parameters [45].

Multiplicity Deadtime Parameters

Multiplicity deadtime parameters δ, c and d are determined by chi-squared, χ^2 minimisation of the Triples-to-Doubles, $\frac{T_r}{D}$, Doubles-to-Singles, $\frac{D}{S}$ and Triples-to-Singles, $\frac{T_r}{S}$ ratios, respectively. Again, these ratios should remain constant for all ^{252}Cf measured when corrected for deadtime.

Determination of the multiplicity deadtime parameter, δ is analogous to the determination of the coincidence deadtime parameter a. Singles, Doubles and Triples count rates were recorded from measurements of ^{252}Cf sources spanning a range of source intensities between 10^3 to 10^6 ns^{-1}.

3.6.3 Summary: JCC-51 Deadtime Parameters

Table 3.3 provides a summary of the measured coincidence and multiplicity mode deadtime parameters for the JCC-51 counter; as determined by Croft, *et al* [48].

Coincidence Deadtime Parameters	
a	812 ns $\pm$4 ns
b	0
Multiplicity Deadtime Parameters	
δ	207 ns $\pm$5 ns
c	145 ns $\pm$4 ns
d	145 ns $\pm$4 ns

Table 3.3: JCC-51 deadtime parameters.

3.7 Summary: JCC-51 Operating Parameters

Table 3.4 provides a summary of the value of the basic operating parameters for the JCC-51, determined from the results of characterisation measurements.

Basic Operating Parameters and Values for the JCC-51	
Operating Parameter	**Value**
Operating HV	1680 V
Pre-delay time, T_p	4.5 μs
Die-away time, τ	51.31 μs $\pm$ 0.27 μs (for procedure adopted)
Coincidence gate width, T_g	64 μs
Coincidence mode deadtime parameters, a and b	812 ns $\pm$4 ns and 0
Multiplicity deadtime parameter, δ	207 ns $\pm$5 ns
Multiplicity deadtime parameter, c	145 ns $\pm$4 ns
Multiplicity deadtime parameter, d	145 ns $\pm$4 ns
Doubles gate fraction, f_d	0.6521 $\pm$ 0.0014
Triples gate fraction, f_t	0.425 $\pm$ 0.053

Table 3.4: Basic operating parameters and values for the JCC-51.

Chapter 4

SIMULATION OF DEADTIME BEHAVIOUR IN PNMC SYSTEMS

Chapters 2 and 3 reviewed both theoretical and practical aspects of correlated neutron counting and deadtime behaviour, together with the motivations driving an investigation into deadtime correction factors for PNMC. Here, a detailed account is given of the development of a simulation method to investigate deadtime behaviour in PNMC systems over a range of operational conditions of a multiplicity counter. The chapter will provide a full description of the pulse train generation and MSR software.

4.1 A Monte Carlo Approach to the Simulation of Deadtime Losses in PNMC

The radiation transport code MCNPX^{TM} (Monte Carlo N-Particle eXtended) [6], together with a bespoke auxiliary code developed by the author using the C++ programming language, was used to simulate ideal neutron pulse trains for a range of spontaneous fission sources and idealised detection geometry; providing an event by event record of the time distribution of neutron captures within the detection system. Stored pulse trains were then perturbed in software to apply the effects of deadtime according to the chosen physical process; for example, the ideal paralyzable (extending) and non-paralyzable deadtime models with an arbitrary dead-time parameter. The action of the MSR electronics was modelled in software to analyse these pulse trains.

This method of Monte Carlo Pulse Train Analysis (MC-PTA) was initially developed to address the first research question posed in chapter 1: *Can existing neutron pulse train analysis techniques be extended to include a full systematic study of deadtime behaviour and effects in passive neutron multiplicity counting systems?*

Note that the detection geometry is idealised in the sense that physical realisation would not be practical but it represents one extreme case with performance indicative of limiting high efficiency, ϵ and low die-away time, τ. This represents the performance expected for future generations of passive neutron multiplicity counting systems.

4.1.1 Motivation

This work has been motivated by the recent work of Croft *et al.* [1] which recognises that the current semi-empirical analytical approaches to dead-time corrections are inadequate in certain situations of practical interest; for example, the assay of bulk quantities of PuO2 fuel feed-stock and the measurement of lean impure scrap and waste materials which have both high (α, n) to spontaneous fission yields and high absolute emission rates.

The need for re-evaluation of existing dead-time corrections has prompted work to improve the empirical models. Once established, this simulation code provided a tool to facilitate a systematic investigation of dead-time behaviour and to support current and future work on the re-evaluation of deadtime correction methods for correlated neutron counting.

4.1.2 Merits of Chosen Approach

The analytical point model is presently the most common approach applied to interpret experimental MSR data. This model can be replaced by a detailed Monte Carlo simulation to create a pulse train that can be analysed in software including allowance for deadtime losses, as demonstrated in the numerical model described by Bondar [2]. The Monte Carlo simulation can take into account explicit physical characteristics which the point model does not incorporate. Table 4.1 compares point model parameters with Monte Carlo simulation.

Parameter	Point Model	Monte Carlo Simulation
Detection Efficiency	ϵ	$\epsilon(\underline{r}, E)$
Multiplication	M	$M(\underline{r}, E)$
Gate Factor	f	f(matrix)
Probability of Capture	$p_C = 0$	$p_C \neq 0$
Induced Fission Multiplicity	ν_{Ij}	$\nu_{Ij}(E)$

Table 4.1: Point Model vs. Monte Carlo Simulation

Simulation allows the effects of deadtime to be directly applied to ideal neutron pulse trains, according to any chosen model. Deadtime behaviour and corresponding deadtime correction factors can then be investigated for a range of sources. In addition, input parameters are fully known, including counter operational parameters and the input system deadtime parameter. This simulation approach therefore allows a full systematic study of deadtime behaviour across a range of input parameters for the MSR, including variation of the coincidence gate width and pre-delay settings. In future work, count rates may be distributed between different numbers of pre-amplifier boards i.e. detector outputs, to investigate the effect of different input channels to the MSR on the deadtime behaviour. This can be used to aid the development of future counter designs.

A software multiplicity counter has the additional advantage that list mode data can be saved so that post-processing of the data can be carried out using many different algorithms.

4.2 Simulation Method Overview

Simulation took place over the following stages:

(1) Neutron pulse train generation

- Modelling neutron captures in MCNPX

- Processing the MCNPX output to generate pulse trains in software

(2) **Simulation of MSR action in software**

(Post-processing option not available in MCNPX)

4.3 Neutron Pulse Train Generation

Neutron pulse trains are the stream of digital electronic pulses representing the time-stamp of neutron captures in the detector; as described in section 2.3.3. Neutron capture may be simulated and used to generate ideal neutron pulse trains in software. Neutron pulse train generation took place over two stages: in the first stage, the radiation transport code MCNPX was used to model neutron captures from a spontaneous fission source in a large ^{3}He detector. A list of neutron capture times for individual neutrons from spontaneous fission events were output to a file known as the MCNPX PTRAC file. The second stage involved processing this output file in software to generate an ideal neutron pulse train, akin to a list mode data file from an actual multiplicity counter. The effect of deadtime could then be overlaid on the pulse train at this stage.

The method of neutron pulse train generation described in detail here is based in essence on a previous approach by Swinhoe, *et al.* [3]. To date, no attempt has been made to carry out a full systematic investigation of deadtime behaviour. In this work, ideal neutron pulse trains are subjected to a range of deadtimes and two deadtime models. This enabled the creation of a tool for the systematic study of deadtime behaviour and hence study of deadtime correction factors for a range of neutron sources.

4.3.1 Modelling Neutron Capture in MCNPX

^{3}He Detector Model

A large ^{3}He neutron detector with 4π geometric coverage was modelled. This detection geometry was chosen to enable generation of ideal neutron pulse trains and thus allow direct comparison of simulated data to existing theory once the effects of deadtime had been applied. Detector parameters were then chosen to maximise detection efficiency and shorten the capture time distribution in order to mimic the expected behaviour of future extreme counter designs. The detector was modelled with a large radius of 1000 m so that the detector could be considered to be self-moderating and hence ensure that the maximum number of neutron interactions led to neutron capture in the ^{3}He. This resulted in a high efficiency, $\epsilon \sim 99.4$ %. As a result, it was not necessary to model a polythene moderator. The density of the fill gas was chosen to be 1.65 kgm^{-3}. This density corresponds to a relatively high pressure of 13.5 atm at 300 K for the detector volume, resulting in a short dieaway time of ~ 3.4 μs.

There are no structural materials and no hydrogen (CH_2) and hence no losses to capture in these materials. The system is self-moderating and since ^{3}He is light, moderation is a reasonably fast process. This, combined with the rapid dieaway time and the high efficiency, allows operation at short gates which translates into high rate applications and the best chance to separate fission events from random events. In many respects this detector represents the ultimate ^{3}He based detection system [49].

^{252}Cf Spontaneous Fission Source Model

A point like ^{252}Cf spontaneous fission source was modelled with small spherical volume (radius 1 mm) at an artificial density of 15,100 kgm^{-3}, and positioned at the centre of the ^{3}He detector in the MCNPX input file geometry (see Appendix F). A spherical volume distribution was defined to sample spontaneous fission neutrons uniformly throughout the source volume. Neutron energies were sampled from a Watt fission energy spectrum:

$$p(E) = C \exp(-E/a) sinh(bE)^{\frac{1}{2}} \tag{4.1}$$

with spontaneous fission parameters a and b equal to 1.175 MeV and 1.04 MeV^{-1} respectively for the nuclide ^{252}Cf. These parameters have been taken from [6]. Energy E is defined in units of MeV.

The use of the spontaneous fission source card in MCNPX enables spontaneous fission events to be sampled from the "correct" multiplicity distribution for the fissile nuclide, a capability which was unavailable in earlier versions of the MCNP code (which used ν one above and one below the mean in a proportion in order to obtain the mean but not the distribution). The ^{252}Cf spontaneous fission multiplicity distribution is given in Table 4.2. Values were taken from Ensslin, *et al* [24], based on the evaluation by Zucker and Holden [34].

ν	P(ν) ^{252}Cf s.f.
0	0.002
1	0.026
2	0.127
3	0.273
4	0.304
5	0.185
6	0.066
7	0.015
8	0.002
$\overline{\nu_1}$	3.757
$\overline{\nu_2}$	11.962
$\overline{\nu_3}$	31.812

Table 4.2: Spontaneous Fission Multiplicity Distribution for ^{252}Cf

The number of fission histories or events (or `NPS` value) was also specified in the MCNPX input file. Once spontaneous fission events were distributed in time (see section 4.3.5), this parameter could be varied in order to select the source intensity. A `NONU` card was used to "turn off" induced fissions within the source material. This meant that the resulting pulse train consisted of neutron events from spontaneous fission only, which is a good approximation for actual ^{252}Cf sources.

Figure 4.1 provides a graphical representation of the multiplicity data for ^{252}Cf presented in table 4.2.

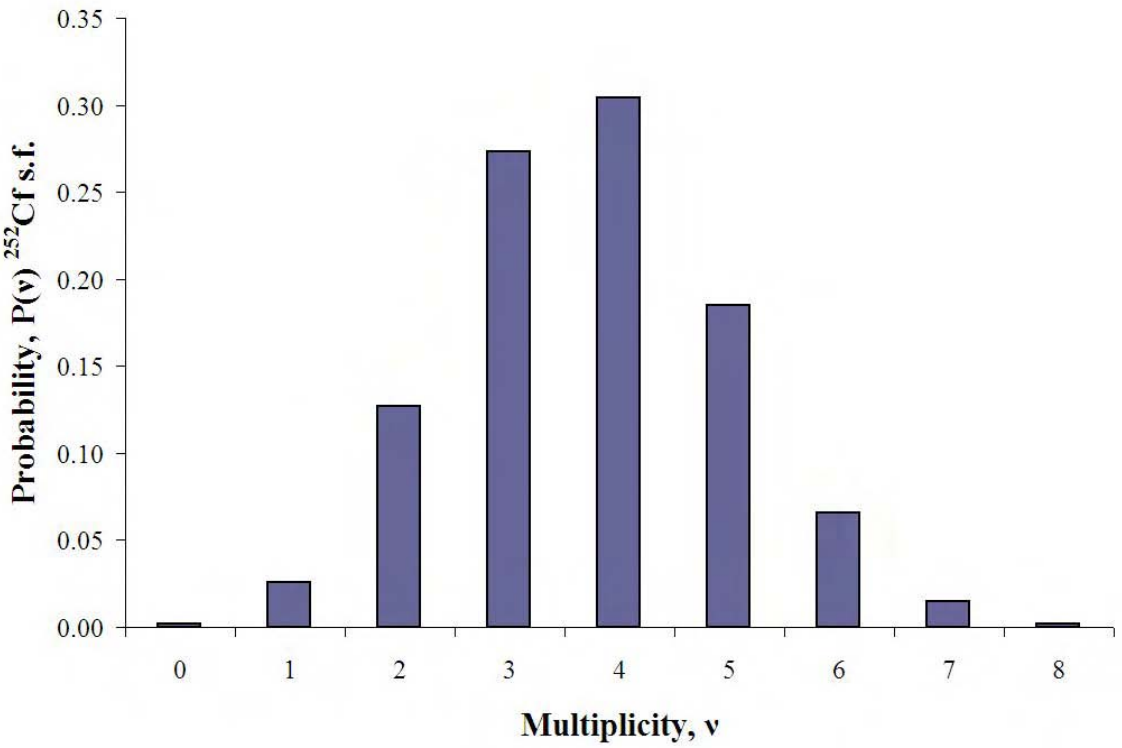

Figure 4.1: Plot of Spontaneous Fission Multiplicity Distribution for ^{252}Cf

Choice of ^{252}Cf

^{252}Cf was chosen to simplify calculations and because ^{252}Cf sources are commonly used for the calibration of PNMC systems, as detailed in section 3.5.2. ^{252}Cf has a multiplication close to one i.e. no induced fission: M = 1. ^{252}Cf can also be taken to have an alpha ratio of zero: $\alpha = 0$. Based on these properties, the Point Model equation 2.6 for the Singles rate in section 2.2.4 becomes:

$$S = mg\epsilon\overline{\nu_{s1}} \tag{4.2}$$

where m is the mass of ^{252}Cf material, g is the specific fission rate, ϵ is the detection efficiency, and $\overline{\nu_{s1}}$ is the first moment of spontaneous fission (average number of prompt neutrons per spontaneous fission). Equation 2.7 for the Doubles rate also simplifies for ^{252}Cf:

$$D = \frac{mg\epsilon^2 f_d \overline{\nu_{s2}}}{2} \tag{4.3}$$

where f_d is the Doubles gate fraction and $\overline{\nu_{s2}}$ is the second moment of spontaneous fission.

Equation 2.8 for the Triples rate also simplifies for ^{252}Cf:

$$T_r = \frac{mg\epsilon^3 f_t \overline{\nu_{s3}}}{6} \tag{4.4}$$

where f_t is the Triples gate fraction and $\overline{\nu_{s3}}$ is the third moment of spontaneous fission.

Detection Efficiency

The detection or capture efficiency of the MCNPX detector, ϵ, for neutrons from the ^{252}Cf source was $\sim 99.4\%$. This was calculated using data in the MCNPX output file.

The point model approximation is valid in this case since all neutrons captured within the ^{3}He can be considered to arise from spontaneous fission reactions in the ^{252}Cf. Contributions from break-up reactions and fission reactions (induced fissions within the source) can be assumed to be negligible compared to the source neutrons from spontaneous fission.

4.3.2 Capture Time Distribution

Coincidence Capture Tally

Neutron captures in ^{3}He were tallied using the coincidence capture tally (FT8 CAP 2003). This recorded the time in shakes (1 shake $\equiv$ 10 ns) from neutron birth at the time of the initiating spontaneous fission event (t = 0) to neutron capture in ^{3}He. This tally was specified in the data card block of the MCNPX input deck as:

```
F8:N 2
FT8 CAP 2003
```

^{3}He captures and moments are tallied in the detector which is cell number 2 in the MCNPX input file geometry (see Appendix F). Optional gating structure (i.e. pre-delay and coincidence gate width [6]) has not been chosen for this tally, since this is overlaid on the pulse train at a later stage in the analysis using the MSR software algorithms. The capture tally is written to the PTRAC file for further analysis, using the following input in the problem physics cards:

```
PTRAC EVENT=CAP FILE=ASC
```

where `FILE=ASC` generates an ASCII output file and `EVENT=CAP` writes coincident capture events to this output `PTRAC` file. `PTRAC` stands for Particle Track Output. The `PTRAC` file is one of several optional files that can be output from MCNPX to provide more detailed information on the problem physics and radiation transport, containing user-filtered particle events [6]. The use of the filter `EVENT=CAP` ensured that only neutron capture events were written to the output file. Whereas all particle events would be written to file without the use of this filter.

PTRAC File

Capture data was written to the PTRAC file for post-processing in software. Each row of the data file represents a single neutron capture event within the ^{3}He detector. The number of rows in the PTRAC file was therefore equal to the total number of neutron capture events in the ^{3}He detector (detection system).

Figure 4.2 provides an example of the first 10 fission events taken from a MCNPX PTRAC file. It can be seen that the PTRAC file comprises four columns of data. The first column lists the fission event (history) number from which the neutron originated. The second column lists the capture time in shakes (1 shake $\equiv$ 10 ns). The capture time is defined as the time from the source fission event to analog capture in ^{3}He. The third column lists the location of the neutron capture in the problem geometry (cell number) i.e. the number of the cell in which the capture occurred. This cell number is flagged with a minus sign if the neutron originated from an induced fission event. The final column lists the source particle number of a given history; for example, the first spontaneous fission history (1 in first column) emitted four spontaneous fission neutrons (4, 3, 2, 1 in fourth column).

1	1.51125E+02	2	4
1	1.89638E+02	2	3
1	2.05616E+01	2	2
1	2.23610E+02	2	1
2	4.81068E+02	2	3
2	1.61312E+01	2	2
2	8.25642E+02	2	1
3	2.79081E+02	2	4
3	2.57855E+02	2	3
3	2.25904E+02	2	2
3	3.24909E+02	2	1
4	5.68490E+01	2	6
4	2.31019E+01	2	5
4	4.92069E+01	2	4
4	2.59631E+02	2	3
4	8.18698E+02	2	2
4	4.79338E+01	2	1
5	2.24794E+01	2	2
5	8.51359E+02	2	1
6	1.12311E+03	2	4
6	4.61950E+02	2	3
6	3.43171E+02	2	2
6	2.59578E+01	2	1
7	8.79569E+01	2	4
7	5.60509E+02	2	3
7	6.37424E+02	2	2
7	2.20377E+02	2	1
8	1.64806E+02	2	3
8	1.39856E+01	2	2
8	3.96633E+02	2	1
9	1.05242E+03	2	5
9	3.90658E+02	2	4
9	1.83795E+02	2	3
9	6.74224E+00	2	2
9	1.88194E+02	2	1
10	2.46336E+02	2	5
10	1.02001E+02	2	4
10	9.90686E+02	2	3
10	7.39004E+02	2	2
10	3.63446E+01	2	1

Figure 4.2: Example of first 10 fission events from a MCNPX PTRAC File

Figure 4.3 provides an example of a single fission event, again taken from a MCNPX PTRAC file. There are four rows of data for this event, corresponding to four captured neutrons. Column one shows that all four captured neutrons originated from the spontaneous fission event history number 1. Column 2 shows that these neutron captures occurred at 151.125, 189.638, 20.562 and 223.610 shakes after the initiating fission event 1, respectively. Column three shows that all neutrons were captured in cell 2, the ^{3}He detector. The top value of column 4 indicates the total number of neutron events recorded for that history i.e. the multiplicity. Figure 4.3 is simply an extract from the data in figure 4.2.

```
1    1.51125E+02    2    4
1    1.89638E+02    2    3
1    2.05616E+01    2    2
1    2.23610E+02    2    1
```

Figure 4.3: Example of first event from a MCNPX PTRAC File

4.3.3 Auxiliary Code

A bespoke auxiliary code was developed by the author to process the PTRAC file data in order to generate the capture time distribution for the detector and the neutron pulse train. All software was written using the C++ programming language.

PTRAC File Handling: File I/O

The first step in generating the neutron capture time distribution and pulse train was to read the PTRAC file to disk for further processing. Note that early working versions of the software read the PTRAC file events into a vector in program memory in order to store these events for later analysis. This imposed a limit on the total number of events that could be allocated space in memory at any one time. The limit was $\sim 2 \times 10^7$ events. This in turn limited the length of the pulse train that could be handled and hence the precision for a given simulated experimental run.

A data structure `event` was defined containing variables `nps, time, cell` and `source` representing the four columns of the PTRAC file:

```
struct event{
   int nps;
   double time;
   int cell;
   int source;}; // data structure event
```

Contributions to `event` were determined by the data in the PTRAC file. This data structure remained the same whether modelling spontaneous fission events or (α, n) events, since the structure of the PTRAC output file remained the same.

The use of structures is standard within C++ and has not been designed specifically for this work. However storing data in this manner, not just capture times as with previous methods, enabled data on capture locations to be preserved alongside the individual capture time values. This feature was added to facilitate future work looking at pulse trains for individual detectors and the effects of summation on counting system deadtime.

Time Conversion

The time of all neutron captures in shakes were converted to nanoseconds by multiplying by the factor 10.

Capture Time Distribution

Binning the capture times recorded in the PTRAC file in software enabled the capture time distribution for the detector to be generated. 10^7 fission events were launched from the ^{252}Cf source in the idealised ^{3}He detector. A capture time histogram was generated with 250 bins of width 0.1 μs each, covering the range from 0 μs to 25 μs. Figure 4.4(a) shows the resulting capture time distribution for the idealised ^{3}He detector. Figure 4.4(b) shows the capture time distribution viewed on a semi-log scale, over a short timescale of the order of one die-away time.

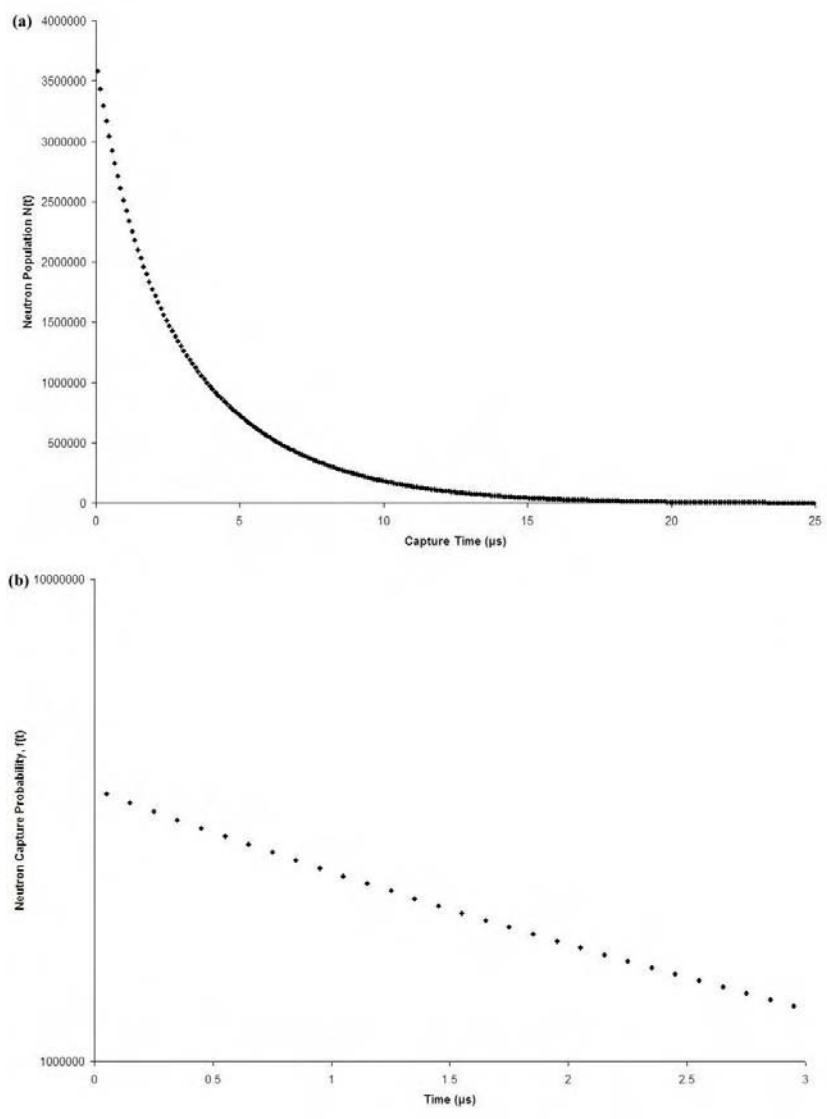

Figure 4.4: (a) Capture time distribution for an idealised ^{3}He detector modelled in MCNPX. (b) Capture time distribution viewed on a semi-log scale, over a short timescale of the order of one die-away time.

At $t = 0$, few to no capture reactions would be expected since fast neutrons must be slowed to thermal energies before the capture reaction becomes dominant. At short timescales, $t \ll \tau$, a weak fast neutron reaction rate is expected. The thermal neutron population is then expected to grow and the reaction rate to follow as it builds. This transient behaviour must happen over extremely short timescales because there is no evidence of it from figure 4.4(b) [50].

Treatment of Zero Neutron Captures

Neutron events that appear in the PTRAC file with a zero time stamp and a zero in the cell number column represent spontaneous fission neutrons that were not captured in ^{3}He. These events were therefore filtered out in software so as not to appear in the first bin of the capture time histogram.

4.3.4 Calculation of Die-Away Time

The die-away time, τ describes the characteristic time for a neutron, once thermalised, to undergo capture or leak from the detection system, as described in section 2.3.1. The die-away time for the detector modelled in MCNPX was calculated to be ~ 3.4 μs from two different fitting methods. The exact value depends on the choice of fitting range and procedure.

Method (1): Fitting the Capture Time Distribution to a Single Exponential

The die-away time was calculated to be 3.401 μs$\pm$ 0.011 μs by fitting the capture time distribution to a single exponential. Performing the fit over the whole curve includes fast neutron contributions to the ^{3}He(n, p) reaction as they are slowed.

Method (2): Fitting the Capture Time Distribution to a Double Exponential

A two component fit was performed for the die-away profile to improve upon the single exponential approximation. This was done on the basis that the early part of the curve may involve non-exponential transients, such as neutron slowing down, that will influence the extraction of the principal component of the distribution. In practical systems other weak but long lived components may be present and it is typical not to include these in a simple exponential fit. In a mathematical sense, the two die-away components can be thought of as the various terms in an expansion solution of the Boltzmann equation, representing the diffusion of neutrons in a finite sized assembly with a complex material shape [50]. The die-away profile was approximated by a double exponential with die-away times τ_1 of 3.546 μs $\pm$ 0.006 μs and τ_2 of 0.807 μs $\pm$ 0.003 μs using the method of Bourva and Croft [51].

4.3.5 Neutron Pulse Train Generation in Software

Following the generation of the capture time distribution in software, ideal neutron pulse train files were generated.

Spontaneous Fission as a Poisson Random Process

Spontaneous fission is a nuclear decay mechanism and is therefore a Poisson random process i.e. each spontaneous fission event has a constant probability of occurrence per unit time [38].

MCNPX does not distribute spontaneous fission events according to the fission rate of the source. Capture times in the PTRAC file are for neutrons starting from fission events that occurred at $t = 0$. The absolute start times of the spontaneous fission events needed to be randomly distributed in time and added to the capture times from the PTRAC file in order to generate a true Poisson pulse train.

Knoll [38] gives an equation to describe the time intervals between successive random events. The probability distribution function $p(t).dt$ that the time between successive events will be in the increment dt about t is given by:

$$p(t).dt = \lambda.exp(-\lambda.t).dt \tag{4.5}$$

where λ is the time averaged mean event rate of the Poisson random pulse train.

Time Distribution of Fission Events

Random starting times for fission events were generated and added to neutron capture times from the MCNPX PTRAC file to give the absolute times of neutron detection. This is statistically equivalent to sampling the time to the next event from a Poisson distribution.

A total experiment (or assay) time, t was defined as the time period for `NPS` fission events to occur for a mean event rate, λ. Time t was calculated separately in Microsoft Excel^{TM}, according to the desired event rate, λ using the following equation:

$$t = \frac{\texttt{NPS}}{\lambda} \tag{4.6}$$

where `NPS` is the number of simulated fission events defined in the MCNPX input file.

A number between 0 and 1 was then generated using a pseudo random number generator [52] and multiplied by the experiment time, t to give the random start time of an individual fission event. This start time was added to the time values of all captured neutrons originating from that fission event.

Time Sorting the Data

After assigning a random time to each event, based on a Poisson distribution, capture times were sorted in ascending order using a standard sort algorithm in C++. This resulted in a capture time distribution in list mode format. The output from this part of the code was an ideal neutron pulse train that could be analysed using a C++ software model of the MSR.

4.4 Simulation of MSR Action in Software

The action of the MSR electronics (as described in section 2.3.6) was modelled in software to analyse simulated pulse trains and mimic the action of hardware MSR (e.g. JSR-14, AMSR).

4.4.1 Pulse Train File Handling: File I/O

The pulse train file was read to disk for further processing. A data structure `event` was defined containing the variable `time` to represent the single column of time values in the pulse train file:

```
struct event{
   double time;}; // data structure event
```

Contributions to `event` were determined by the data in the pulse train file.

This single variable file input was used to enable two file types to be read into software:

- Pulse train files from neutron pulse train generation software
- List mode data files (as in the ESARDA exercise detailed in chapter 5) from an assay performed prior to processing in software or an on-line experiment.

Both file types will contain a single column of data listing neutron capture times.

Pulse train files were read into the MSR software in segments, in order to mimic repeated counting of an item and to generate statistical uncertainties on the mean count rates. The number of segments could be defined by the user by specifying a value for the variable `segments`. Where `int segments = 1` is defined, MSR analysis will be conducted for a single segment i.e. over the entire pulse train.

4.4.2 MSR Parameters

Table 4.3 lists the MSR parameters that were defined in software, together with the corresponding software variable name.

Parameter	Symbol	Software Variable
Coincidence gate width	T_g	`Tg`
Pre-delay	T_p	`Tp`
Long-delay	T_L	`Tl`

Table 4.3: MSR Software Parameters

T_L is typically fixed in the firmware. For the ideal case, setting the pre-delay to zero i.e. `Tp` $= 0$ and setting the coincidence gate width equal to the total experiment time, `Tg` $= t$ (i.e. $T_g \gg$ die-away, τ) ensures all event times are included in the analysis.

4.4.3 Triggering

The software uses triggering for every pulse in the train [2]. This method of triggering is known as Signal Triggered Inspection (STI). Each individual neutron capture event (originating from a fission event) acts as a trigger, defining or extending a pre-delay, T_p, reals plus accidentals (R + A) gate width, T_g, long delay, T_L and final accidentals (A) gate width, T_g.

The signal trigger (trigger pulse) itself is affected by system deadtime; for example, if the trigger falls within the deadtime of another trigger event (the preceding pulse), this trigger is lost. This influence of deadtime on the correlated rates extracted by random signal triggering or inspection (RTI) will be different. RTI is not covered in this thesis because it is not commonly used owing to the overall statistical precision being poor.

4.4.4 MSR Algorithm

The MSR algorithm acts forwards in time, hence the trigger time is compared to any events arriving after that trigger event in time and falling within the gate widths.

Gating Structure

MSR pulse train analysis was conducted using the standard algorithm for multiplicity analysis: each neutron event acted as a trigger and extended a pre-delay, Reals plus Accidentals (R + A) gate and Accidentals (A) gate following a long delay time.

Accumulator and Scaler Counters

Events falling within the gate width defined by the time of the trigger event are tallied i.e. used to increment an up-down counter or accumulator. The number of counts in the coincidence gate are therefore recorded at the time of the trigger event, providing a sample of the gate totals.

Upon the action of the next trigger event, accumulator totals are transferred to scaler counters representing the number of events per gate width. This generates a multiplicity histogram, representing the frequency of the number of events observed in the coincidence gate width. MSR histogram data is then analysed using factorial moments analysis to calculate the Singles, Doubles and Triples count rates using the method detailed in section 3.5.6.

4.5 Simulation of Deadtime Behaviour

Pulse trains could be perturbed using a single system deadtime parameter, δ to overlay the effects of deadtime according to any chosen model i.e. paralyzable and non-paralyzable deadtime models.

4.6 Simulation Method Summary

In summary, figure 4.5 provides an overview of the simulation method. This highlights the ability to vary the point model parameters ϵ, m, g, α and M. In addition, the system deadtime parameter, δ and the gating structure overlaid on the pulse train can be varied. These features of the simulation would not be possible in practical counting systems.

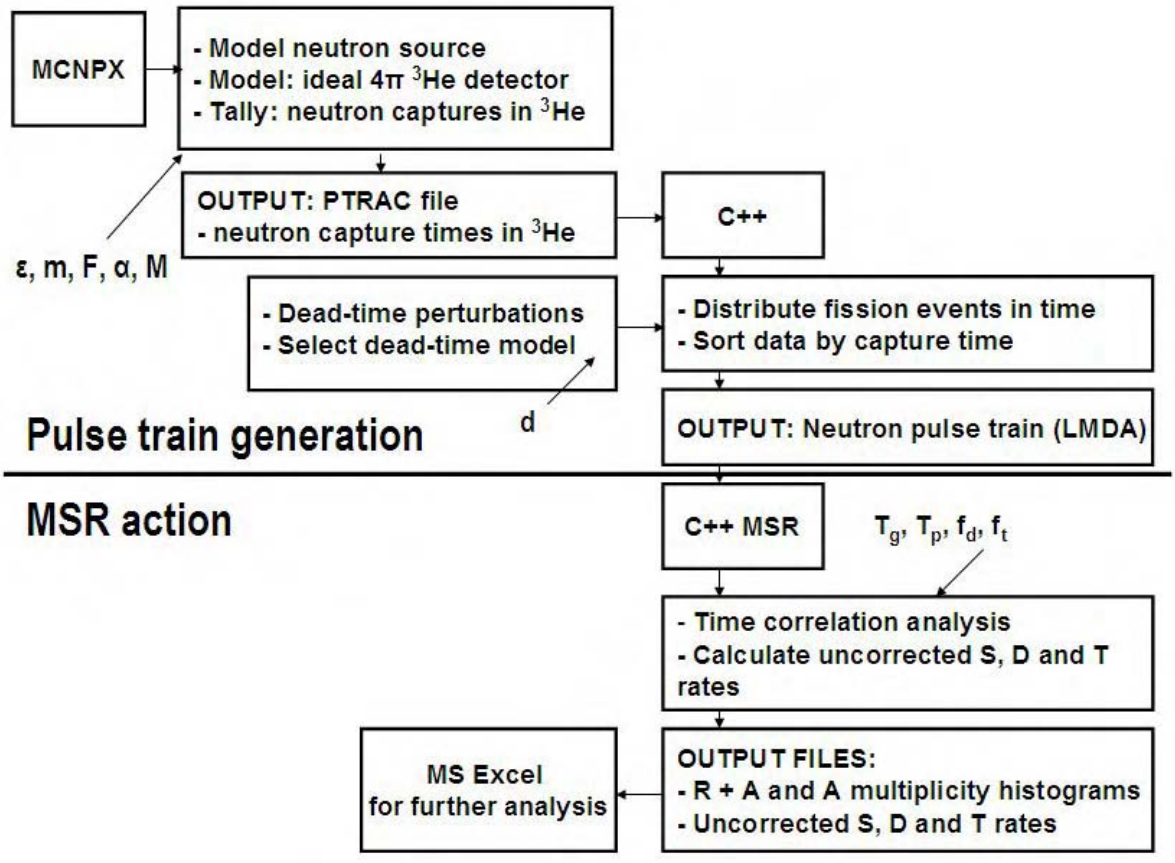

Figure 4.5: Overview of Simulation Method

Chapter 5

MULTIPLICITY INTER-COMPARISON EXERCISE

The MSR software algorithms coded for this thesis work were submitted to an international inter-comparison exercise on neutron multiplicity analysis. This chapter briefly reviews the European Safeguards Research and Development Association (ESARDA) Multiplicity Benchmark Exercise, performed by the ESARDA NDA Working Group. The author submitted simulation results for phase IV of this exercise and contributed to the statistical analysis and final report. This report is currently being reviewed and is due for publication in the ESARDA bulletin. The report is included in appendix A in the form in which it will appear in print for reference.

5.1 ESARDA NDA Working Group

The ESARDA Working Group on techniques and standards for Non-Destructive Analysis (NDA-WG) was established with the objective of providing the safeguards community with expert advice on: NDA methods, procedures on standards and reference materials, and the performance of NDA methods; as stated in [53]. As part of meeting this objective, the group determines the reliability of NDA methods where possible by inter-comparison exercises of safeguards measurements. These exercises may involve measurements by participant laboratories on a common set of samples, or inter-comparison of the codes used for data analysis [54].

5.1.1 Technical Activities

The activities of the NDA-WG are outlined in a recent report by Peerani and Weber [54]. One of the main technical areas of activity for the ESARDA NDA-WG is the modelling of NDA instruments, primarily using Monte Carlo techniques.

Three benchmark exercises have been carried out since 2003 in order to assess the capabilities of Monte Carlo modelling to reproduce experimental data. The ESARDA Multiplicity Benchmark is one such exercise, carried out to compare the different algorithms and codes used in the simulation of neutron multiplicity counters. This encourages best practice and the continuous improvement of neutron NDA measurements.

5.2 ESARDA Multiplicity Benchmark Exercise

Phase IV of the benchmark closely ties in with the themes discussed in this thesis. Thesis chapters 2 and 3 describe the pulse train obtained from neutron detection in a multiplicity counter that can be fed into a MSR for time correlation analysis. Chapter 4 describes the development of a simulation method for pulse train generation (including deadtime effects) and pulse train analysis using a software MSR. Phase IV of the benchmark involved software processing of the digital pulse trains that were obtained from LIST mode data acquisition using an Active Well Coincidence Counter (AWCC): a Canberra JCC-51 and a multi-event datation system (MEDAS) card. Neutron multiplicity measurements were performed prior to the benchmark in the PERLA laboratory at the JRC site in Ispra, Italy. Pulse trains were distributed to all participant laboratories as LIST mode data files and analysed independently in software by each participant.

Results of phase IV were used to assess the relative performance of the different algorithms used for pulse train analysis. Comparison of this kind facilitates the validation of MSR software algorithms against experimental data, with a view to investigate the replacement of hardware MSR with software for future practical applications.

5.2.1 Participants

Eleven laboratories participated in the benchmark exercise: European Commission Joint Research Centre (JRC), Los Alamos National Laboratory (LANL), Canberra Industries (University of Birmingham), Institute for Physics and Power Engineering (IPPE), Institut de Radioprotection et Surete Nucleaire (IRSN), Commissariat a l'Energie Atomique (CEA-DAM and CEA-LMN), Chalmers University, Institute of Isotopes of the Hungarian Academy of Sciences (IKI), AREVA, and the University of Michigan. There were twenty-three contributing scientists in total. A full list of participants can be found in table 4 of the ESARDA report [4] (see Appendix A).

5.3 Author's Contribution

The author participated in phase IV of the multiplicity benchmark. The MSR software developed by the author, described in chapter 4 of this thesis, was used to independently perform multiplicity analysis of the pulse trains contained in the LIST mode data files. Singles, Doubles and Triples count rates, together with their statistical uncertainties, were determined for the six source cases and submitted as the data sets labelled "Canberra" in Table 3 of the final report [4].

Once data had been collated from all participants, in a blind fashion, the author also contributed to statistical analysis of the results from phase IV. This analysis produced figures 4, 5a, 5b and 5c in the ESARDA report [4] (see appendix A) and led to contribution to the write up on the results of phase IV in section 5 of the same report [4].

5.3.1 Report for the ESARDA Bulletin

The final report on phases III and IV of the ESARDA Multiplicity Benchmark has been drafted and is due for publication in the ESARDA bulletin. The report is included in appendix A for completeness and for reference.

Chapter 6

A NEW THEORETICAL APPROACH TO DEADTIME CORRECTION FOR PNCC

Traditionally, deadtime correction factors for neutron coincidence counting (NCC) are based on the paralyzable model. Both the Singles and Doubles rate correction factors are approximated by an exponential dependence similar to those for a pure random (Poissonian) neutron source. However, the pulse trains are not random for fission sources. This chapter presents the development of alternative deadtime correction factors for the Singles and Doubles rates derived from NCC, to extend their application to correlated neutron sources. Note that NCC is a standard technique for accountancy measurements and for process hold-up determination, for example, in gloveboxes. For spent fuel assay PNMC is often not viable due to high (α, n) emission rates whereas PNCC may be. Therefore the fact that this work concentrates on Singles and Doubles (but not Triples) does not diminish the practical importance.

6.1 Motivation

As presented in chapter 3, ^{252}Cf is an important spontaneous fission source for characterisation of neutron counters and determination of calibration parameters, including both NCC and multiplicity deadtime parameters. It has been observed in work presented by the author, Evans, *et al* [55] (see appendix C) that, even at low event rates, correlated neutron counting using ^{252}Cf suffers a deadtime effect. In contrast to counting a random neutron source (e.g. AmLi to a good approximation), deadtime losses do not vanish in the low rate limit. Consequently, deadtime corrected count rates are not equivalent to true count rates. This is because neutrons are emitted from spontaneous fission events in time-correlated 'bursts', and are detected over a short period commensurate with their lifetime in the detector (characterised by the system die-away time, τ).

Even at low event rates when spontaneous fission events themselves are unlikely to overlap, neutrons within the detected 'burst' are subject to intrinsic deadtime losses since within the group there is a high instantaneous rate. Therefore, it is somewhat surprising that the deadtime loss within the group is not taken into account in deadtime correction algorithms in the leading NCC analysis software (e.g. Canberra NDA2K and Los Alamos National Laboratory (LANL) INCC).

6.1.1 Thought Experiment

The concept that deadtime losses can occur even in the limit that the Singles rate tends to zero can be illustrated by the example of a spallation neutron 'burst' of high multiplicity, $\nu \sim 50$ say. Spallation neutrons can arise as a result of a cosmic ray interaction with a high Z material such as lead (Pb) counter shielding. The next event could, for the sake of argument, occur one day later. Assuming 100% detection efficiency, this single event would result in 50 neutrons being observed in a 24 hour observation period, the assay time in this example. This can be thought of as a pulse train of maximum period 24 hours, with just a single pulse consisting of a burst of 50 neutrons.

The 50 neutrons would be detected over a time scale of the order of a few μs in a counter with short die-away time, and therefore appear as a high instantaneous rate within a short coincidence gate. Overlapping events within the burst will result in the pulse train being subject to a large deadtime effect. Since the next event occurs one day later, this scenario does not correspond to a high sustained event rate. From this illustration, there is a clear need to build the effect of correlations into the correction factors for deadtime losses, even at low ($\sim$ zero) average event rates.

Mathematical Illustration

The average (sustained) count rate for a single neutron burst of multiplicity, $\nu = 50$ in a 24 hour observation period can be calculated using the following:

$$Average\ count\ rate = \frac{50\ neutrons}{3600 \times 24s} = 5.79 \times 10^{-4} n/s \tag{6.1}$$

Within a single coincidence gate width of 4.5 μs for a counter with short die-away time, however, the instantaneous rate is calculated from:

$$Instantaneous\ count\ rate = \frac{50\ neutrons}{4.5 \times 10^{-6} s} = 1.11 \times 10^{7} n/s \tag{6.2}$$

The instantaneous count rate in this case is a factor of $\sim 10^{10}$ larger than the average count rate.

6.1.2 Deadtime Losses in Neutron Counting at Low Rates with ^{252}Cf

For ^{252}Cf the effect is less severe than in the cosmic ray thought experiment, but nevertheless in Evans, *et al* [55] (appendix C) it has been demonstrated that a deadtime effect can be observed even at low count rates. The effect was emphasised by modelling a neutron counter with high efficiency and short die-away time; representing a future counter design. This led to extending present deadtime correction formalisms in an attempt to quantify this effect. In this work, Monte Carlo simulation and subsequent numerical calculation were used to address this problem, as opposed to assuming an empirical correction factor as has been the tradition in the past.

New solutions are presented here as to how the equations for the deadtime correction factors may be modified. Empirical results from simulation, quantifying the magnitude of the effect for different deadtimes and covering a range of gate fractions, are then presented.

6.2 Traditional NCC Deadtime Correction

Traditionally, the count rates obtained from PNCC are corrected for deadtime using parameters extracted based on the expectation that the Reals-to-Totals ratio, $\frac{R}{T}$ for ^{252}Cf will be constant, as explained in section 3.6.1. For consistency with previous notation, this will herein be referred to as the Doubles-to-Singles ratio, $\frac{D}{S}$. The Reals-to-Totals ratio, $\frac{R}{T}$ and Doubles-to-Singles ratio, $\frac{D}{S}$ are numerically equivalent. However, during an assay, the Reals and Totals rates are obtained directly from the the shift register hardware while Doubles and Singles are derived from the measured multiplicity histograms.

6.2.1 Traditional NCC Deadtime Correction Factors

The traditional form of the deadtime correction factors (DTCFs) for the Singles and Doubles rates obtained from standard NCC are based on a simple paralyzable model.

Singles DTCF

The traditional deadtime correction formalism for NCC Singles counting relates the deadtime corrected Singles rate, S_c to the measured Singles count rate, S_m through the following transcendental expression:

$$S_c \approx S_m . \exp(\delta . S_c) \tag{6.3}$$

The simple paralyzable form of the Singles deadtime correction factor is therefore defined as:

$$DTCF_S \approx \frac{S_c}{S_m} \approx \exp(\delta . S_c) \tag{6.4}$$

Practically, this is normally applied as:

$$DTCF_S \approx \exp(\frac{a + b.S_m}{4} . S_m) \tag{6.5}$$

This exponential form of the deadtime correction factor is referred to in a discussion by Swansen [46]. The current form of the NCC deadtime parameter is empirical [56].

Doubles DTCF

By extension, the traditional deadtime correction formalism for NCC Doubles counting relates the deadtime corrected Doubles rate, D_c to the measured Doubles count rate, D_m through the following expression:

$$DTCF_D \approx \frac{D_c}{D_m} \approx \exp(4.\delta . S_c) \tag{6.6}$$

The factor 4 in the exponential is empirical. The theoretical basis, drawn on by [46], of the factor 4 is unknown and currently no formal discussion in literature exists. By analogy to equation 6.5, this correction factor is normally applied as:

$$DTCF_D \approx \exp((a + b.S_m) . S_m) \tag{6.7}$$

6.3 New Theoretical Approach

6.3.1 Developing an alternative formalism for the Singles DTCF

Applying equation 6.4 for the Singles DTCF is straightforward when simulated data is analysed because S_c is known. The existing expression for the Singles deadtime correction factor is dominated by the Singles rate with no treatment for correlation within the pulse train. For a correlated neutron source, however, correlated events within the fission burst itself can also lead to deadtime losses, as previously described. The deadtime correction factor for Singles should therefore include terms for correlations. Empirically it is proposed here that additional exponential terms may be added to the correction factor, to account for deadtime arising from higher order correlations. The Singles deadtime correction factor would therefore, to first order in S, D and T_r, take the following form:

$$\frac{S_c}{S_m} = DTCF_S = \exp(\delta.S_c + \text{“}s_1.D + s_2.T_r + 0\text{”}) \tag{6.8}$$

where “s_1” and “s_2” are constants to be determined. The terms enclosed in quotations relate to the correlations and have been determined by Croft [57] as described in section 6.3.2. The additional term $\exp(\text{“}s_1.D\text{”})$ is added to take into account the effect of correlations on the pulse train analysis i.e. the effect of Doubles on the Singles rate deadtime in this case. Quotations “ ” are used to emphasise that the above discussion is not quantitative, but indicates that some dependence of the kind should exist. In equation 6.9 Triples and higher terms are neglected since Triples rates are often low in practical applications due to low detection efficiency ($\epsilon \ll 100\%$) and low Triples gate fractions ($< \frac{1}{2}$):

$$DTCF_S \approx \exp(\text{“}s_1.D\text{”}).\exp(\delta.S_c).1 \tag{6.9}$$

6.3.2 Revised Singles DTCF

Croft [57] has proposed an alternative form for the Singles DTCF:

$$DTCF_S \approx [1 + \frac{(D_c/f_d)}{S_c}.\frac{\delta}{\tau_{eff}}].\exp(\delta.S_c) \tag{6.10}$$

in the limit where $\frac{\delta}{\tau_{eff}} \ll 1$ and $\frac{\delta}{\tau_{eff}}$ is roughly constant for a given system. This was inspired by the work of Matthes & Haas [58], Haas [59], Haas & Swinhoe [60], Pederson, *et al.* [61], and Srinivasan [62].

The terms in equation 6.10 are justified by the following arguments:

- The Singles deadtime correction factor should have a direct dependence on deadtime to first order and is therefore linearly related, in the multiplier, to a single system deadtime parameter, δ.

- The form of the deadtime correction factor is thought to include a direct dependence on deadtime yet be independent of gate fraction. That is the deadtime affects the pulse train and not the processing overlaid on top of it. Since deadtime effects are manifest in the pulse train itself, deadtime is thought to be independent of gate fraction[6], f_d i.e. independent of pre-delay and coincidence gate width.

- The deadtime imposed by correlated events is expected to depend on parameters related to the proportion of correlation in the pulse train (which will in turn depend on the source multiplicity distribution). The level of correlation in the pulse train can be characterised by the ratio $\frac{D}{S}$. The Doubles-to-Singles ratio, $\frac{D}{S}$ can therefore be thought of as the "volume control" on the level of correlation in the pulse train.

- The deadtime correction is inversely proportional to a single exponential dieaway, τ_{eff}. This is defined as the effective dieaway time of the detection system, when approximated to a single exponential. The ratio $\frac{1}{\tau_{eff}}$ therefore determines the timescale over which events are detected i.e. how concentrated events from an individual burst are or how close together in time.

[6]Dividing D_c by f_d eliminates the gate fraction dependence. This can be shown via the cancellation of the f_d terms in the following expression, derived from the Doubles point model equation for ^{252}Cf (equation 6.16):

$$\frac{D_c}{f_d} = \frac{mg\epsilon^2\frac{\overline{\nu_{s2}}}{2}f_d}{f_d} \tag{6.11}$$

- The 'in-burst' deadtime correction factor is independent of mass (i.e. "rate") except through multiplication, M.
- Equation 6.10 is also dimensionally correct. Dividing D by S also eliminates the rate (non-multiplying mass) dependence for a given fissioning system. Likewise $\frac{\delta}{\tau_{eff}}$ is dimensionless.

Equation 6.10 can be expressed as:

$$DTCF_S \approx K_S . \exp(\delta . S_c) \tag{6.12}$$

where K_S is defined as the vanishing (Singles) rate deadtime CF multiplier i.e. this parameter determines the deadtime in the limit where the event rate tends to zero. K_S is given by the following expression:

$$K_S \approx [1 + \frac{(D_c/f_d)}{S_c} . \frac{\delta}{\tau_{eff}}] \tag{6.13}$$

For a given system, K_S is a constant for ^{252}Cf. Values for this constant have been derived for a range of system deadtime parameters and gate fractions from empirical results presented in section 6.5. For actual Pu assays, K_S will depend on the leakage self-multiplication, M_L and random to spontaneous fission neutron production rate, α; that is on the item dependent $\frac{(D_c/f_d)}{S_c}$ value.

6.3.3 Developing an alternative formalism for the Doubles or Reals DTCF

By analogy to equation 6.12, the Doubles correction factor can be expressed as:

$$DTCF_D \approx K_D . \exp(4 . \delta . S_c) \tag{6.14}$$

where K_D is defined as the vanishing (Doubles) rate deadtime CF multiplier. Again, K_D is a modifier to the traditional NCC Doubles DTCF. Initially, the factor 4 has been retained from the original expression. K_D is also item dependent and will be discussed in more detail later in section 6.5.2.

6.4 Simulation

Deadtime correction factors have been simulated over a range of source intensities for ^{252}Cf. Simulation provides a means to:

- **Investigate the functional form** of the revised Singles and Doubles DTCFs for PNCC.
- **Evaluate performance** of revised DTCFs, relative to traditional NCC DTCFs.

Simulated measured Singles and Doubles rates were recorded at a range of values of system deadtime parameter (for a constant gate fraction) and range of gate fractions (for a constant system deadtime parameter). By this method, the proposed alternative formalisms for the Singles and Doubles DTCFs, given by equations 6.12 and 6.14, were evaluated.

Ideal neutron pulse trains were generated for ^{252}Cf using the simulation method developed in chapter 4 and published in Evans, *et al* [63] (see appendix C). A ^{252}Cf source was modelled as a point isotropic source positioned at the centre of an idealised ^{3}He detector, using the MCNPX$^{\text{TM}}$ model described in section 4.3.1. Thirteen pulse trains were generated in total. An assay time of 600 s was chosen in each case, with 10 counting cycles for statistical analysis.

A range of ^{252}Cf source intensities were simulated, between 6.262×10^{3} ns^{-1} (6.262 kHz) and 2.505×10^{5} ns^{-1} (0.251 MHz). The detection efficiency was $\sim$ 99.4% and the die-away profile could be approximated by a double exponential with die-away times 3.06 μs and 4.41 μs, with relative intensities 74% and 26%. Table 6.1 shows the full range of ^{252}Cf source intensities chosen, where each row of the table relates to an individual pulse train.

The first column of table 6.1 displays the number of source spontaneous fission events, or `NPS` value, defined in the MCNPX$^{\text{TM}}$ input file. Changing this variable allows the source intensity, or neutron emission rate, to be tuned to a given value.

The average number of prompt neutrons emitted per fission, or first moment of spontaneous fission, $\overline{\nu}_{s1}$ is 3.757 for ^{252}Cf (see table 4.2). Multiplying the number of spontaneous fission events by the first moment gives the average number of prompt neutrons emitted from spontaneous fission events over the 600 s assay period and thus available for neutron capture (values are listed in the second column). Dividing these values by the assay time gives the average source intensity, listed in the third column.

Taking the average number of prompt neutrons emitted over a 600 s assay period, then multiplying by the detection efficiency ($\epsilon \sim 99.4$ %) and dividing by the number of time segments (10 in this case), gives the average number of captured neutrons per segment. Due to software limitations this value should not exceed 2.000×10^7, as noted in section 4.3.3.

Number of Spontaneous Fission Events (NPS)	Average Number of Prompt Neutrons	Average Source Intensity (ns^{-1})	Average Number of Captured Neutrons per Segment
1.000×10^6	3.757×10^6	6.262×10^3	3.736×10^5
2.000×10^6	7.514×10^6	1.252×10^4	7.471×10^5
3.000×10^6	1.127×10^7	1.879×10^4	1.121×10^6
4.000×10^6	1.503×10^7	2.505×10^4	1.494×10^6
5.000×10^6	1.879×10^7	3.131×10^4	1.868×10^6
6.000×10^6	2.254×10^7	3.757×10^4	2.241×10^6
7.000×10^6	2.630×10^7	4.383×10^4	2.615×10^6
8.000×10^6	3.006×10^7	5.009×10^4	2.989×10^6
9.000×10^6	3.381×10^7	5.636×10^4	3.362×10^6
1.000×10^7	3.757×10^7	6.262×10^4	3.736×10^6
2.000×10^7	7.514×10^7	1.252×10^5	7.471×10^6
3.000×10^7	1.127×10^8	1.879×10^5	1.121×10^7
4.000×10^7	1.503×10^8	2.505×10^5	1.494×10^7

Table 6.1: Calculated Source Intensities for Simulated ^{252}Cf Sources.

Simulated measured Singles and Doubles rates were recorded at zero deadtime, $\delta = 0$. These values are equivalent to true count rates. Ideal pulse trains were then perturbed by overlaying the effect of a paralyzable deadtime model. Simulated measured Singles and Doubles rates were recorded at the range of system deadtime parameters given in table 6.2.

δ (μs)
0.010
0.050
0.075
0.100
0.150

Table 6.2: Range of system deadtime parameters, δ used in the simulations.

The shift register settings of pre-delay, T_p, coincidence gate width, T_g, and long delay, T_L, were fixed at values of 0.3 μs, 4.5 μs and 200 μs, respectively in the main results presented. Hence the Doubles gate fraction, f_d remained constant whilst the deadtime was varied. Empirical simulation results could be used to determine the following:

- Dependence of vanishing Singles rate DTCF multiplier, K_S on system deadtime parameter, δ
- Dependence of vanishing Doubles rate DTCF multiplier, K_D on system deadtime parameter, δ

The Point Model equations provide one method to calculate the gate fraction, f_d. Re-visiting the ^{252}Cf Point Model equations in chapter 4 for the Singles and Doubles rates leads to an expression for $\frac{D_c}{S_c}$ from which f_d can be derived. The Singles and Doubles rates for ^{252}Cf are given by the following expressions:

$$S_c = (mg).\epsilon.\overline{\nu}_{s1} \tag{6.15}$$

$$D_c = (mg).\epsilon^2.f_d.\frac{\overline{\nu}_{s2}}{2} \tag{6.16}$$

The gate fraction, f_d can therefore be derived from the following expression:

$$\frac{D_c/f_d}{S_c} = \epsilon.(\frac{\overline{\nu}_{s2}}{2}/\overline{\nu}_{s1}) \tag{6.17}$$

Using this expression as an alternative means to calculate the gate fraction, as opposed to using the standard expression for detection system die-away time, τ, eliminates any uncertainty that may arise as a result of using an effective system die-away time, τ_{eff} from a single exponential approximation. Since $\frac{D_c/f_d}{S_c}$ is a term in the revised form of the Singles and Doubles DTCFs, equation 6.17 can also be used in the calculation of K_S (equation 6.13) and K_D (equation 6.25).

The first and second moments of spontaneous fission can be calculated from data given in the MCNPX^{TM} output file and are displayed in table 6.3. $\overline{\nu}_{s1}$ and $\overline{\nu}_{s2}$ have uncertainties associated with them due to experimental uncertainty and evaluation, but in the MCNPX^{TM} model the multiplicity distribution is exact. The Point Model assumptions are valid in this case because ^{252}Cf was modelled as a point source i.e. there is no contribution to the captured neutrons from induced fission ($M = 1$) or from (α, n) reactions ($\alpha = 0$).

	^{252}Cf Spontaneous Fission Moment
$\overline{\nu}_{s1}$	3.757
$\overline{\nu}_{s2}$	5.974

Table 6.3: First and second moment of spontaneous fission, $\overline{\nu}_{s1}$ and $\overline{\nu}_{s2}$ for a point source of ^{252}Cf modelled in MCNPX^{TM}.

Simulated measured rates were recorded for a range of gate fractions between 0.141 and 0.743, listed in table 6.4. Gate fractions were varied by fixing the MSR pre-delay, T_p at a constant value of 0.3 μs and varying the coincidence gate width, T_g between 0.5 μs and 6.0 μs in increments of 0.5 μs. The system deadtime parameter was also held constant at a value of 0.01 μs for these simulations to determine the dependence of the Singles and Doubles DTCFs on gate fraction.

T_p (μs)	T_g (μs)	f_d
0.3	0.5	0.141
0.3	1.0	0.255
0.3	1.5	0.347
0.3	2.0	0.423
0.3	2.5	0.488
0.3	3.0	0.542
0.3	3.5	0.589
0.3	4.0	0.629
0.3	4.5	0.664
0.3	5.0	0.694
0.3	5.5	0.720
0.3	6.0	0.743

Table 6.4: Range of coincidence gate widths, T_g and calculated gate fractions, f_d used in simulation of the MSR.

In this case, empirical simulation results could be used to determine the following:

- Dependence of vanishing Singles rate DTCF multiplier, K_S on gate fraction, f_d
- Dependence of vanishing Doubles rate DTCF multiplier, K_D on gate fraction, f_d

6.5 Empirical Results

DTCF multipliers K_S and K_D were determined by fitting empirical simulation data to the forms of the DTCFs proposed in equations 6.12 and 6.14. Curve fitting was performed using the Deming non-linear weighted least-squares fitting method [64] as implemented in the DEM4_27 code [65] which was available in the BASIC programming language. This approach has been previously applied to the analysis of calibration data collected by IAEA inspectors from NDA instruments; as detailed by Goldman, *et al.* [66]. Results obtained using the Deming method were consistent with Microsoft Excel^{TM} Solver, with the limitation that Solver could not facilitate a full uncertainty analysis.

Fits to the data were found to improve by allowing the multipliers in the exponential, n_S and n_D to vary, as opposed to using a value of 1 in the case of Singles and a factor of 4 in the case of Doubles. Simulated data were therefore fit to the following forms of the Singles and Doubles DTCFs:

$$\frac{S_c}{S_m} = DTCF_S \approx K_S . \exp(n_S . \delta . S_c) \tag{6.18}$$

where n_S is a free parameter derived from the data itself.

$$\frac{D_c}{D_m} = DTCF_D \approx K_D . \exp(n_D . \delta . S_c) \tag{6.19}$$

where n_D is again a free parameter derived from the data itself.

Table 6.5 provides a summary of the K_S, K_D, n_S and n_D parameters derived from the Deming fitting method, together with their uncertainties.

δ (μs)	$K_S \pm \sigma(K_S)$	$n_S \pm \sigma(n_S)$	$K_D \pm \sigma(K_D)$	$n_D \pm \sigma(n_D)$
0.010	1.0058 $\pm 2.5 \times 10^{-6}$	1.0059 $\pm 1.6 \times 10^{-11}$	1.0099 $\pm 1.6 \times 10^{-5}$	4.0458 $\pm 1.3 \times 10^{-10}$
0.050	1.0288 $\pm 1.1 \times 10^{-5}$	0.9924 $\pm 6.9 \times 10^{-11}$	1.0502 $\pm 3.6 \times 10^{-5}$	3.9512 $\pm 3.0 \times 10^{-10}$
0.075	1.0432 $\pm 1.1 \times 10^{-5}$	0.9830 $\pm 6.6 \times 10^{-11}$	1.0758 $\pm 4.3 \times 10^{-5}$	3.9041 $\pm 3.5 \times 10^{-10}$
0.100	1.0575 $\pm 1.5 \times 10^{-5}$	0.9752 $\pm 8.7 \times 10^{-11}$	1.1019 $\pm 5.1 \times 10^{-5}$	3.8611 $\pm 4.0 \times 10^{-10}$
0.150	1.0862 $\pm 1.8 \times 10^{-5}$	0.9613 $\pm 1.1 \times 10^{-10}$	1.1550 $\pm 7.5 \times 10^{-5}$	3.7929 $\pm 5.6 \times 10^{-10}$

Table 6.5: DTCF parameters derived from non-linear weighted least-squares curve fitting to the simulation data as a function of δ, together with their uncertainties[7].

[7]Note that the uncertainties in the K_S, K_D, n_S and n_D parameters are very much smaller than the precision with which the parameters have been determined within the Deming fitting method. It was however not deemed necessary to re-code the Deming fitting method in this case.

From equations 6.12 and 6.14, n_D is expected to vary with n_S as follows:

$$n_D \approx 4 \cdot n_S \tag{6.20}$$

$$\frac{n_D}{n_S} \approx 4 \tag{6.21}$$

Table 6.6 shows the ratio $\frac{n_D}{n_S}$ calculated from the data in table 6.5, together with the calculated uncertainty on this ratio.

δ (μs)	$\frac{n_D}{n_S} \pm \sigma(\frac{n_D}{n_S})$
0.010	4.022 $\pm 1.469 \times 10^{-10}$
0.050	3.982 $\pm 4.080 \times 10^{-10}$
0.075	3.972 $\pm 4.431 \times 10^{-10}$
0.100	3.959 $\pm 5.412 \times 10^{-10}$
0.150	3.945 $\pm 7.344 \times 10^{-10}$

Table 6.6: Ratio $\frac{n_D}{n_S}$ derived from fitted simulation data, expected to be close to 4.

Figure 6.1 shows n_S and n_D against system deadtime parameter, δ. Values of n_S and n_D are seen to be close to 1 and 4, respectively, and remain approximately constant over the range of simulated source intensities. Uncertainties in n_S and n_D are plotted, but are small.

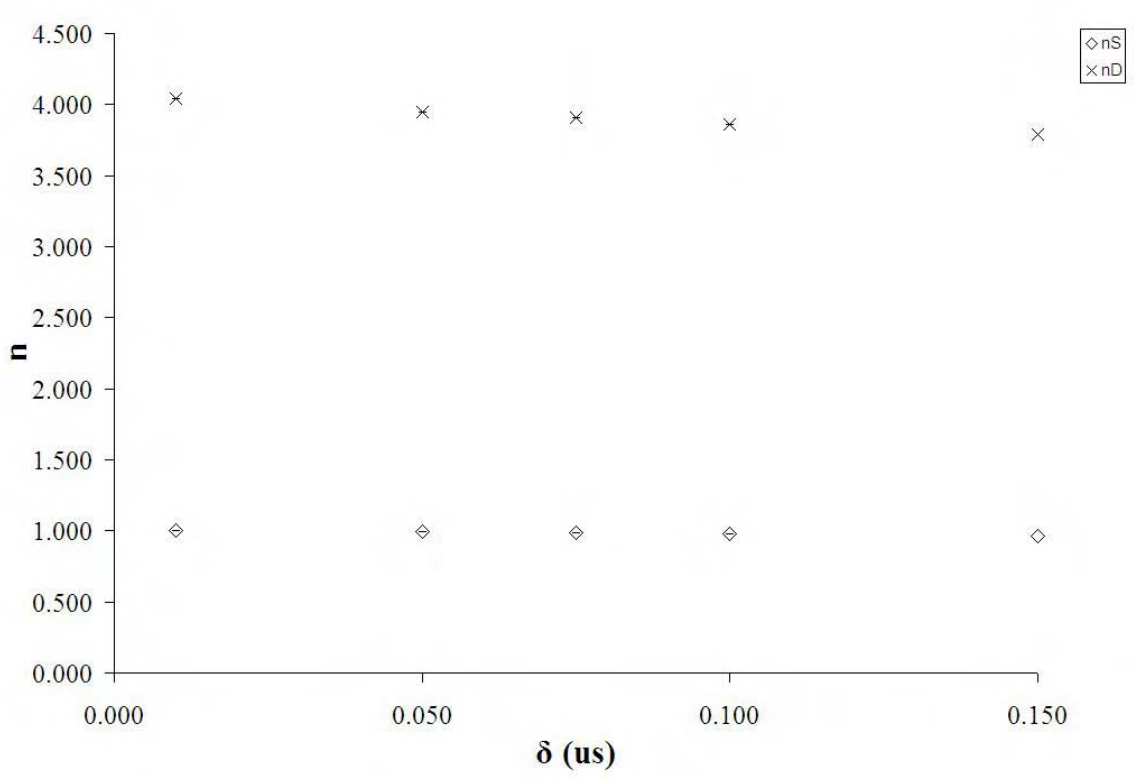

Figure 6.1: n_S and n_D vs. system deadtime parameter, δ.

6.5.1 Dependence of Singles and Doubles DTCFs on System Deadtime Parameter

The empirical results demonstrate the Singles DTCF to be dependent on system deadtime parameter and independent of gate fraction (see figure 6.3) in the functional manner expected. This analysis supports the proposed form of the Singles DTCF given by equation 6.10. Figure 6.2(a) shows a linear dependence of the vanishing Singles rate DTCF multiplier, K_S on system deadtime parameter, δ.

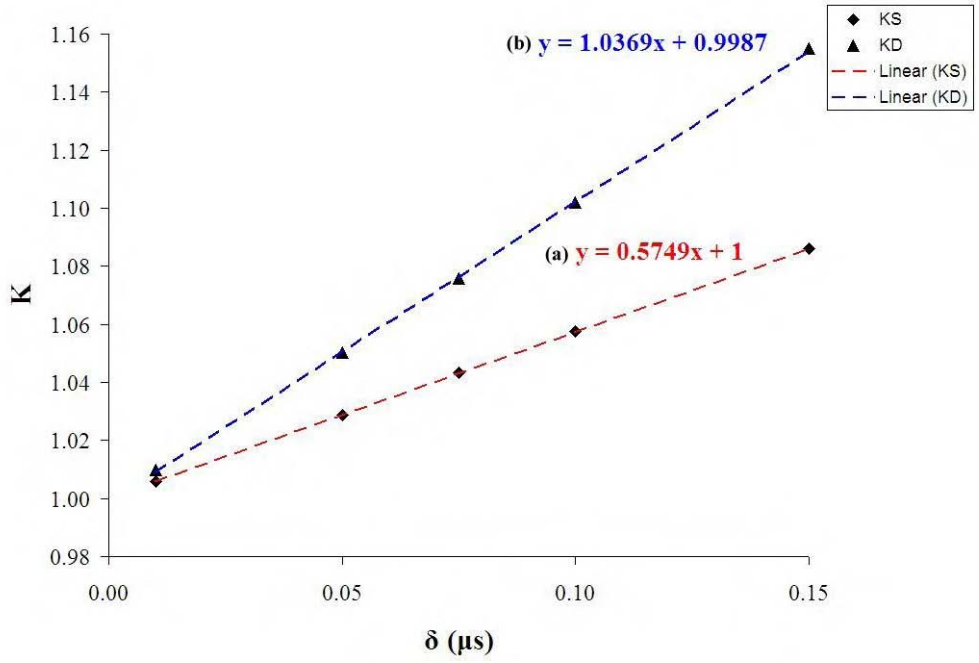

Figure 6.2: (a) Vanishing Singles rate DTCF multiplier, K_S vs. system deadtime parameter, δ (b) Vanishing Doubles rate DTCF multiplier, K_D vs. system deadtime parameter, δ ($K \rightarrow y$; $\delta \rightarrow x$) Uncertainties in K are plotted, but are small.

The following function was derived from a standard linear fit to the data in figure 6.2(a):

$$K_S = 1 + 0.5749.\delta \tag{6.22}$$

A generalisation of equation 6.10 for the linear fit to the data is given by:

$$K_S \approx [\theta_1 + \theta_2.\frac{(D_c/f_d)}{S_c}.\frac{\delta}{\tau_{eff}}] \tag{6.23}$$

where θ_1 is the intercept on a plot of K_S vs. δ, and the gradient is given by $\theta_2.\frac{(D_c/f_d)}{S_c}.\frac{1}{\tau_{eff}}$.

The intercept θ_1 was expected to be unity, but was allowed to be a free parameter.

Equation 6.23 was used to calculate the value expected for the gradient in an absolute sense using parameters obtained from the simulation. This gave a value between 0.465 and 0.516, depending on the chosen value of τ_{eff} (with lower limit corresponding to a single exponential approximation and upper limit corresponding to a two component fit to the dieaway curve i.e. 3.40 μs and 3.06 μs, respectively). It is interesting to note that twice the value of this upper limit of 0.516 is 1.032, which closely corresponds to the gradient of the graph in figure 6.2(b) for Doubles. Perhaps this justifies further study for systems of widely different characteristics to see if there is a general relation. For example, this is reminiscent of the $\sim$ factor 4 between the Singles DTCF and Doubles DTCF in traditional PNCC. This might also fall out of a deeper theoretical treatment and future work is proposed with I. Pázsit, Professor of Nuclear Engineering at Chalmers University.

Note that τ_{eff} is used on the basis of the understanding that the die-away of real systems do not follow a single exponential. For example, if there are 3 components to the die-away, $\frac{1}{\tau_{eff}}$ is a combination of τ_1, τ_2 and τ_3. The parameter $\frac{1}{\tau_{eff}}$ can therefore be treated as an empirical parameter, expressed as the following:

$$\frac{1}{\tau_{eff}} = \frac{1}{f(\tau_1, \tau_2, \tau_3)} \tag{6.24}$$

where $f(\tau_1, \tau_2, \tau_3)$ is a function that depends on the region of the die-away curve fitted. Equation 6.24 is a valid assumption for both K_S and K_D, since the DTCFs will need to include a multiplier on the gradient, θ_2 and λ_2 (see equation 6.25).

6.5.2 Dependence of Singles and Doubles DTCFs on Gate Fraction

Figure 6.3(a) shows the vanishing Singles rate DTCF multiplier, K_S to be independent of Doubles gate fraction, f_d. The slight downward trend in figure 6.3(b), indicated by the negative gradient of magnitude 0.0044, shows that the vanishing Doubles rate DTCF multiplier is, however, dependent on gate fraction. Results showing a similar trend are presented in appendix G for system deadtime parameter values: 0.050 μs, 0.075 μs, 0.100 μs and 0.150 μs. To account for this dependence, the vanishing Doubles rate DTCF multiplier can therefore be written as the following:

$$K_D \approx [\lambda_1 + \lambda_2 . \frac{(D_c/f_d)}{S_c} . \frac{\delta}{\tau_{eff}} . f_d] \tag{6.25}$$

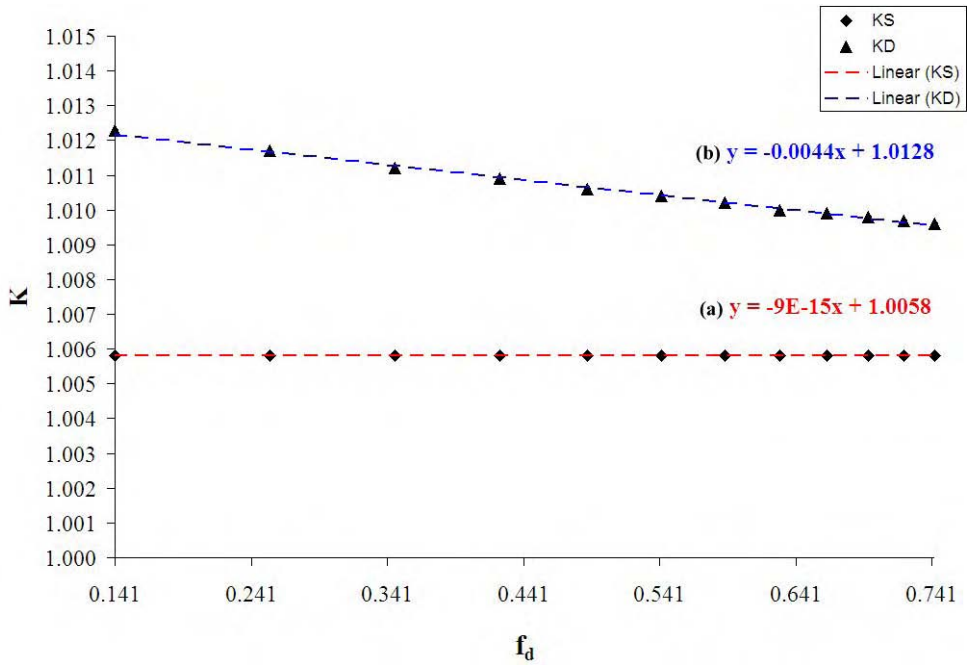

Figure 6.3: (a) Vanishing Singles rate DTCF multiplier, K_S vs. Doubles gate fraction, f_d (b) Vanishing Doubles rate DTCF multiplier, K_D vs. Doubles gate fraction, f_d. System deadtime parameter, $\delta = 0.01$ μs. Uncertainties in K are plotted, but are small.

6.6 Comparison

Here, both the traditional and revised forms of the DTCFs are applied to the simulated measured Singles and Doubles rates (acquired over a range of δ values) and compared. Singles and Doubles DTCFs should correct the measured rates to obtain a constant $\frac{D}{S}$ ratio. In other words, the ratio ξ should be unity across the range of count rates simulated:

$$\xi = \frac{\frac{D_c}{S_c}|_{\delta}}{\frac{D_c}{S_c}|_{\delta=0}} = 1 \tag{6.26}$$

Table 6.7 shows the true $\frac{D}{S}$ ratios ($\delta = 0$), together with statistical uncertainties on this ratio, as a function of true Singles rate ($\delta = 0$). Statistical uncertainties were obtained from the propagation of uncertainties in the true Singles and Doubles rates i.e. simulated Singles and Doubles rates at $\delta = 0$, via the following expression:

$$\sigma(\frac{D}{S}) = \frac{D}{S} \cdot \sqrt{(\frac{\sigma(D)}{D})^2 + (\frac{\sigma(S)}{S})^2} \tag{6.27}$$

where $\sigma(S)$ and $\sigma(D)$ are the statistical uncertainties in the true Singles and Doubles rates, respectively. The pulse train was divided into 10 time segments. True Singles and Doubles rates are the mean count rates, averaged over the individual count rates recorded across the 10 segments. Uncertainties are therefore expressed as the standard error of the mean count rates.

$S_c \pm \sigma(S_c)$	$D_c \pm \sigma(D_c)$	$\frac{D}{S} \pm \frac{\sigma(\frac{D}{S})}{\frac{D}{S}}$ (%)
6224 $\pm$ 3	6531 $\pm$ 7	1.0494 $\pm$ 0.11
12451 $\pm$ 3	13061 $\pm$ 10	1.0490 $\pm$ 0.08
18676 $\pm$ 4	19589 $\pm$ 13	1.0489 $\pm$ 0.07
24899 $\pm$ 5	26110 $\pm$ 18	1.0487 $\pm$ 0.07
31123 $\pm$ 4	32640 $\pm$ 10	1.0488 $\pm$ 0.03
37348 $\pm$ 4	39169 $\pm$ 14	1.0487 $\pm$ 0.04
43577 $\pm$ 6	45700 $\pm$ 14	1.0487 $\pm$ 0.03
49804 $\pm$ 5	52207 $\pm$ 18	1.0482 $\pm$ 0.04
56032 $\pm$ 7	58750 $\pm$ 21	1.0485 $\pm$ 0.04
62255 $\pm$ 7	65273 $\pm$ 29	1.0485 $\pm$ 0.05
124528 $\pm$ 10	130596 $\pm$ 52	1.0487 $\pm$ 0.04
186789 $\pm$ 12	195997 $\pm$ 72	1.0493 $\pm$ 0.04
249055 $\pm$ 14	261360 $\pm$ 81	1.0494 $\pm$ 0.03

Table 6.7: True $\frac{D}{S}$ ratios ($\delta = 0$) and associated statistical uncertainties as a function of true Singles rate, S_c ($\delta = 0$).

The true Doubles-to-Singles ratios, $\frac{D}{S}$ for the range of simulated ^{252}Cf sources are listed in column 2 of table 6.7. It can be shown that in the case where $\epsilon \rightarrow 1$, then $\frac{D_c}{S_c} > 1$ via the following expression; derived from the Singles and Doubles point model equations for ^{252}Cf (equations 6.15 and 6.16):

$$\frac{D}{S} = \frac{mg\epsilon^2 f_d \frac{\overline{\nu_{s2}}}{2}}{mg\epsilon\overline{\nu_{s1}}} \tag{6.28}$$

As $\epsilon \rightarrow 1$, equation 6.28 becomes:

$$\frac{D}{S} \approx \frac{f_d \frac{\overline{\nu_{s2}}}{2}}{\overline{\nu_{s1}}} \tag{6.29}$$

where $f_d \approx 0.65 \pm 1.42 \times 10^{-3}$, $\overline{\nu_{s2}} = 11.962$ and $\overline{\nu_{s1}} = 3.757$.

$$\therefore \frac{D}{S} > 1 \tag{6.30}$$

Statistical uncertainties in the true $\frac{D}{S}$ ratios were used to assign lower and upper bounds in the expected deviation in the ratio ξ (given by equation 6.26) from unity, listed in table 6.8.

S_c	Ratio ξ	Lower Bound	Upper Bound
6224	1.000000	0.998853	1.001147
12451	1.000000	0.999159	1.000841
18676	1.000000	0.999317	1.000683
24899	1.000000	0.999274	1.000726
31123	1.000000	0.999661	1.000339
37348	1.000000	0.999638	1.000362
43577	1.000000	0.999670	1.000330
49804	1.000000	0.999644	1.000356
56032	1.000000	0.999621	1.000379
62255	1.000000	0.999536	1.000464
124528	1.000000	0.999591	1.000409
186789	1.000000	0.999625	1.000375
249055	1.000000	0.999683	1.000317

Table 6.8: Ratio ξ together with lower and upper bounds on this ratio.

An ideal DTCF should be able to correct the measured $\frac{D}{S}$ within these bounds i.e. the deviation in the ratio ξ from unity should not exceed these bounds therefore the deviation in the corrected $\frac{D}{S}$ ratios should not exceed the uncertainties in the true $\frac{D}{S}$ ratios.

6.6.1 Deadtime Corrected Doubles to Singles Ratios using the Traditional Theoretical Approach

When traditional NCC DTCFs are applied, figure 6.4 provides an illustration that the $\frac{D}{S}$ ratio does not correct to a constant value in the limit that the Singles tends to zero. Figure 6.4 therefore shows the deviation from unity (where unity is the expected value for Cf). A 0.5% deviation in the $\frac{D}{S}$ ratio can be calculated (at the lowest count rate, at the highest value of δ) compared to the true value (at $\delta = 0$), when performing deadtime correction using the traditional NCC DTCFs. This is significant compared to the small 0.1% statistical uncertainty in the true $\frac{D}{S}$ ratio at this count rate. The deviation of this ratio from unity is just 0.01 % when performing deadtime correction using the revised NCC DTCFs. The magnitude of this effect is emphasised by the extreme efficiency of the chamber modeled and the choice of δ.

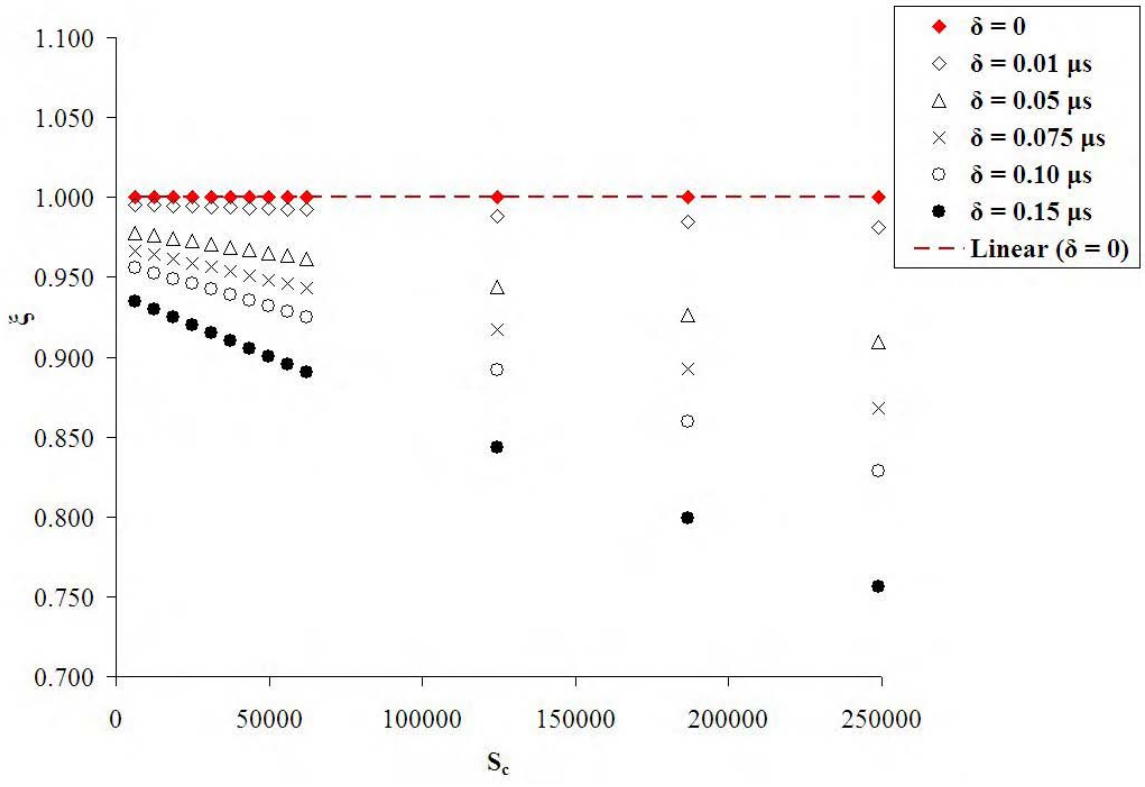

Figure 6.4: Ratio ξ using traditional NCC deadtime correction factors vs. S_c

6.6.2 Deadtime Corrected Doubles to Singles Ratios using the New Theoretical Approach

Figure 6.5 shows that the ratio ξ is consistent with unity and the new approach is able to correct the measured $\frac{D}{S}$ ratio within the statistical uncertainties in the true $\frac{D}{S}$ ratio. The blue solid diamonds on the curve illustrate the lower and upper bounds for the statistical uncertainties in the true $\frac{D}{S}$ ratio, as listed in table 6.8 i.e. the simulated $\frac{D}{S}$ ratio when $\delta = 0$. All corrected rates lie within these bounds.

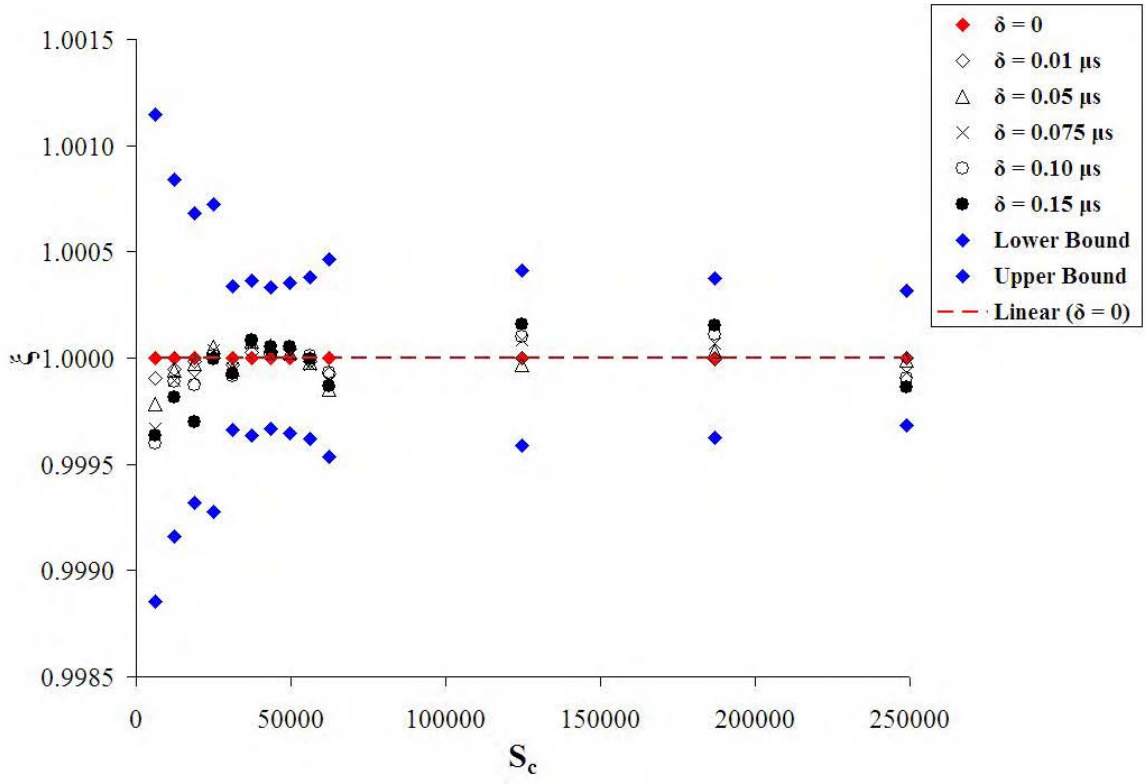

Figure 6.5: Ratio ξ using revised NCC deadtime correction factors vs. S_c. The $\delta = 0$ case lies on the unity line.

6.7 Practical Implications

6.7.1 Calibration using ^{252}Cf

Conventionally, assay system calibration is performed using ^{252}Cf. A bias in the ratio ρ_0 for ^{252}Cf has been observed even in the limit of low rates and a correction factor has been applied. The quantity ρ_0 is defined as the Doubles-to-Singles ratio for a non-multiplying metallic item of ^{240}Pu. The ratio ρ_0 can also be defined for ^{252}Cf since $M = 1$ and $\alpha = 0$. This is given by the following expression:

$$\rho_0(^{252}\text{Cf}) = \frac{D_c}{S_c} \tag{6.31}$$

The first and second moments of spontaneous fission for ^{252}Cf and ^{240}Pu are compared in table 6.9.

	^{252}Cf s.f.	^{240}Pu s.f.
$\overline{\nu}_{s1}$	3.757	2.156
$\overline{\nu}_{s2}$	5.974	3.825

Table 6.9: First and second moments of spontaneous fission for ^{252}Cf and ^{240}Pu.

The multiplicity distribution for ^{240}Pu is softer than that of ^{252}Cf i.e. the spontaneous fission moments are lower for ^{240}Pu than ^{252}Cf, hence the ^{240}Pu multiplicity distribution has a lower mean multiplicity. A conversion factor is therefore expected to be needed to relate ρ_0 for ^{252}Cf to ^{240}Pu when applying calibration data to real items:

$$\rho_0(^{240}\text{Pu}) = \rho_0(^{252}\text{Cf}) \times DTCF \times Conversion\ Factor \tag{6.32}$$

for a non-multiplying sample e.g. Pu metal. The conversion factor is just a ratio of nuclear data. Therefore, this presents a future need to quantify the difference in the relative effects of deadtime for ^{252}Cf and ^{240}Pu.

$$DTCF \approx \frac{\frac{K_D}{K_S}|_{^{252}\text{Cf}}}{\frac{K_D}{K_S}|_{^{240}\text{Pu}}} \tag{6.33}$$

which can be evaluated from equations 6.23 and 6.25.

6.7.2 In Application

Item dependent correction factors will need to be applied when measuring multiplying items such as Pu oxides. Then factors come about naturally via the appearance of the term $\frac{D_c}{S_c}$ in the expressions for K_S (equation 6.23) and K_D (equation 6.25).

Chapter 7

CONCLUSIONS AND RECOMMENDATIONS FOR FUTURE WORK

7.1 Summary and Conclusions

In chapter 1, the following main research question was posed:

- *Can existing neutron pulse train analysis methods be extended to include a full systematic study of deadtime behaviour and effects in passive neutron counting systems?*

In answering this question, a simulation method has been established for the systematic investigation of deadtime losses over a range of neutron sources, source intensities and operational parameters of a neutron counter. The development of this method was presented in chapter 4. This led to a further research question:

- *Are there differences between the deadtime correction factors for uncorrelated (e.g. AmLi) and correlated neutron sources (e.g. Cf)?*

Differences between deadtime losses in random neutron sources (e.g. AmLi) and correlated fission sources (e.g. Cf) have been found and attributed to deadtime losses within fission bursts themselves. Results are presented in appendices B, C and D, which are expanded upon in chapter 6.

New forms of the Singles and Doubles deadtime correction factors for PNCC are presented in chapter 6, together with empirical simulation data which supports the functional form of these correction factors. Simulation data has shown that these formalisms are applicable to correlated neutron sources. In addition, the new deadtime correction factors have improved performance compared to the traditional NCC deadtime correction factors, when correcting for deadtime based on a constant $\frac{D}{S}$ ratio.

The revised deadtime correction formulae explicitly make allowance for "within burst losses" at low sustained rates. This allows the small biases to parameters such as ρ_0 to be corrected and provides the appropriate allowance in switching between fission sources. The effect of multiplication on these deadtime losses was considered in the following research question:

- *To what extent does multiplication (e.g. Pu items) impact the deadtime correction factors (impact the existing theoretical approaches to deadtime correction)?*

As the multiplication, M, becomes greater than one, the pulse train becomes more correlated e.g. the term $\frac{D_c}{S_c}$ in the vanishing (Singles or Doubles) rate deadtime correction factor multiplier increases; first introduced in section 6.3.2. As a result, the deadtime correction factor becomes larger due to the greater probability of neutrons being closer together in time. This effect has not been studied in the same detail as the first two research questions, but remains an open research question for future work, alongside other topics discussed in section 7.2.

7.2 Recommendations for Future Work

7.2.1 Experimental Validation

The high efficiency and short die-away time counter used for this work does not exist in practice and therefore empirical validation of results could only be performed via simulations. The validity of new deadtime correction factors presented in chapter 6 to current state of the practice systems could be performed via experiment on systems of diverse type (e.g. including variations in efficiency, system die-away time and system deadtime parameter). Experiments could also be performed using a range of fission neutron sources with different neutron multiplicities, and assaying both multiplying and non-multiplying items.

7.2.2 Extension of Modelling Beyond the Ideal Case

The simulation work could also be extended beyond the ideal case to cross-check against experimental results. Both experimental work and extended simulations can be used to determine the limits of traditional NCC deadtime correction algorithms i.e. assign an upper limit on efficiency and lower limit on system die-away time for the regime in which traditional algorithms may be applied.

The simulation work can be extended to more realistic cases to include the following [49]:

- Distribution of count rates between different numbers of pre-amplifier boards, varying the number of input channels to the MSR
- He-3 pulse shape variation
- Discriminator action
- Derandomisers
- MSR clock speeds
- Finite time resolution of the MSR
- Extension of MSR algorithms to the coding of the fast accidentals method i.e. sampling the A gate more frequently than the R + A gate
- Investigation of Random Triggered Inspection (RTI) versus Signal Triggered Inspection (STI)

7.2.3 Improved MSR Algorithms

List mode data provides a complete record of an assay therefore analysis algorithms used during the post-processing of this data should be optimised to extract all available information. A future research question is proposed:

- *Are existing algorithms for the shift register the most efficient? Is there merit to an improved sampling regime for the MSR?*

7.2.4 Inverse Calculations

The forward simulation method has been successfully applied to the extension of deadtime correction factors for correlated neutron counting. Inverse calculations are still needed for practical applications [49].

7.2.5 Triples DTCF

The new forms of the deadtime correction factors for PNCC developed in this work can be extended to derive a deadtime correction factor for Triples count rates.

7.2.6 Correlated Neutron Counting Applied to the Assay of Spent Nuclear Fuel

Temporally correlated neutron counting techniques are being considered for the assay of spent nuclear fuel under a current research program; as discussed by Tobin, *et al* [67].

Spent nuclear fuel contains ^{244}Cm which can account for greater than 95% of the neutron emission [68]. When placed in a chamber, the fuel pin neutrons that emerge in to the moderator are detected and can be used as a trigger to sense induced fissions from those that return; as proposed by Menlove, *et al* [69].

These experiments, aimed at Pu accountancy in new reprocessing cycles, take place at high rates. The approaches developed here are expected to have direct applicability in this emerging field.

References

[1] S. Croft, R.D. McElroy, S. Philips, M.F. Villani, and L.G. Evans. Dead Time Behaviors in Passive Neutron Correlation Counting. In *Proc. of WM'07*, Tucson, AZ, USA, February 2007. Paper #7258.

[2] L. Bondar. Computerized Multiplicity Counter. In *Proc. of the 19th Annual ESARDA Symposium on Safeguards and Nuclear Material Management*, Montpellier, France, 13-15 May 1997.

[3] M.T. Swinhoe. Generation of Pulse Trains for the ESARDA NDA Benchmark Exercise. Technical report, Los Alamos National Laboratory (LANL), February 2004. LA-UR-04-0834.

[4] P. Peerani, A. Weber, M.T. Swinhoe, and L.G. Evans. Esarda Multiplicity Benchmark Exercise Phase III and IV Final Report, 2009.

[5] S. Croft. Private Communication, June 2006.

[6] D.B. Pelowitz. *MCNPX User's Manual Version 2.5.0*. Los Alamos National Laboratory (LANL), April 2005. LA-CP-05-0369.

[7] N. Dytlewski. Dead-time corrections for multiplicity counters. *Nuclear Instruments and Methods in Physics Research A*, 317:492–494, 1991.

[8] I. Pázsit and L. Pál. *Neutron Fluctuations: A Treatise on the Physics of Branching Processes*, pages 294–312. Elsevier, 2008.

[9] M.T. Swinhoe. Private Communication, October 2008.

[10] International Atomic Energy Authority (IAEA). IAEA Safeguards Glossary: 2001 Edition, 2001. Available from: http://www-pub.iaea.org/MTCD/publications/PDF/nvs-3-cd/PDF/NVS3_prn.pdf (Last accessed 5 January 2009).

[11] A.M. Meeks and J. Chapman. Development of the Remote-Handled Transuranic Waste Radioassay Data Quality Objectives. Technical report, Oak Ridge National Laboratory (ORNL), 1991. ORNL/TM-13362.

[12] N. Ensslin, D. Reilly, H. Smith Jr., and S. Kreiner, editors. *Passive Non-destructive Assay of Nuclear Materials*. Los Alamos National Laboratory

(LANL), March 1991. NUREG/CR-5550 LA-UR-90-732
Available from: http://www.lanl.gov/orgs/n/n1/panda/.

[13] S. Croft, S. Philips, E. Alvarez, K. Lambert, J. Guerault, L. Passelegue, C. Mathonat, and G.Widawski. Nuclear Calibration of a Large Volume Calorimeter. In *Proc. of WM2009*, Phoenix, AZ, USA, March 2009.

[14] F. Bronson. To Sample or not to Sample - An Investigation into the Uncertainty from Sampling followed by Laboratory Analysis versus *in-toto* Gamma Spectroscopy for situations of Non-Uniform Radioactivity Distributions. In *Proc. of WM2008*, Phoenix, AZ, USA, February 2008.

[15] T. Gozani. *Active Non-destructive Assay of Nuclear Materials; Principles and Applications*. US Nuclear Regulatory Commission (NRC), Washington DC, 1981. NUREG/CR-0602.

[16] A. Worrall. Private Communication, September 2008.

[17] B. Barré, editor. *All about nuclear energy from Atom to Zirconium*. Arevacom, 2008.

[18] P.D. Wilson, editor. *The Nuclear Fuel Cycle: From Ore to Waste*. Oxford University Press (United Kingdom), 1996.

[19] Nuclear Decommissioning Authority. *Nuclear Decommissioning Authority Plutonium Options*, 2008.

[20] A. Worrall. Private Communication, February 2009.

[21] Report prepared for the Department for Environment, Food and Rural Affairs and the Nuclear Decommissioning Authority by Pöyry Energy Limited. *The 2007 UK Radioactive Waste Inventory Main Report*, March 2008.
Available from http://www.nda.gov.uk/ukinventory/
(Last accessed 29 December 2008).

[22] Defra. *Radioactive Wastes in the UK: A Summary of the 2007 Inventory*, March 2008.
Available from http://www.nda.gov.uk/ukinventory/
(Last accessed 29 December 2008).

[23] D. D. Eisenhower. Atoms for Peace Speech. IAEA, December 1953.
Available from http://www.iaea.org/About/history_speech.html
(Last accessed 14 February 2009).

[24] N. Ensslin, W.C. Harker, M.S. Krick, D.G. Langner, M.M. Pickrell, and J.E. Stewart. *Application Guide to Neutron Multiplicity Counting*. LANL, November 1998. LA-13422-M Manual.

[25] J. Sprinkle. DOE-HQ on NDA Future Needs. PowerPoint Presentation, July

an Integrated Approach? In *Proc. of the 49th Annual Meeting of the INMM*, Nashville, TN, USA, July 2008.

[68] H.O. Menlove K.E. Thomas, E.A. Hakkila and J.S. Hong. Safeguarding the Direct Use of Plutonium in CANDU Reactors (DUPIC). In *Proc. of Global'93 - Future Nuclear Systems: Emerging Fuel Cycle and Waste Disposal Options*, Seattle, Washington, USA, September 12-17 1993.

[69] S.H. Menlove H.O. Menlove and S.J. Tobin. Verification of Plutonium content in Spent Fuel Assemblies Using Neutron Self-Interrogation. In *Proc. of the 50th Annual Meeting of the INMM*, Tucson, AZ, USA, July 2009.

Appendices

Appendix C: Paper Published in Proceedings of Waste Management 2009 (peer reviewed)

Appendix D: Paper Published in Proceedings of the INMM 49th Annual Meeting 2008

Appendix F: MCNPX Input File

```
cf2b.x
c cell cards
1     1 -15.1     -1             $ cf-252 sphere
2     2 -0.00165   1 -2          $ He-3 4pi detector
3     0            2             $ External void

c surface cards
1     SO 0.1                    $ cf-252 sphere, point like
2     SO 100000                 $ detector sphere, radius = 1000m

c materials cards
c material one is cf-252
M1    98252 1.0
c material two is He-3 detector
M2     2003 1.0
NONU $ fission turnoff
c energy and thermal cards
MODE N
PHYS:N J 100 3J 1
c analog capture
CUT:N 2J 0 0
c SF source, spherical volume distribution
SDEF  PAR = SF
      ERG = D1
      CEL = 1
      SUR = 0 $ volume distribution
      POS = 0.0 0.0 0.0 $ defines centre of sphere
      RAD = D2 $ power law with a=2 to sample uniformly in cell volume
SP1 -3 1.175 1.04 $ Watt fission spectrum for Cf-252
SI2 0.09 $ value of radius
SP2 -21 $ power law, defaults to a=2
c tally specification cards
FC8 coincidence capture tally
F8:N 2
FT8 CAP 2003
c variance reduction cards
IMP:N 1 1 0
c output control cards
PRINT 38 110 117 118
c ptrac capture file
PTRAC EVENT=CAP FILE=ASC
NPS 50000000
```

Appendix G: Additional Results: Dependence of Singles and Doubles Vanishing Rate DTCF Multiplier on Gate Fraction

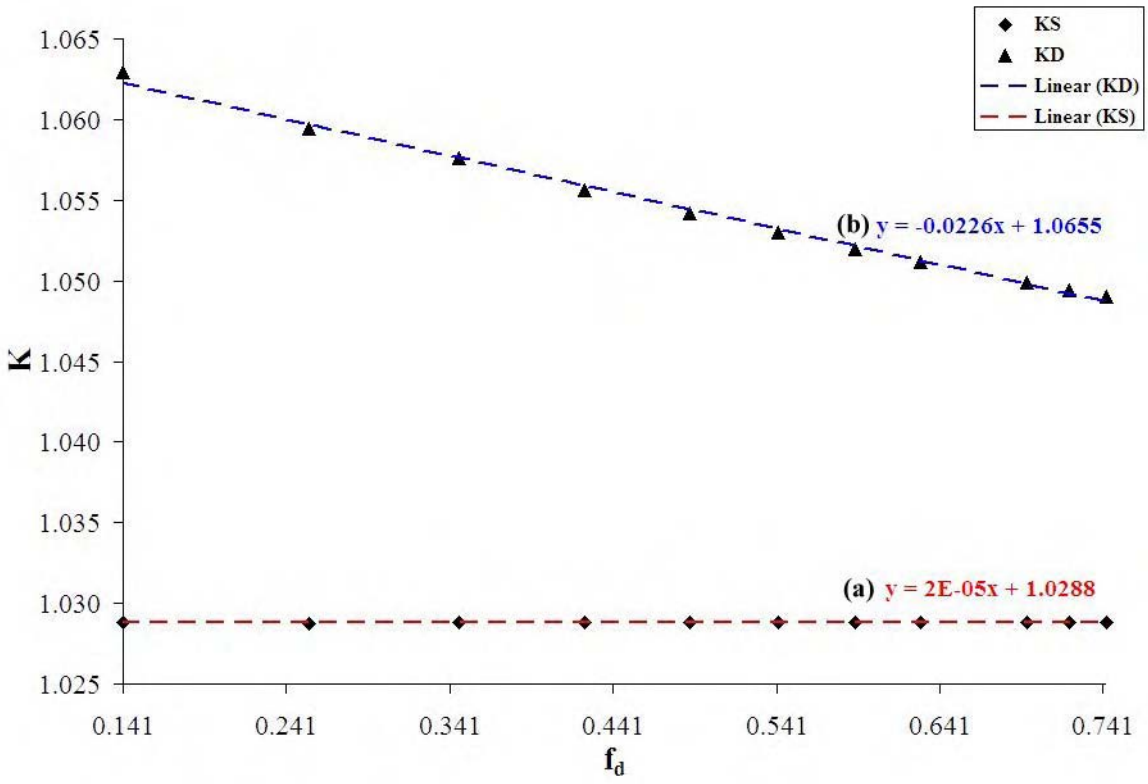

Figure 1: (a) Vanishing Singles rate DTCF multiplier, K_S vs. Doubles gate fraction, f_d (b) Vanishing Doubles rate DTCF multiplier, K_D vs. Doubles gate fraction, f_d. System deadtime parameter, $\delta = 0.05$ μs.

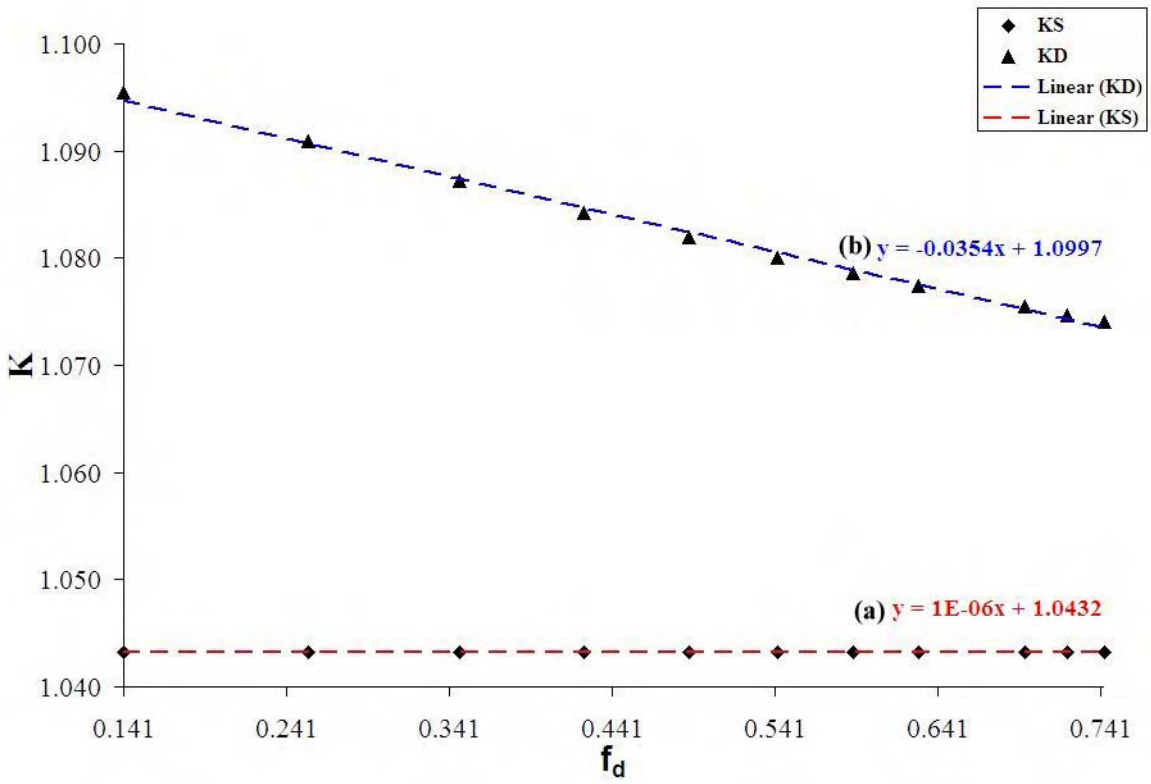

Figure 2: (a) Vanishing Singles rate DTCF multiplier, K_S vs. Doubles gate fraction, f_d (b) Vanishing Doubles rate DTCF multiplier, K_D vs. Doubles gate fraction, f_d. System deadtime parameter, $\delta = 0.075$ μs.

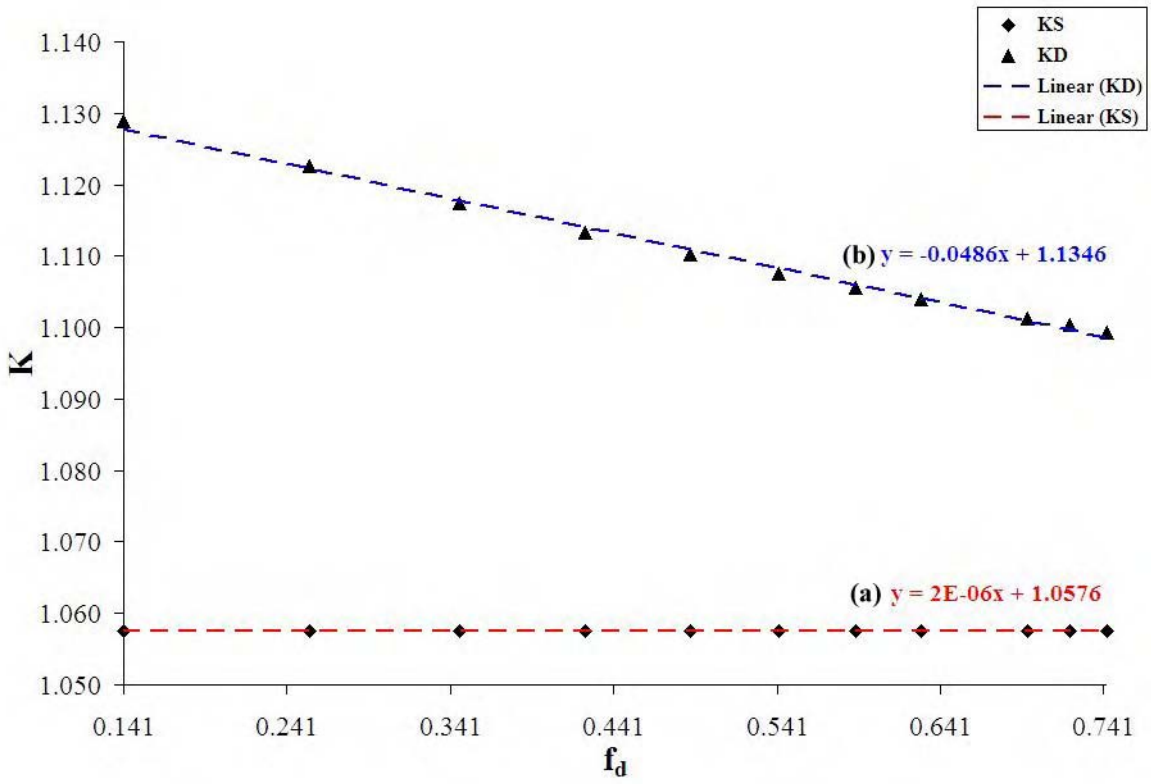

Figure 3: (a) Vanishing Singles rate DTCF multiplier, K_S vs. Doubles gate fraction, f_d (b) Vanishing Doubles rate DTCF multiplier, K_D vs. Doubles gate fraction, f_d. System deadtime parameter, $\delta = 0.100$ μs.

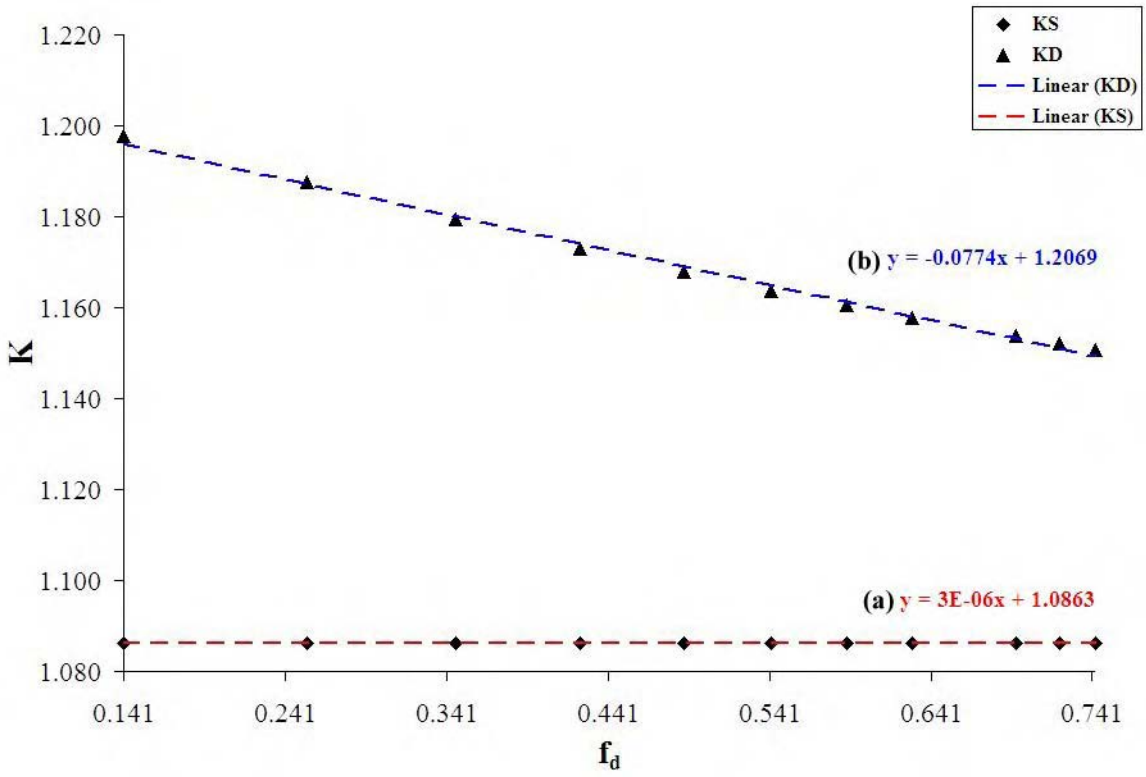

Figure 4: (a) Vanishing Singles rate DTCF multiplier, K_S vs. Doubles gate fraction, f_d (b) Vanishing Doubles rate DTCF multiplier, K_D vs. Doubles gate fraction, f_d. System deadtime parameter, $\delta = 0.150$ μs.